UNIVERSITÉ LAVAL

Study of Molecular Interactions and Surface Alignment Control of Liquid Crystals

Thèse

Amalya Minasyan

Doctorat en physique
Philosophiae doctor (Ph.D.)

Québec, Canada

Résumé

Le contrôle de l'alignement des molécules de cristaux liquides (CL) est d'une importance majeure pour la plupart des applications électro-optique comme les afficheurs, les modulateurs et les atténuateurs variables. Ce contrôle est réalisé plus spécifiquement par les interactions entre les molécules de CL et la surface adjacente. L'alignement par la surface est ainsi un des facteurs clés pour l'amélioration des performances des systèmes basés sur les CL. Cette thèse rapporte une étude expérimentale sur le contrôle de l'alignement des molécules de CL par la surface, et explore des avenues pratiques.

Dans un premier temps, des CL nématiques à double fréquence (DF-NLC) et des films minces de mésogènes réactifs (MR) déposés sur la surface intérieure d'une cellule, ont été utilisés pour produire des structures polymères stabilisées en surface. Pour former ces structures, une interpénétration partielle entre les molécules de CL et de MR a été réalisée pendant l'application d'un couple diélectrique (positif ou négatif) sur le système de matériau. Après une courte période d'interpénétration entre la couche de MR et les CL, une exposition UV a été appliquée pour polymériser totalement le système de matériau. Ces systèmes ont démontré un fort potentiel pour le contrôle de l'alignement des CL par la surface. Ils permettent la « programmation » de cellule de CL présentant une diffusion de la lumière électriquement contrôlable, pouvant être utilisé dans des applications telles que des fenêtres intimités et l'éclairage intelligent. Des analyses électro-optiques et microscopiques ont été faites pour caractériser ces structures. Nous avons montré que les modulations de contraste de la lumière diffusée, ainsi que la dépendance de la polarisation et les temps de réponses peuvent être améliorées de façon notable par le contrôle à double fréquence.

Dans un deuxième temps, des CL chiraux double fréquence (DF-CLC) ont été utilisé pour produire des structures stabilisées en surface, qui, en addition d'une diffusion contrôlable, ont montré des phénomènes de réflexion résonante. Des couches de MR orientées et partiellement polymérisées furent utilisées comme couche d'alignement pour les DF-CLC. Le rôle du temps de pré-polymérisation des MR sur les propriétés des cellules ont été étudiées par des analyses électro-optiques et spectroscopiques. Nos études morphologiques

ont démontré que l'interdiffusion des molécules entre la couche de MR et le volume des CL durant le procédé de programmation génère des agrégats polymères sur les surfaces internes de la cellule, qui sont à l'origine de la diffusion contrôlable de la lumière.

Abstract

The alignment control of liquid crystal (LC) molecules is of great importance for the most of LC based electro-optical applications such as displays, modulators, and variable attenuators. This control realises, particularly, by the interactions between LC molecules and the adjacent surface. This makes the surface alignment one of the key factors for the improvement of LC-based devices' performance. This PhD thesis reports an experimental study of alignment control of LC molecules by surfaces, and explores the possibility of practical avenues.

First, dual frequency nematic LCs (DF-NLC) and thin reactive mesogen (RM) films, cast on internal surfaces of cell substrate, were used to build surface polymer stabilized structures. To form these surface-stabilized structures, a partial interpenetration between the LC and RM molecules was allowed while applying an orienting dielectric torque (positive or negative) to the material system. Then, after a short interpenetration period between the RM layer and the bulk LC, UV exposition was added to definitely cure the material system. These systems demonstrated great potential for the surface alignment control of LCs, enabling the ‘‘programming’’ of LC cells with electrically controllable light scattering, which can be used in privacy windows and smart lighting applications. Electro-optic and microscopic studies were done to characterize these surface-stabilized structures. We showed that the contrasts of light scatter modulation, polarization dependence and response times can be noticeably improved by the dual-frequency control.

Afterward, dual frequency chiral LCs (DF-CLC) were used to build surface-stabilized structures, which in addition to the controllable scattering, showed also resonant reflection phenomenon. Partially cured and oriented RM layers were used as alignment layers for DF-CLC. The role of the pre-curing duration of RM in the behavior of the cell was observed by electro-optical and spectroscopic studies. Our morphological studies showed that the molecular interdiffusion between RM layer and bulk LC during the programming process generates polymer aggregates on the cell's internal surfaces, which are at the origin of formation of controllable light scattering.

Table of Contents

Résumé iii

Abstract v

Table of Contents vii

List of Figures ix

Remerciements xvii

Foreword xix

Chapter 1 Introduction 1

1.1 Objectives 4

1.2 Thesis structure 6

Chapter 2 Introduction to Liquid Crystals 7

2.1 Liquid crystals 7

2.2 Nematic and cholesteric phases 12

2.3 Properties of liquid crystals 14

2.3.1 Optical anisotropy 14

2.3.2 Dielectric anisotropy 16

2.3.3 Elasticity 19

2.4 Alignment by surfaces 20

2.5 Field induced reorientation: Electro-optical effect 24

2.6 Light scattering in liquid crystals 28

Chapter 3 Thin Orienting Surface Layers with Azobenzen Dyes 31

3.1 Introduction 35

3.2 Material systems and samples 37

3.3 Photo sensitivity study in two anisotropy matrices 38

3.4 Photo sensitivity study in a polymer matrix 44

3.5 Summary and conclusions 47

Chapter 4 Surface Polymer Stabilized Dual Frequency Nematic Liquid Crystals 49

4.1 Introduction 55
4.2 Materials and Methods 56
4.3 Experimental Setup and Process 58
4.4 Stationary Mode Characterization 60
4.5 Dynamic Characterization 65
4.6 Discussion 67
4.7 Conclusion 71
Chapter 5 Surface Polymer Stabilized Dual Frequency Chiral Liquid Crystals 73
5.1 Introduction 77
5.2 Materials and methods 84
5.3 Experimental setup and process 86
5.4 Haze measurements 94
5.5 Discussion 95
5.6 Conclusions 103
Chapter 6 Conclusion 105
Bibliography 109

List of Figures

Figure 2.1 Schematic presentation of the solid, liquid crystal, and liquid phases. *7*

Figure 2.2 Molecules in the liquid crystal phase. The director shows the direction of preferred direction. Axis of each molecule makes an angle with the director. (After Ref. [35]) *8*

Figure 2.3 Molecular structure of a typical liquid crystal. (After Ref. [36]) *9*

Figure 2.4 Gay-Berne potential U(r) as function of intermolecular distance r between elongated molecules. Black elipsoids mimic the pairs of interacting molecules in different geometry of interaction. Both scales are arbitrary. (After Ref. [42]) *11*

Figure 2.5 Schematical representation of nematic a) and cholesteric b) phases *12*

Figure 2.6 Example of chiral molecule: Bromochlorofluoromethane enantiomers (After ref. [48]) *13*

Figure 2.7 The refractive index ellipsoid of a uniaxial liquid crystal with the optic axis parallel to the z axis. The refractive index n_o of the ordinary ray is independent of propagation. The refractive index n_e of the extraordinary ray is larger than no for a liquid crystalline material of positive birefringence (After Ref. [5]). *15*

Figure 2.8 Orientation of a LC molecule by an electric field. In (a) the molecule has positive dielectric anisotropy, while in (b) it has a negative dielectric anisotropy. (After Ref. [35]) *16*

Figure 2.9 Frequency dependence of dielectric constants for the dual frequency LC: MLC2048. (After Ref. [53]) *19*

Figure 2.10 The three basic types of deformation in liquid crystals: a) splay deformation b) twist deformation and c) bend deformation *20*

Figure 2.11 Alignment by surfaces: a) planar alignment b) homeotropic alignment and c) tilted alignment *21*

Figure 2.12 Schematic representation of rubbing process (After Ref. [61]) *23*

Figure 2.13 A nematic liquid crystal cell with a liquid crystal molecule oriented an angle θ measured from the xy-plane. An electric field E is applied along the z-axis. The molecule experience a torque that tend to reorient the molecule in a direction of applied field. (After Ref. [44]) *25*

Figure 2.14 A planar nematic liquid crystal cell with strong surface anchoring: a) external field off, b) external field on 26
Figure 2.15 The structures of cholesteric textures. (After Ref. [68]) 27
Figure 2.16 Scattering of light depending on particle size: from smaller to larger particles 29
Figure 2.17 LC Privacy Glass from Innovative Glass Corporation. (From http://www.innovativeglasscorp.com/lc-privacy) 30

Figure 3.1 Schematic representation of the mesogenic azobenzene dye (Beam 5721) molecular structure used in our study. It is a mixture of 4 components: 4-n-butyl-4'-ethoxyazobezene, 4-n-butyl-4'-pentyloxyazobezene 4-n-butyl-4'-heptyloxyazobezene and 4-n-butyl-4'-decyloxyazobezene. 32
Figure 3.2 Azobenzene molecule can convert betwwen trans and cis isomers upon absorption of light. (After Ref. [71]) 32
Figure 3.3 Statistical photo-orientation of azo molecules. The molecules aligned along the polarization direction of the incident light absorb, isomerize, and re-orient. The final state of molecules is perpendicular to the light polarization. Those molecules cannot absorb and remain fixed. (After Ref. [71]) 33
Figure 3.4 Polarization selective absorption spectra of the thin layer of RM doped by MAD. "par" and "perp" are cases when the polarization of the probe beam was, respectively, parallel and perpendicular to the director of the RM. The excitation of the material was done by an LED operating at 375 nm and polarized along the direction of the RM's director. 39
Figure 3.5 Absorption spectra of the MAD doped bulk NLC for probe polarizations, parallel (« par ») and perpendicular (« perp ») to the director. Ground state, excited state by LED, natural (a) relaxation (excitation by Argon ion laser) and forced (b) relaxation cases are presented for both polarizations. Intensity of LED excitation was 2,6mW/cm^2. Power of the argon ion laser was 60 μW (I=0,71mW/cm^2). 41
Figure 3.6 The natural and forced relaxation of MAD doped NLC absorption observed at 450 nm (mainly cis absorption) without and with an argon ion laser of 0,71 mW/cm^2 power. 43

Figure 3.7 Ground state and excited, by a linearly polarized (vertical) UV LED of 2.6 mW/cm2 power (operating at 375 nm) absorption spectra observed with a probe beam polarized parallel and perpendicular to the polarization of the LED. *44*
Figure 3.8 Dynamics of the photo induced birefringence of the MAD doped PMMA film induced by using an excitation at λ=488nm and detected at λ=632 nm. The excitation beam is switched on at t ≈ 5 sec and switched off at t ≈ 55 sec. *45*
Figure 3.9 Demonstration of the PID in the MAD doped PMMA for excitation intensity of 2,4W/cm^2 at 514 nm. *47*

Figure 4.1 Photopolymerization of reactive mesogens: at left we have monomers (free molecules), and at right we have polymer with interconnected monomers. (After Ref. [100]) *49*
Figure 4.2 Method for the spatial control of the pretilt angle: (a) Planar cell filled with LC-RM mixture; (b) LC-RMs mixture separation in the external electric field (pre-cure voltage); (c) formation of the polymer layer in the vicinity of the LC cell substrates by local UV lightinduced polymerization (UV curing); (d) cell with spatially varied pretilt after curing. (After Ref. [101]) *50*
Figure 4.3 Schematic illustration of the fabrication of PSLCs. a) Photoreactive monomers dissolved in a LC before polymerization. b) Polymer network stabilizing the LC orientation after polymerization by UV irradiation (After Ref. [102]) *51*
Figure 4.4 Schematic presentation of major steps of the fabrication of S-PS-DF-NLC cell (see text for details). *58*
Figure 4.5 Schematics of the general experimental setup used for the "programming" and for the electro-optic study of the haze and angular dependence of light scattering of S-PS-DF-NLC cells. The half-wave plate λ/2 and the diaphragm were used later for electro-optic tests only (see hereafter). *59*
Figure 4.6 Qualitative demonstration of (a) cell's scattering in its ground state (left picture, U _ 0 V), when subjected to U = 110 V at 1 kHz (central picture) and when subjected to U = 80 V at 80 kHz (right picture). (b) The comparative histograms for three key cases (vertical arrows show the scanned zones). The cell was programmed with 110 V at 1 kHz. *61*

Figure 4.7 Normalized (ground state; U = 0 V) angular distribution of scattered light power for the S-PS-DF-NLC cells programmed in the presence of an electric field of 110 V at 1 kHz (dashed curve) and at 70 kHz (solid curve). *62*
Figure 4.8 Stationary dependence of ballistic light transmission upon the voltage applied to the S-PS-DF-NLC cell with frequency (a) 1 kHz and (b) 70 kHz. The cell was programmed with U = 110 V at 70 kHz...... *63*
Figure 4.9 Angular dependence of the probe beam's transmission of the S-PS-DF-NLC cell that was programmed with U = 110 V at 70 kHz. Squares, circles, and triangles represent, respectively, ground state (U = 0 V) as well as excited homeotropic (110 V at 1 kHz) and excited planar (60 V at 70 kHz) states. *64*
Figure 4.10 Transmission versus time for different transitions for two perpendicular polarizations (solid line, vertical; dashed line, horizontal). Excitation switching is performed (at t ≈ 5.6 s) from 110 V at 1 kHz to 0 Vand then (at t ≈ 12.4 s) from zero to 110 V at 1 kHz. The S-PS-DF-NLC cell was programmed with 110 V at 70 kHz. *65*
Figure 4.11 Transmission versus time during the natural relaxation process for two perpendicular polarizations (solid line, vertical; dashed line, horizontal). The S-PS-DF-NLC cell was programmed with 110 V at 70 kHz. *66*
Figure 4.12 Transmission versus time for an S-PS-DF-NLC cell that was programmed at 70 kHz. Switching is performed at t ≈ 4.4 s from 1 kHz (110 V) to 80 kHz (80 V) and back to 1 kHz (110 V) at t ≈ 11.2 s. Curves for two polarizations (solid line, vertical; dashed line, horizontal) are practically coinciding...... *68*
Figure 4.13 Ground-state microphotography (by using Zeiss polarization microscope) of the S-PS-DF-NLC cell that was programmed at 70 kHz. *69*
Figure 4.14 Schematic demonstration of the possible mechanism of slowing of the S-PS-DF-NLC's reaction due to the difference between (a) free relaxation and (b) forced back reorientation. The polymer aggregate (solid curve 1) is bent (dashed curve 2) toward the surface AB by the negative torque...... *70*

Figure 5.1 Schematic presentation of a PDLC cell and its operation principle. Dotted horizontal lines (at distance d0) show transparent electrodes (e.g., ITO). Two circles (of diameter dd) show the LC droplets (filled vertical ellipses showing the LC molecules; when

voltage V0 is applied to the ITOs) dispersed within the polymer matrix. A and B represent incident rays at normal and tilted angles, while A' and B' show the transmitted and scattered rays, respectively.....78
Figure 5.2 Schematic presentation of a PSLC cell and its operation principle. Dotted horizontal lines (at a distance d0) show transparent electrodes. Short horizontal lines (a) show the monomer molecules (not necessarily aligned along the LC molecules, shown by horizontal filled ellipses). Large curved lines (b) show the polymer walls and bundles. The application of voltage V0 initiates nonuniform LC reorientation (c) and corresponding light scatter.....80
Figure 5.3 Schematic presentation of fabrication of a nonuniform PSLC cell. The original mixture is exposed from one side of the cell (a) and the diffusion of monomers creates higher polymer network density from that side of the cell (b). 81
Figure 5.4 Schematic presentation of the fabrication of a S-PSLC. The partially cured RM layer is cast and aligned on the internal surface of the cell (a). Partial interpenetration between the RM and LC molecules is allowed before the photo polymerization of the RM (b).....82
Figure 5.5 Schematic presentation of the fabrication of an oriented (programmed) S-PSLC cell. The partially cured RM layers are cast and aligned on the internal surface of the cell (a). Partial interpenetration between the RM and LC molecules is allowed under an applied electric field (b) before the photo polymerization of RM layers (c). 83
Figure 5.6 Transmission spectra of the S-PS-CLC cell that was programmed with U=60V voltage at 1kHz. A single frequency CLC was used as LC. The RM wasn't cured before applying the programming voltage (Δtpp = 0 min.). Curves 1 – before programming and 2 – after programming (in ground state, U=0V); 3 – after programming (excited by U=75V at 1kHz).....87
Figure 5.7 Transmission spectra of the S-PS-DF-CLC cell programmed with U=40V at 1kHz. The RM was not cured before applying the programming voltage (Δtpp = 0 min). Curves 1 - 0V; 2 – 120V at 1kHz; 3 – 120V at 90kHz. 88
Figure 5.8 Transmission spectra of the S-PS-DF-CLC cell (programmed with U=40V voltage at 1kHz with the RM cured for Δtpp = 30 minutes). Curves 1 - 0V; 2 – 90V at 1kHz; 3 – 90V at 90kHz.....89

Figure 5.9 Schematic representation of the experimental setup used for the measurement of the reflection spectra. WLS - Supercontinuum White Light Laser, S-sample, F - neutral density filter, BS – beam splitter cube, IS - integrating sphere..... 90
Figure 5.10 Reflection spectra of the S-PS-DF-CLC cell (programmed at U=40V at 1kHz with RM cured for Δtpp = 30 minutes) during the natural relaxation from homeotropic (U=80V at 1kHz) to ground state (U=0V). Curves 1 – 0 sec; 2 –60 sec; 3 – 180 sec; 4 – 1260 sec..... 91
Figure 5.11 Reflection spectra of the S-PS-DF-CLC cell (programmed at U=40V at 1kHz with RM cured for Δtpp = 30 minutes) during forced relaxation (from 80V at 1kHz to 80V at 80kHz). Curves 1 – 0 sec; 2 –0.2 sec; 3 – 0.8 sec; 4 – 20 sec. 91
Figure 5.12 Transmission spectra of the S-PS-DF-CLC cell (programmed at U=40V at 1 kHz, with the RM precured for Δtpp = 1.5 minutes) in stationary states. 1 - 0V; 2 – 160V at 1kHz; 3 – 160V at 90kHz. The vertical dashed arrow shows the wavelength (632.8nm) used for haze measurements. 92
Figure 5.13 Transmission spectra of the S-PS-DF-CLC cell (programmed at U=40V at 1kHz, with the RM pre-cured for Δt_{pp} = 1.5 minutes) during the natural relaxation after the switch off of the voltage from the state with 160V at 1kHz. Curves 1 – 160V at 1kHz; 2 – relax 30 sec; 3 – relax 120 sec; 4 – relax 1800 sec; 5 – 0V. 92
Figure 5.14 Transmission spectra of the S-PS-DF-CLC cell (programmed at U=40V at 1 kHz, with the RM pre-cured for Δtpp = 1.5 minutes) during the forced relaxation after the switching the voltage from the state 160V at 1kHz to 160V at 90kHz. 1 – 160V at 1kHz; 2 – relax 0.5 sec; 3 – relax 0.7 sec; 4 – relax 2.1 sec; 5 – 160V at 90kHz. 93
Figure 5.15 Schematics of the experimental setup used for the electro-optical haze measurements of S-PS-DF-CLC cells. 94
Figure 5.16 The angular dependence of the probe beam's transmission (haze) of the S-PS-DF-CLC cell (programmed with U=40V at 1kHz with RM procured for Δtpp = 1.5 minutes). Squares, circles and triangles represent respectively ground state (U=0V), excited homeotropic (160V at 1kHz) and excited "helicoidal" (160V at 90kHz) states. Inverted triangles (top curve) correspond to the reference glass plate. 95

Figure 5.17 Micro photography of the S-PS-DF-CLC cell (in transmission) with RM cured for Δtpp = 1.5 minutes, recorded by using polarizing microscope (crossed polarizers). The corresponding driving conditions are shown on the right top corners of images. *98*

Figure 5.18 Digital zoom on the Figure 5.17 images (recorded in transmission by the polarizing microscope) to demonstrate the defect structures a-in the homeotropic and b-in the planar excited states. The outlined zones are linear defects (1 and 2), polymer rich region (3 and 4) and planar cholesteric structures with different numbers of half periods (5 and 6). *99*

Figure 5.19 Transmission spectra of the S-PS-DF-CLC cell (programmed at U=40V at 1 kHz, with the RM precured for Δt_{pp} *= 1.5 minutes) for various stationary voltages applied at 1kHz.* *100*

Figure 5.20 AFM scan of the substrate with RM pre-cured for Δtpp = 1.5 minutes. (a) – Surface morphology in 3D and (b) – surface presented in 2D (left) and amplitude profiles (right) in two perpendicular directions (top and bottom). *102*

Remerciements

Ces travaux de recherche ont été réalisés dans le laboratoire du COPL à l'université Laval sous la direction de professeur Tigran Galstian. Mes premiers remerciements lui sont adressés, pour m'avoir permis de faire ma thèse dans son groupe de recherche, pour son accueil et son aide tout au long de mes travaux de recherches.

Je tiens aussi à remercier l'ensemble du personnel du laboratoire pour toute leur aide au quotidien, notamment Patrick Larochelle, Hugues Auger et Souleymane Toubou Bah, ainsi que le Dr. Amir Tork de la compagnie TLCL pour son aide en chimie.

Je voudrais remercier également mes collègues Karen Allahverdyan et Jean-Philippe Bédard Arcand pour m'avoir accompagné dans mon travail au laboratoire en m'initiant aux expériences et aux montages de caractérisation dans le laboratoire, ainsi que pour les nombreuses discussions enrichissante sur mon sujet.

Je voudrais remercier ensuite mon superviseur lors de mon master à Erevan, le professeur Rafik Hakobyan pour l'aide qui m'a apporté durant mes études.

Mon attraie pour la science et en particulier la physique n'aurait pas été le même sans Arthur Davtyan qui a été mon enseignant en secondaire. Je tiens donc à la remercier à travers ce manuscrit.

Je remercie tous mes amis et proches qui m'ont permis indirectement de pouvoir réaliser ce travail, plus particulièrement Kristine, Karen et Margarit. Mais aussi, Yannick, Elina, Ani et Vahe, et tous ceux que j'oublie mais sans qui ces années de thèse à Québec n'aurait pas été les mêmes.

Je remercie également Matthieu Chazot, pour son aide et son support pendant l'écriture et la réalisation de ma thèse. Il a su trouver les mots pour m'aider à persévérer dans toutes les circonstances.

Enfin, je dédie ce mémoire à mes parents, ma sœur et mon frère, pour leur soutien et leur affection tout au long de mon travail.

Foreword

This thesis includes three peer-reviewed manuscripts published in scientific journals during my PHD project. I am the principle author of all of them. You shall find the information about each author and their contribution to the published works below.

- A. Minasyan, A. Tork, and T. Galstian, "Study of photo isomerization and photoinduced anisotropy of a mesogenic azobenzen dye mixture in various solid and liquid matrices," *Proc. SPIE 9288, Photonics North 2014, 92880N*, 2014.

Center for Optics, Photonics and Laser, Department of Physics, Engineering Physics and Optics, Laval University, Pav. d'Optique-Photonique, 2375 Rue de la Terrasse, Québec, Canada G1V 0A6

Conributions: For this pubication, I realized the entire experimental part, participated in conference Photonics North 2014 as a poster presenter and writed the first version of manuscript after having a discution with Professor Tigran Galstian about the content. Amir Tork was participated in subject discutions. The manuscript then was revised and completed by Tigran Galstain.

- A. Minasyan and T. Galstian, "Surface-polymer stabilized liquid crystals with dual-frequency control," Appl Opt. , vol. 52, no. 22, pp. E60–E67, 2013.

- A. Minasyan and T. Galstian, "Surface polymer-stabilized dual frequency chiral liquid crystals," Liquid Crystals Reviews, vol. 2, no. 1, pp. 60-71, 2014.

Center for Optics, Photonics and Laser, Department of Physics, Engineering Physics and Optics, Laval University, Pav. d'Optique-Photonique, 2375 Rue de la Terrasse, Québec, Canada G1V 0A6

Conributions: For these pubications, I realized the entire experimental part and writed the first version of manuscripts after having a discution with Professor Tigran Galstian about the content. The manuscripts then were revised and completed by Tigran Galstain.

Chapter 1

Introduction

Liquid crystals (LCs) were discovered over a century ago [1]. They were considered as a ‘‘new’’ state of matter that exhibits intermediate phases where they flow like liquids, yet possess some physical properties of crystals. Since this discovery many LCs were synthesized and studied [2] [3] [4]. They attracted the interest of scientists of various fields and engineers due to their exceptional anisotropic (optical and dielectric) properties and the easy control of their orientation by external fields. Due to the high degree of long scale orientational correlation and the anisotropic shape of the molecules of LC, they exhibit a high degree of macroscopic anisotropy. Dielectric anisotropy of LCs [5] [1] combined with the fact that it is orientationally flexible leads to a reorientation of the molecules of LC under the influence of a low voltage electric field (1V). This renders the LCs of such importance to electro-optic devices. They have found wide commercial applications over the latest decades in electro-optical liquid crystal display (LCD) devices such as watches, calculators, mobile telephones, computer monitors, notebooks. They are also used in many non-display applications such as spatial light modulators, fast light shutters, thermometers, tunable filters, tunable lenses, etc.

The operation of above mentioned LC based electro-optic devices is based on the electrically variable orientation of their director (average orientation of the long molecular axis). The alignment control of LC molecules is of great importance in almost all LC device applications. This control is made by applying an external field (magnetic, electric), as well as by the surface interactions between LC molecules and the internal surface of substrate. Since the LC flows, in order to be studied in laboratory or used practically in devices, the thin layer of LC (typically of few micrometres) is usually enclosed between two glass substrates in so called sandwich-like cell geometry. The interactions between LC molecules and adjacent surface influence the LC alignment, and determine the ordering of molecules in the bulk of LC cell in the absence of the external fields (ground-state

alignment). These interactions are complex and highly dependent on the LC and the substrate in question. The ground-state alignment of LC molecules is very important in LC-based devices (in majority of LC applications) where ground-state alignment is used as a default state that is retrieved once the excitation is switched off. The speed of that (relaxation) transition also is defined by those surface interactions. Thus the study and control of surface/LC interactions is of vital importance for the performance of LC based electro-optical devices.

Various methods were developed to obtain a predetermined ground-state alignment of the LC. This was mainly obtained via the surface-mediated interactions between the "pure" LC layer and the solid "discrete" interfaces. The most widely used method is the mechanical rubbing of polymer layers with a cloth. That creates reorientation of molecular chains and nanometric grooves on the surface of the polymer and thus induces a preferred alignment direction for the LC. This process, however, has several drawbacks (generating static charge, attracting dust, etc.) which come from the contact type of the method. Alternative methods, such as vacuum deposition and photo alignment, exist today, but they are complex, expensive or/and not available commercially [6] [7]. In addition, those surfaces (except the photo aligned ones) are efficient for the uniform alignment of LCs. Their market acceptance remains rather limited both for in-plane patterning [7] and for out-of-plane pretilt control [8] [9]. These limitations motivate the search for alternative methods of alignment of LCs enabling more functionalities and better performance of LC-based devices.

The major drawbacks of LC-based devices are their slow response times and the request to use polarizers for their operation. This increases the cost, decreases the light efficiency and reliability of those devices. These characteristics were significantly improved by a new family of materials, anisotropic composites, consisting of LCs and polymers, developed for light scattering electro-optical applications [10] [11] [12] [13] [14] [15]. Polymer Dispersed LC (PDLC) and Polymer Stabilized LC (PSLC) have shown useful electro-optical performance.

PDLCs are composite materials where a small amount of LC ($\approx 30\%$) is incorporated in a polymer matrix, forming LC droplets with a micrometers sized diameter [16] [17] [18] [19]. The operation principle of this device is very simple: in its ground state (field – off state), the director's orientation of the LC is not the same in different droplets, the effective refractive index of those LC droplets is different from the refractive index of the polymer matrix, and the device strongly scatters light. Upon application of an electric field LC molecules are reoriented in each droplet in such way that the LC molecules are now aligned parallel to the electric field. If the ordinary refractive index of LC is matched with that of the polymer, the device appears transparent in the field – on state.

In bulk PSLC a small amount of the polymer ($\approx 5\%$) is dispersed in a LC anisotropic matrix [20] [21]. The aim is to ''stabilize'' the LC alignment by elastic interactions between the polymer network and LC. The texture of the LC is not significantly influenced by the formation of the polymer network, so in the field – off state the device is transparent. Application of the electric field causes light scattering due to the appearance of orientation defects because of the polymer network keeping LC molecules in their initial orientation near the polymer walls while the bulk LC molecules reorient under the field application. This electrically controllable light scattering has an attractive potential for the electro-optical applications such as light shutters, privacy and smart windows, projective displays, variable illumination LED systems and paper-like reflective displays.

Despite the fact that such material systems have certain advantages versus ''pure'' LC layers, they have significant drawbacks, which are of rather fundamental character. One of them is the haze: the presence of scattering in the ''transparent'' state for the tilted incident light. The second drawback of those material systems is the high driving voltages required when compared to ''pure'' LC layers.

It was recently shown that very limited degree of interpenetration between the LC molecules and the surface polyimide alignment layer may be obtained in the presence of external fields [22]. The use of the "soft" polymer interfaces (instead of using polyimide) can provide a more efficient interpenetration and more flexibility for the configuration of the ground-state LC alignment, which then may affect the performance of the LC cell in the

excited state. In the scope of this thesis we are exploring the possibility of using thin reactive mesogen (RM) layers, cast on the internal surfaces of the LC cell substrates as "soft" polymer interfaces, with the aim to control both the in-plane organization of LC molecules and their out-of-plane alignment, and also add several functionalities such as shorter response times and polarization independence.

1.1 Objectives

LC alignment is the key technology needed to improve the performance of LC-based electro-optic devices. The uniform and well-defined alignment is requested in most LCDs. To achieve this alignment certain substrate surface treatment is needed. The mechanical rubbing of polymer surfaces is the most used method to obtain a single domain uniform alignment of LC's in the LCD industry [6]. Despite the several advantages of this method (relative simplicity, technological robustness), there are serious drawbacks coming from the contact type of this method, which are mechanical damage, generation of fine dust particles and accumulation of static charges. In addition, this method cannot be used to produce the multi-domain alignment or to align the LC in closed volumes. Therefore the study of the alternative methods, which could replace the rubbing technology, attracts the interest of the many scientists of LC research field and ours also.

The main objective of this thesis is the investigation of new strategies of production of surface alignment layers for LC's in-plane and out-of-plane alignment control and improvement of LC based electro-optical devices' performance. We concentrated our works in two more specific objectives.

The first one is to obtain a controllable pretilt angle for a uniform alignment control of LCs. The motivation comes from the demand for intermediate pre-tilt angle, which can improve the LCD's performance and characteristics (faster response times, lower voltages). This demand has been increased after than new LCD mode, no-bias-bend (NBB) pi cell, operating in the no-bias optically compensated bend (OCB) mode, was reported as a candidate to fasten the response times [23]. Nowadays, most LCDs use planar alignment

layer with low degree of pretilt angle of 0° - 10° by using rubbing technique or vertical alignment layer with pretilt angle of 85° - 90° by using UV exposure technique. There are several approaches to obtain intermediate pretilt angles such as oblique deposition of SiOx [24], amorphous fluorinated carbon thin film via an ion-beam [25], mixture of planar and vertical polyimides [26], stacked alignment layers [27]. However, these approaches have problems of stability and reproducibility. Moreover, they are not suitable for mass production due to complexity of process.

We think that a non-contact method such as photo alignment is the most promising for a liquid crystal alignment [7]. Among the photo alignment materials the azobenzens are interesting because they can be reoriented with a light beam in visible or UV and it is possible to dope them in the different polymer matrixes for fixing their orientation [28]. Therefore, we attempted to use a layer of reactive mesogen (RM) doped with mesogenic azo dye to create an out-of plane alignment (pretilt angle) of LC molecules via the appropriate reorientation of azobenzene molecules in a host RM thin "command layer" by irradiating the layer with a polarized light.

The second specific objective is to create ('program') the controllable surface polymer stabilized structures for the non-uniform alignment control of LCs. Recently, the surface polymer stabilized LCs (S-PSLCs) systems using RM thin layers cast on an internal surface of LC cell substrates were reported [29] [30] [31]. They showed great potential for the control of the ground state LC alignment, enabling the fabrication of cells with electrically controllable light scattering, which can be used in various ''smart lighting'' applications such as privacy/smart windows and variable (Flash, LED) illumination systems. Among the important advantages of S-PSLCs systems (comparing for example with bulk PDLCs) is the fact that the alignment defects are formed mainly at the LC interface. Thus the viewing angle can be significantly improved and also the operation voltages can be significantly reduced (compared to PDLC and PSLC systems).

While the response times of S-PSLCs are noticeably faster compared to pure NLCs [29] [30] [31], we were looking for to further improve their performance by using dual frequency LCs (DF-LCs) in the S-PSLC geometry. DF-LCs are interesting for improving the switching speeds [32] because an external field of low frequency can align the director

along the field, while an external field of higher frequency aligns the director perpendicular to the field. So, changing frequency of the field one can switch the director very fast because the director always suffers a torque from a field. Thus, DF-LCs may enable not only obtaining of the different 'programming' regimes (with low or high frequencies), but also having more possibilities of control during the post-programming operations. The more specific goals of this part of work are to improve the modulation contrast, response times and obtain a polarization independent performance of S-PSLS cells.

1.2 Thesis structure

This thesis focuses on study of the interactions of liquid crystals with the interfaces, from both scientific and practical points of view. At first, a general introduction to the liquid crystals, concerning their properties and alignment techniques is done in Chapter 2. Three following chapters are based on the published articles and represent two different approaches employed for the LC surface alignment control. Each of these chapters includes complementary literature review own to the method employed. In Chapter 3 we present the experiments and results of the first approach based on the use of the light for the LC alignment control. In Chapter 4 we present the second approach of LC alignment control by using ''soft'' RM/LC interface ''programmed'' and controlled by the electric field, using a dual-frequency nematic liquid crystals. Further, the same approach employed to dual frequency chiral liquid crystals is presented in Chapter 5. A general conclusion to the entire study is finally done in Chapter 6.

Chapter 2

Introduction to Liquid Crystals

2.1 Liquid crystals

We know from basic physics that many substances can exist in different state of matter or so-called phases. We classify them to solids, liquids and gases. But this classification in not complete: many organic substances do not possess a single change of state (or phase transition) between the crystal and the liquid (Figure 2.1). It's Reinitzer [33] that in 1888 discovered a phase of matter between solid and liquid states, while observing the melting behavior of organic substance related to cholesterol. He noticed that at 145.5C the substance becomes cloudy liquid and at 178.5C it turns to a clear liquid. This substance was then characterized by Lehmann [34] , who had developed a series of optical polarization microscopes. Lehmann recognized that he was looking at a different state of matter than that of classical solids, liquids, and gases. He named the new phase of a matter existing between solid and liquid states ‘‘liquid crystal’’, basing on physical properties that this phase possess. This state are also known as mesomorphic (from greek: intermediate form) or mesophase.

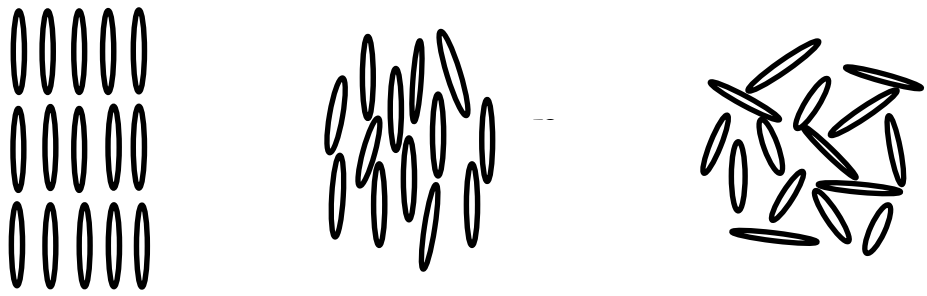

Figure 2.1 Schematic presentation of the solid, liquid crystal, and liquid phases.

As we know the solid phase possesses the positional order, (the molecules occupy certain positions) and also it possesses orientational order. When solid melts to a liquid, both types of order are lost. When solid melts to a liquid crystal, the positional order can be lost, but some of orientational order remains [35]. The molecules in liquid crystals are free to move like in liquids, but at the same time they tend to remain pointing along the certain direction called director (Figure 2.2). The orientational order in liquid crystals is described quantitatively by an average function called the order parameter

$$S = < \frac{3}{2} cos^2\theta - \frac{1}{2} > , \qquad (2.1)$$

where θ is the angle between the director and the axe of the molecule (Figure 2.2). The order parameter decreases when temperature in liquid crystals increases, and above the liquid phase transition temperature T_c becomes 0. Typical values for the order parameter in liquid crystals are between 0.3 and 0.9.

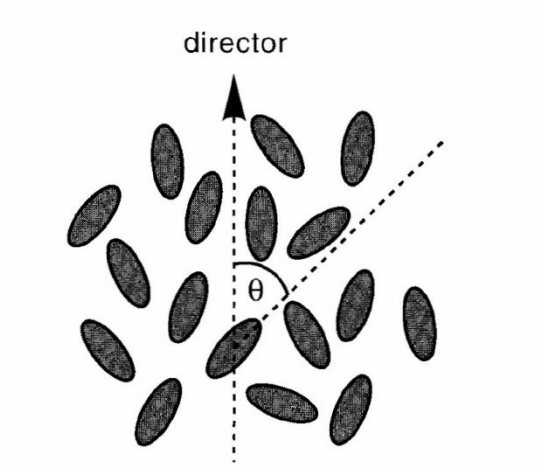

Figure 2.2 Molecules in the liquid crystal phase. The director shows the direction of preferred direction. Axis of each molecule makes an angle with the director. (After Ref. [35])

The physical and optical properties of liquid crystals are depending on their constituent molecules [3] . The Figure 2.3 shows the chemical structure of the most common occurring liquid crystals [36].

In general, to form the liquid crystal phase the molecules must be first of all elongated, and must have a rigid core which will often contain an aromatic element. Also there will be a polarizable group, e.g. CL, CN, CN_2, and in addition to a long flexible chain attached to the core. The flexible chain will usually be an alkyl(C_nH_{2n+1}) or alkoxy($C_nH_{2n+1}O$) group [37]. The molecules such as those shown in Figure 2.3 comprise the two or more aromatic rings connected by a linkage group X, and at the end connected to the side-chain R and terminal group R'.

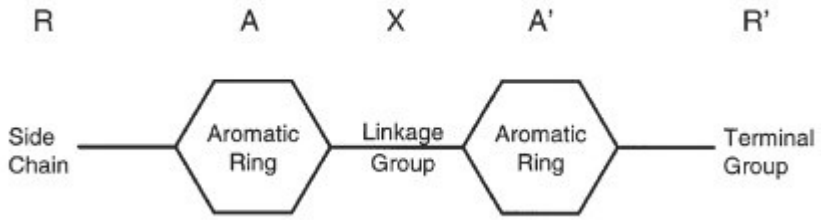

Figure 2.3 Molecular structure of a typical liquid crystal. (After Ref. [36])

There are variety of theoretical models [1] which try to describe the formation of the liquid crystalline phase. The general points of these theories about main factors influencing in the formation of the liquid crystalline phase are

- the molecules should contain the rigid core plus the flexible element which allows some degree of disorder to avoid the formation of the crystalline phase
- the length of the molecule respect to the width of latter should be of order of 6:1 and
- the molecule should contain an element capable of the long-range dipolar interactions.

One of the most successful theories was introduced by Maier and Saupe [38]. The so called Maier-Saupe theory (also called mean field theory) assumes that the most important force to form the liquid crystalline phase is the dispersion force between molecules. The dispersion forces (also known as London forces) are a type of the Van der Waals attractive forces that occurs between two induced electric dipoles [39]. The origin of these forces is in random fluctuations in the electronic structure of the molecules. These fluctuations lead to inducing the temporary dipoles in molecules interacting with each other. The molecules stay close to each other and continue to fluctuate in synchrony in order to maintain their dipoles and stay interacted with each other. To calculate the force field, it is usually considered an average of six nearest neighbours, so the mean field approximation of the potential field is assumed. Since a molecule in nematic phase has a higher rotational freedom about its long axis than in a crystal, it is reasonable to assume that this approximation is appropriate in this situation. Also the liquid crystalline materials contain significant dipole or anisotropic electronic polarizability, which lead to long-range interactions and high ordered molecular organisation along the preferred direction. The molecule of liquid crystal will so experience the force to point along that preferred direction, and so that force will be proportional to the order parameter S [37]. The interaction energy of the liquid crystal molecule with its surroundings is then shown to be

$$W_{int} = -\frac{A}{V^2} S \left(\frac{3}{2} cos^2\theta - 1\right), \qquad (2.2)$$

where V is the molar volume, S is the order parameter, and A is a constant determined by the transition moments of molecules.

The nature of intermolecular interactions in liquid crystals can be quite different including Coulomb interactions, *dipole- dipole* (Keesom interaction), *dipole- induced dipole* (Debye interaction), i*nduced dipole- induced dipole* (dispersion or London interaction), steric interactions, and hydrogen bonds. One consequence of the shape anisotropy of liquid crystal molecules is that the dispersion forces became dependent on their mutual

orientation. These anisotropic attractive forces are the important factor in driving molecules into a favorable mutual orientations and ordering in liquid. Moreover, for anisotropic shape molecules, the repulsive steric forces are also orientation-dependent, and this is usually a determinant factor of mutual alignment of molecules. For spherical molecules, the Lennard-Jones (or 6–12) potential is often used [39] [40] to describe the intermolecular interactions of the molecules. For elongated molecules consisting of several atoms, the Gay–Berne potential [41], taking into account a mutual orientation of elongated molecules is considered. This is basically an appropriately scaled Lennard–Jones potential that allows two particles to approach each other closer parallel to the short axis compared with approaches along the long axis. From Figure 2.4 one may see how the equilibrium distance and the depth of the energy minimum differ for differently oriented molecules [42].

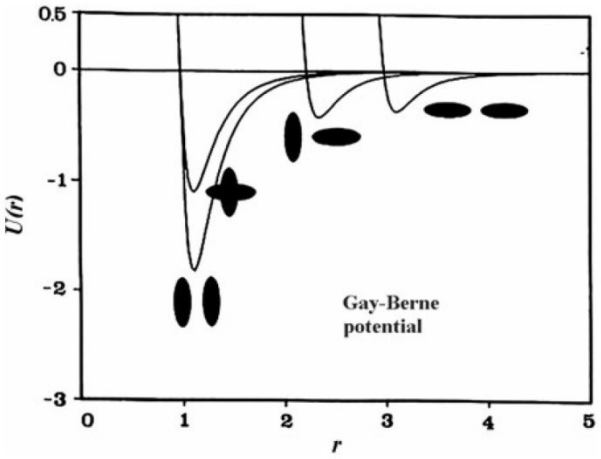

Figure 2.4 Gay-Berne potential *U(r)* as function of intermolecular distance *r* between elongated molecules. Black elipsoids mimic the pairs of interacting molecules in different geometry of interaction. Both scales are arbitrary. (After Ref. [42])

The most widely studied and used in liquid crystals are thermotropic liquid crystals, whose physical and optical properties are function of temperature. Thermotropic liquid crystals are classified in three main classes depending on their molecular structure: nematic, cholesteric and smectic. In this work we have used only two types of these classes: nematic liquid crystals (NLC) and cholesteric liquid crystals (CLC), so we will present them in more details.

2.2 Nematic and cholesteric phases

Nematic liquid crystals (NLCs) are among the most explored and studied anisotropic fluid [1] [43] [19] materials. They are used in a diverse applications including different types of displays [44], modulators [45], tunable lenses [46] , filters and beam/image processing devices [47] Operation of these devices is mainly based on the electrically variable orientation of the liquid crystal director.

The nematic liquid crystal phase is the closest to the liquid. The interactions between the molecules tend to arrange, on average, parallel to each other, thereby defining a preferred direction of their axes of symmetry. This preferential alignment axis defines the axis of symmetry of the phase, the nematic axis, indicated by a unit vector $\boldsymbol{n}$ called the director. The schematic representation of the rodlike liquid crystal molecules in nematic phase is shown in (Figure 2.5a). The molecular arrangement is positionally random and similar as in a liquid, which gives to this phase high fluidity. However, there is some order of directional correlation, which is the cause of the anisotropic properties of this phase. The nematic phase molecules are centrosymetrique, their physical properties are the same for the +**n** and –**n** directions. If the molecules carry the permanent electric dipole, they will be organized in such a way that the collective dipole moment of the system is zero.

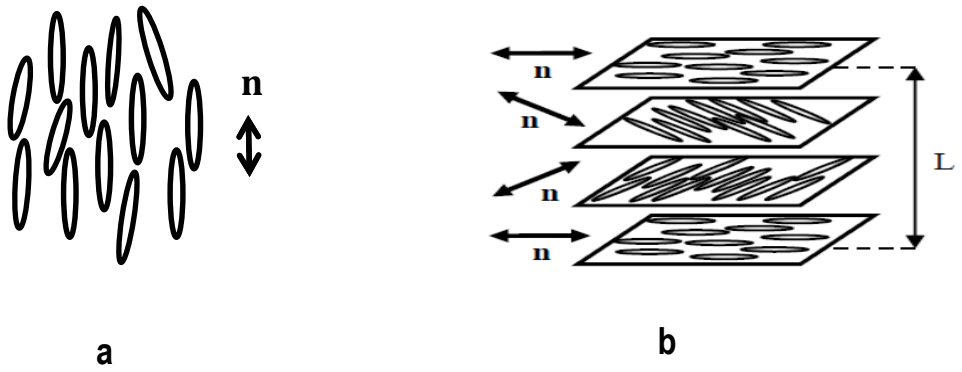

Figure 2.5 Schematical representation of nematic a) and cholesteric b) phases

Many organic compounds are chiral (their mirror image is not superimposable on them) because they contain at least one asymmetric carbon (Figure 2.6, after ref. [48]). If we dissolve a chiral molecule in a nematic liquid crystal, the chiral nematic phase forms. A main result of this phase is in the occurrence of a helical structure. This type of chiral nematic phase is called cholesteric phase. Like a nematic phase, this phase has a long-range orientational order, but no-long range positional order. The difference is that director is not fixed in the space as in the nematic phase. The intermolecular forces between molecules favor alignment between molecules at a slight angle to one another. Locally, the molecules are still oriented in the average along a director **n**, but macroscopically the direction of **n** varies spatially describing a helix about a coil axis perpendicular to **n** (Figure 2.5b). This helical structure is characterized by two parameters: its pitch (**P**) and its direction of rotation. The pitch is the distance that the director makes by rotating one full turn. Because of the equivalence of **-n** and **n**, the spatial period L (Figure 2.5b) is equal to one-half of the pitch.

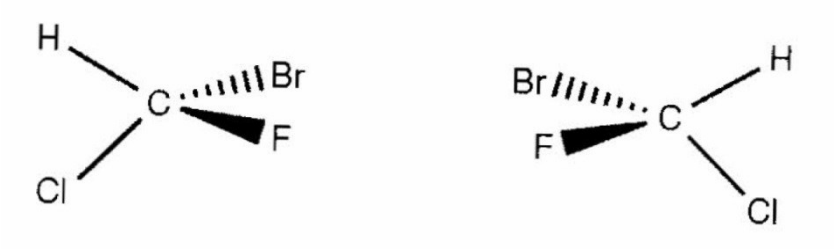

Figure 2.6 Example of chiral molecule: Bromochlorofluoromethane enantiomers (After ref. [48])

The repeated helical structure of the director gives rise to a Bragg reflection for the normally incident light [1]. This phenomenon takes place for the wavelengths near the resonance wavelength $\lambda_R = n_{av} * P$, where $n_{av} = \frac{2*n_\perp + n_\parallel}{3}$ is the average refractive index of the LC, $n_\perp$ and $n_\parallel$ being the local ordinary and extraordinary refractive indexes of the LC, respectively. The spectral width of the resonance band is proportional to the pitch of the helix and the local birefringence $\Delta n = n_\parallel - n_\perp$ of the liquid crystal, $\Delta\lambda_R = \Delta nP$. Circularly polarized light of the same circularity to the helical structure is reflected because of the constructive interference of the light reflected from the different layers, while

circularly polarized light of the opposite circularity to the helical structure is not reflected because of the destructive interference. So, if the normally incident light is unpolarised, then the 50% of the light will be reflected. It is possible to achieve a more than a 50% of reflection by introducing a polymerizable monomer into a cholesteric medium exhibiting thermally induced helicity [49] [50].

2.3 Properties of liquid crystals

All the special properties of LCs come from their strong anisotropy [1] (optical, dielectric, magnetic, mechanical, etc.). This anisotropic property of the LC molecules is due to their rodlike shape of the molecules (anisotropy shape). Most of the NLC are uniaxial; the material has a single axis of symmetry. Free rotation around the long molecular axis gives an axis off symmetry which is parallel to the director. So the properties of the material along the direction perpendicular to that symmetry axis are same, whereas they are different along the axis parallel to the director.

2.3.1 Optical anisotropy

The aligned NLCs are uniaxial, and therefore birefringent, exhibiting different optical properties of light traveling with electric field parallel or perpendicular to the director or optical axis. The electric vector of the incident plane polarized light propagating through the NLC split into the ordinary ray (o) which propagates in the plane perpendicular to the optical axis and extraordinary ray (e) propagating in the plane which include the optical axes and ray direction (Figure 2.7). The refracting index of the ordinary ray n_o is constant and independent of propagation direction, whereas the refractive index of the extraordinary ray $n_e(\theta)$ varies with the ray propagation angle θ with respect to the plane perpendicular to the optical axis according to

$$n_e(\theta) = \left(\frac{cos^2\theta}{n_o^2} + \frac{sin^2\theta}{n_e^2}\right)^{-1/2} \qquad (2.3)$$

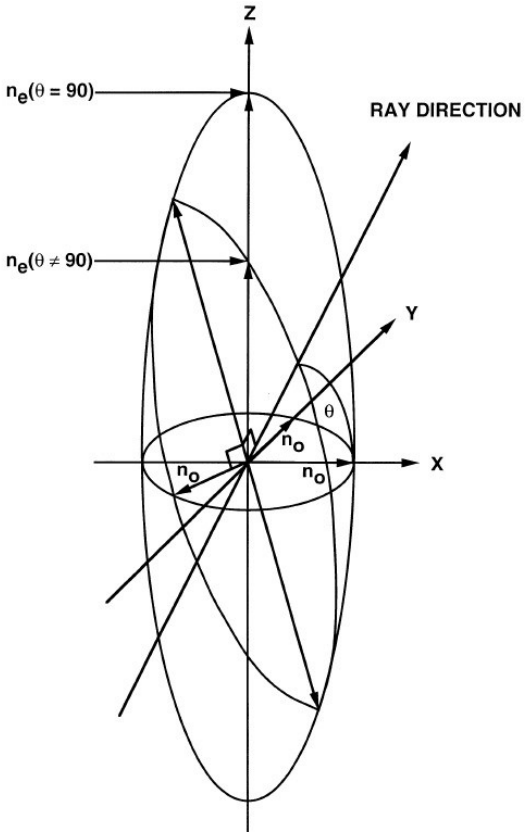

Figure 2.7 The refractive index ellipsoid of a uniaxial liquid crystal with the optic axis parallel to the z axis. The refractive index n_o of the ordinary ray is independent of propagation. The refractive index n_e of the extraordinary ray is larger than no for a liquid crystalline material of positive birefringence (After Ref. [5]).

The birefringence of the medium depends on the propagation direction and is defined as

$$\Delta n(\theta) = n_e(\theta) - n_o \qquad (2.4)$$

The maximum birefringence occurs when electric field of the e-ray is parallel to the optical axis ($\theta = 90^\circ$). The optical anisotropy $\Delta n = n_e - n_o$ in LCs is generally higher than in the crystals and is about 0.1 to 0.2.

2.3.2 Dielectric anisotropy

Most of LCs molecules are not charged; however, sometimes the bonding between the atoms can cause a slight separation of the positive and negative charge in molecules and so create the permanent electric dipole. In the absence of the electric field the molecules are oriented in the way that accumulative electric dipole of all molecules is zero, even if orientational order is present. The situation changes if an electric field is applied to the material. As shown in Figure 2.8 the opposite charged parts will experience the forces in opposite directions, and the electric torque will cause the molecules to rotate until the electric dipole line up with the electric field. This will tend to orient the molecule parallel or perpendicular to the electric field, depending on how the separation of charge occurs: along or across the long axis of the molecule. If each molecule carries a permanent dipole parallel (or approximately parallel) to the longitudinal axis, the dipole will be oriented (by the E field) along the long axis ($\varepsilon_{\parallel} > \varepsilon_{\perp}$, dielectrically positive). And if there is a permanent dipole, which is more or less perpendicular to the long axis, the situation is reversed ($\varepsilon_{\parallel} < \varepsilon_{\perp}$, dielectrically negative) [1] .

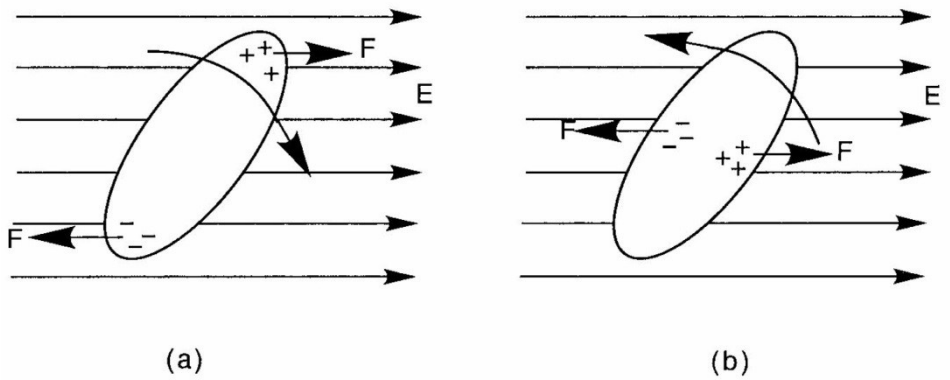

Figure 2.8 Orientation of a LC molecule by an electric field. In (a) the molecule has positive dielectric anisotropy, while in (b) it has a negative dielectric anisotropy. (After Ref. [35])

In many liquid crystal molecules the bonding of atoms does not produce any separation of charges. Those molecules respond to an electric field in another way. The electric field applied to the molecule displaces the positive charges slightly in one direction and the

negative charges in the other direction, and so induces an electric dipole. Once the dipole moment is induced the electric field acts on the molecule in the same way as in the case of the permanent dipole in any medium. In the nematic LCs the polarizability of the molecules is different for directions parallel to the long axis of the molecule and perpendicular thereto. The difference $\Delta\varepsilon = \varepsilon_{\parallel} - \varepsilon_{\perp}$ may be positive (e.g., E7, 5CB, TL216) or negative (MBBA), depending on the chemical structure of the constituent molecules of the NLC.

The dielectric permittivity's in the LCs depends on the temperature and the frequency. The $\Delta\varepsilon$ decreases as the temperature of the medium increases. The frequency dependence (dispersion) can be described from the physical origin of the induced polarization of the molecules. Generally there are three contributions to the induced polarization of the liquid crystal molecules: electronic, vibrational, and orientational polarization [44]. The electronic contribution is due to field-induced displacement of the electron cloud in the molecule. The magnitude of the dipole induced moment depends on the orientation of the molecule in the electric field. The vibrational contribution is due to a deformation of the nuclear skeleton of the liquid crystal molecule. Orientational polarization is arising from the partial alignment of the permanent dipoles in liquid crystal molecules. These three mechanisms of polarisation have different characteristic relaxation times. Among them, the orientational polarisation, which related to the reorientation of permanent electric dipoles of molecules, is the slowest with the time scales ranging from 10^{-9} to 10^{-2}s. At relatively low frequencies of electric field (e. g., 1kHz) all three contributions participate in the overall polarization. As the frequency increases, the orientational polarization becomes negligible because of the insufficient time to respond to the reversed electric field.

In general $\varepsilon_{\parallel}$ and $\varepsilon_{\perp}$ have the different dispersion regions. For the rodlike molecules of the liquid crystals orientatational contribution of permanent dipoles for $\varepsilon_{\perp}$ is negligible, while for the $\varepsilon_{\parallel}$ the orientational contribution of permanent dipoles is significant. According to Debye's theory, the frequency dependence of the dielectric constants of polar molecules can be written as

$$\varepsilon_{\parallel} = \varepsilon_{\parallel H} + \frac{(\varepsilon_{\parallel L} - \varepsilon_{\parallel H})}{1 + (f/f_R)^2}$$

$$\varepsilon_{\perp} \approx constant \qquad (2.5)$$

where $\varepsilon_{\parallel H}$ is the dielectric constant at high frequencies ($f_R \ll f$) and $\varepsilon_{\parallel L}$ is the dielectric constant at low frequencies ($f \ll f_R$). The relaxation frequency $f_R = 1/(2\pi\tau)$ is related to the relaxation time τ of the orientational motion of the molecules. In the case, when the static value of $\varepsilon_{\parallel}$ (for low frequencies) exceeds that of $\varepsilon_{\perp}$, there is a possibility that $\varepsilon_{\parallel}$ becomes smaller than $\varepsilon_{\perp}$ in the relaxation frequency region, as a result of a low frequency dispersion in $\varepsilon_{\parallel}$(see eq. 2.5). Thus, the dielectric anisotropy will change its sign from positive to negative at a certain cross-over frequency. For some LCs it occurs at relatively low cross-over frequencies (near the 50kHz), and we call them dual frequency liquid crystals (DFLC).

One of the disadvantages in the LC based devices is that turn-off relaxation process is long. The turn-on process can be accelerated and be can made sufficiently fast by increasing of external field. The turn-off process can also be accelerated if we use DFLC. A DFLCs are the mixtures usually composed of two types of materials [51]: 1) Compounds possessing a positive dielectric anisotropy at low frequencies (positive compounds). These compounds ensure frequency dependence of the mixtures thanks to the fact that their dielectric anisotropy decreases with the increase of the frequency. 2) Compounds possessing a negative dielectric anisotropy at high frequencies (negative compounds). These compounds ensure the large negative dielectric anisotropy for the high frequency region below the megahertz for whole mixture [52].

The frequency dependence of the dual frequency nematic liquid crystal (DFNLC) that we used in this work is presented in Figure 2.9. The crossover frequency of MLC2048, the frequency at which the dielectric anisotropy changes sign is around of the 30kHz [53]. This frequency is generally determined by the relaxation frequency of the positive compound. There are various factors that determine relaxation frequency, such as molecular length [54] [55], viscosity and order parameter [56].

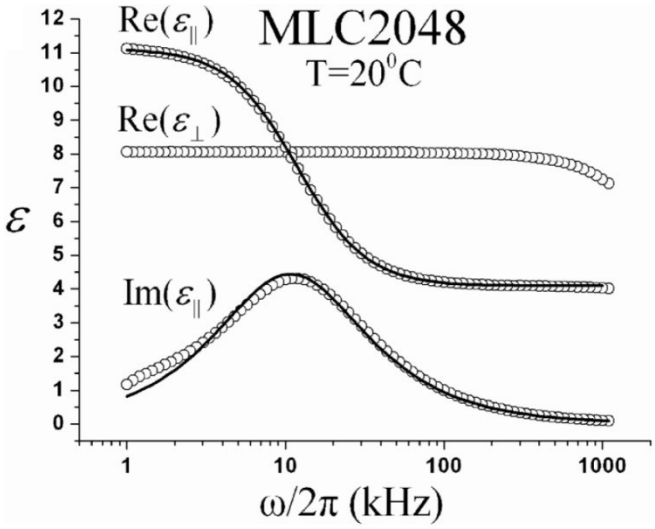

Figure 2.9 Frequency dependence of dielectric constants for the dual frequency LC: MLC2048. (After Ref. [53])

The DFLCs are very interesting for improving the switching speed [32] because an external field of low frequency can align the director along the field, while at the higher frequency the director aligns perpendicular to the field. So, changing frequency of the field one can switch the director very fast because the director always suffers a torque from a strong field. Since the field is never switched off, the slow free relaxation process of the director is excluded.

2.3.3 Elasticity

The existence of a long-range orientational order in liquid crystal is at the root of its elastic properties. At rest, all the molecules of a nematic liquid crystal are aligned parallel to a fixed **n** direction. This configuration corresponds to the equilibrium configuration and minimum free energy state. Any deviation from this perfect order increases the free energy of the system. Upon application of a distorting force, such as electric field or surface forces, a liquid crystal will undergo a deformation. The balance between the distorting force's torque and the elastic torque will then determine the static deformation pattern of the liquid

crystal. Any static deformation of liquid crystals can be presented as a combination of a three basic deformations. These are splay, twist, and bend deformations, as shown in Figure 2.10. Following the notation of the Oseen-Frank theory [1], the elastic energy density of the deformed nematic liquid crystal that can be given by

$$F_d = \frac{1}{2}K_{11}(div\mathbf{n})^2 + \frac{1}{2}K_{22}(\mathbf{n}\cdot rot\mathbf{n})^2 + \frac{1}{2}K_{33}(\mathbf{n}\times rot\mathbf{n})^2 \qquad (2.6)$$

where K_{11}, K_{22} and K_{33} are the elastic constants (Frank constants), associated to splay, twist and bend deformations, respectively. The elastic constants determine the spatial and temporal response of the liquid crystal director to applied external fields.

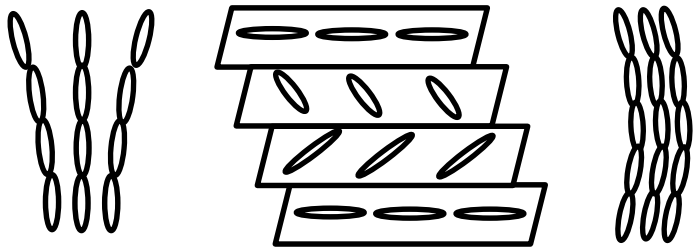

Figure 2.10 The three basic types of deformation in liquid crystals: a) splay deformation b) twist deformation and c) bend deformation

2.4 Alignment by surfaces

There are two types of alignment forces which act in different ways on the liquid crystals: the volume forces (such as electric fields, magnetic fields), and the surface forces. The surfaces are very important for understanding and controlling the behavior of LC. Without any physical or chemical treatments of surfaces, the liquid crystal will have many domains and many discontinuities in orientations, which will cause a light scattering and liquid crystal will appear cloudy.

The surface interactions between substrate and LC are complex and highly dependent on the material and the substrate in question. These interactions are fundamental for understanding the phenomena of alignment in the liquid crystals. The most important factors determining the LC alignment near the surfaces include dipolar interactions, Van der Waals forces, steric interactions, hydrogen bonding, surface topography and elastic properties of liquid crystals.

The chemical interaction between the surface and the LC is one of the factors that can influence the orientation of the molecules. Surfaces, by their chemical nature, can generate a planar, homeotropic, tilted alignment of the molecules (Figure 2.11). The liquid crystal molecules align parallel to the substrates in the planar alignment, perpendicular to the surfaces in the hoemeotropic alignment, and tilted to the substrates with a certain polar angle, called pretilt angle, in the tilted alignment. Actually, the tilted alignment with the pretilt angle less than 10^{o} is usually called planar alignment. In order to obtain planar alignment substrates with rubbed polyimide films are used. Homeotropic alignment is generally obtained by using substrates with hydrophobic films such as silane compounds [57]. The SiO evaporation method can give any of the planar, homeotropic and tilted alignments by changing evaporation angle [24].

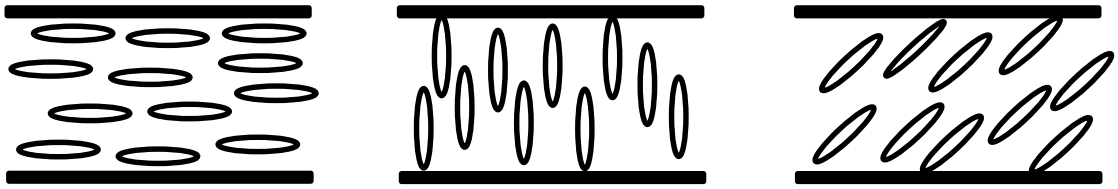

a b c

Figure 2.11 Alignment by surfaces: a) planar alignment b) homeotropic alignment and c) tilted alignment

In the volume of the liquid crystal, all directions are equivalent for the director. This is no longer true when in contact with a surface, where the symmetry of the mesogenic phase is

broken by the presence of the other phase than the liquid crystal. In the vicinity of an interface, in the absence of external fields, the liquid crystal is aligned with the surface director $\mathbf{n_s}$ parallel to a privileged $\mathbf{n_f}$ called easy axis direction. This axis corresponds to the orientation that minimizes the energy of the interface, the anisotropic part of which is called anchoring energy. Any deviation of $\mathbf{n_s}$ from $\mathbf{n_f}$ increases the energy of the system and creates a anchoring torque which tends to bring $\mathbf{n_s}$ parallel to $\mathbf{n_f}$. The anchoring energy depends on an interaction between aligning layer and liquid crystal molecules near the surface. In most cases, the alignment of the liquid crystal molecules near the substrate is hardly changed by the applied external fields (electric or magnetic). Such interaction between the aligning layer and liquid crystals is called strong anchoring. In the case of strong anchoring, the alignment of the liquid crystal molecules (in bulk) gets back to the initial orientation after removing the external field. In the case of a so called weak anchoring, the orientation of the liquid crystal molecules near the surface can be changed upon application of external fields. In this case the orientation of the liquid crystal molecules (in bulk) is different from the initial orientation.

The LC alignment in bulk is determined by the orientational ordering of the first LC monolayer adsorbed on the substrate [58] [59]. Then through LC molecule-molecule interactions this orientation propagate in volume by the effect of the elasticity of the medium [1]. It is therefore very important to be able to properly orient liquid crystals near the surfaces.

The rubbing method is the dominant alignment process since it was reported by Mauguin eighty years ago [60]. It consists of rubbing a spin-coated polymer (usually polyimide) surface using a rotating drum covered by a cloth with short fibers (Figure 2.12, after ref. [61]). This process orients the polymer film by printing a micro-relief and orienting the polymer chains of the surface in the direction of rubbing. The orientation of the film is then transmitted to the liquid crystal molecules by short-distance interactions (Van der Waals forces and hydrogen bonds). The orientational distribution of the first LC monolayer absorbed on the rubbed polyimide substrate can be determined from the optical second-harmonic generation (SHG) measurement of surface [62]. The alignment film thus provides to the liquid crystal molecules an azimuthal orientation in the rubbing direction and also

yields a polar direction called pretilt angle (Figure 2.12). The pretilt angle is very important in electro-optical applications. If there is no pretilt angle, the rodlike molecules of liquid crystal molecules can turn in two ways when reorienting by an electric field applied perpendicular to their molecular axis. That will create a disclination lines (orientational inhomogeneities) and multiple domains. A small pretilt angle will facilitate the turning of the molecules under the applied electric field, and ensure a single domain alignment. In addition, it will not only ensure a single domain alignment, but also speed up a response time.

The technique of rubbing is widely used in the LCD industry [6] since its implementation is relatively simple, faster and more reproducible when compared to the other techniques. The polyimide films are the dominant alignment materials used in the industry not only for their alignment characteristics, but also for thermal stability and superior electric properties. They are also relatively inexpensive and easy to apply.

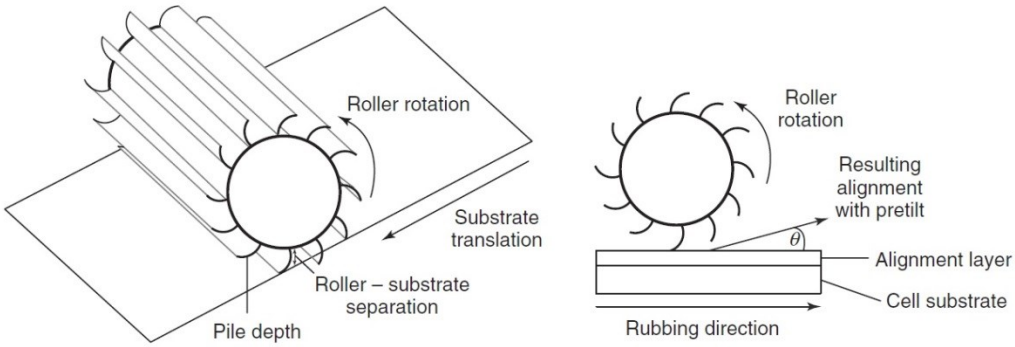

Figure 2.12 Schematic representation of rubbing process (After Ref. [61])

Despite the apparent achievements of rubbing technology, there are some serious drawbacks of this method that comes from the contact type of this method. Movement of the rotating roller rubbing on the polymer surface leads to the accumulation of static charges and the generation of fine dust particles that can decrease the basic characteristics of the device. The application of rubbing technology in large LCD creates additional difficulties in precise control of rubbing characteristics on huge substrate areas. The use of

this method is also problematic in the case of projection screens, because traces of rubbing become visible, when the enlarged image is formed. Finally, this method, in principle, cannot be used to align the LC in closed volumes.

An alternative method of alignment that is currently experiencing wide popularity is the photo-alignment, which consists of altering a polymer layer by irradiating it with light, usually in the ultraviolet. Photoalignment has many obvious advantages in comparison with the rubbing method. These advantages include elimination of static charges and impurities, controllable pretilt angle and anchoring energy, possibility to produce multidomain alignment, the ability for LC alignment on curved substrates, and finally, possibility to align the LC in closed volumes [7]. The method that we are most interested in and that attracted a lot of attention is the use of the photoreorientation of azobenzene components. In our group of research we have used azobenzene dye doped systems in the bulk [63] [64] or in the surface layer [65] [66] to induce reorientation of the host matrix by using the photoreorientation of the azobenzene dye molecules. In the scope of this thesis, presented in Chapter 3, we have attempted to use a mesogenic azo dye (MAD) doped into the RM surface thin film and expose the film by a laser beam, in order to reorient the azobenzene molecules, and so the RM matrix and the polymerize this film by UV exposition to fix this alignment.

2.5 Field induced reorientation: Electro-optical effect

As was mentioned already a liquid crystal molecule can be reoriented by an application of an electric field. The reorientation of the liquid crystal molecules will lead to local birefringent changes in the cell, and thus modifying the transmission properties of the cell. For an applied electric field **E**, the relation between the electric field and displacement **D** can be written in the form

$$\boldsymbol{D} = \varepsilon_{\perp}\boldsymbol{E} + (\varepsilon_{\parallel} - \varepsilon_{\perp})(\hat{\boldsymbol{n}} \cdot \boldsymbol{E})\hat{\boldsymbol{n}} \,. \qquad (2.7)$$

The molecular torque produced by the electric field is then given by [36]

$$\boldsymbol{\Gamma} = \boldsymbol{D} \times \boldsymbol{E} = (\varepsilon_{\parallel} - \varepsilon_{\perp})(\hat{\boldsymbol{n}} \cdot \boldsymbol{E})(\hat{\boldsymbol{n}} \times \boldsymbol{E}). \qquad (2.8)$$

If we consider the planar aligned nematic liquid crystal cell and an electric field is applied perpendicular to the cell substrates, then the electrostatic torque can be written in the form

$$\Gamma = (\varepsilon_{\parallel} - \varepsilon_{\perp})E^2 \sin\theta \cos\theta, \qquad (2.9)$$

where θ is the tilt angle of liquid crystal director from the boundary surface (see Figure 2.13). We can notice that the electrostatic torque is proportional to the E^2, which is independent of the polarity of the field. It means that reversing the electric field direction will not change the direction of the torque. That means, that even AC electric field of the high frequencies can create the same electrostatic torque, and reorient the liquid crystal molecules, which have high rotational viscosity.

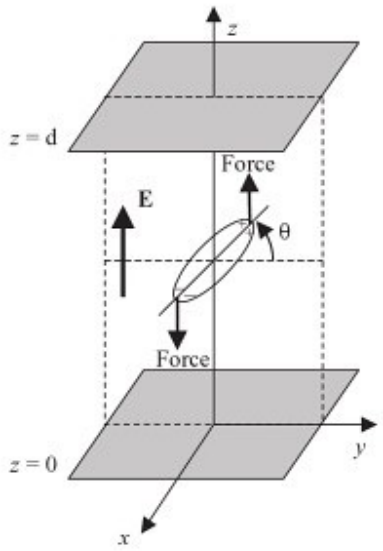

Figure 2.13 A nematic liquid crystal cell with a liquid crystal molecule oriented an angle θ measured from the *xy*-plane. An electric field E is applied along the *z*-axis. The molecule experience a torque that tend to reorient the molecule in a direction of applied field. (After Ref. [44])

It is important to note that the strength of the electric field necessary to reorient the liquid crystal molecules is relatively low. If we consider one molecule, the electric interaction energy will be low compared with the thermal fluctuation energy $\approx k_B T$. That's why in

liquids the disordered motion of the molecules will prevent any reorientation of the molecules. The situation is different in the liquid crystals, which molecules fluctuate together with strong angular correlation [67]. In this case the electrostatic torque applied to the group of the molecules (fluctuating together) is more important, and so the liquid crystal can be reoriented with the electric voltages of the order of 1V [1].

We can notice that for the $\varepsilon_{\parallel} > \varepsilon_{\perp}$, the minimum electrostatic energy occurs when the long axis of the liquid crystal molecule is parallel to the applied electric field. In the liquid crystal cell with strong anchoring conditions the reorientation of molecules near the surface will be zero. The reorientation of the molecules inside the cell will induce the distortion of director distribution, and that will create an elastic restoring torque that tends to prohibit the reorientation. As a result, the reorientation angle of the liquid crystal molecules will not only depend on the applied electric field, but also on the elastic forces in the bulk and the anchoring conditions on the surfaces. This reorientation is not occurring gradually as the strength of the applied field is increased. If we consider the nematic liquid crystal cell with the strong anchoring boundary conditions ($\theta(0) = \theta(d) = 0$), then the reorientation of the molecules will occur for the voltage exceeding some threshold value $V_{th} = \pi\sqrt{\frac{K}{\Delta\varepsilon}}$.

The reorientation process under the applied electric field for the nematic liquid crystal cell which initially has planar alignment is presented schematically in Figure 2.14. The NLC cell (with $\varepsilon_{\parallel} > \varepsilon_{\perp}$) reorients gradually upon the application of the electric field and provides a homeotropic alignment for a critical voltage $U = U_c$.

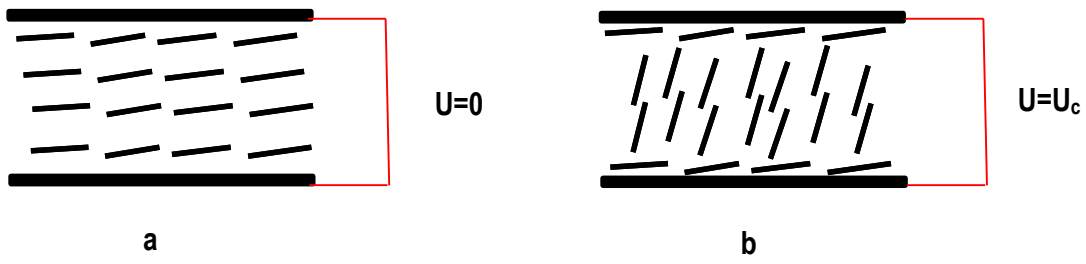

Figure 2.14 A planar nematic liquid crystal cell with strong surface anchoring: a) external field off, b) external field on

For the chiral liquid crystals the planar alignment texture differs from the planar alignment for the nematics [68]. The chiral liquid crystal with a given pitch in a planar texture adopts the structure shown in Figure 2.15(a). In this texture, the helecal axis of CLC is perpendicular to the cell substrates, and a material reflects light centered at the wavelength

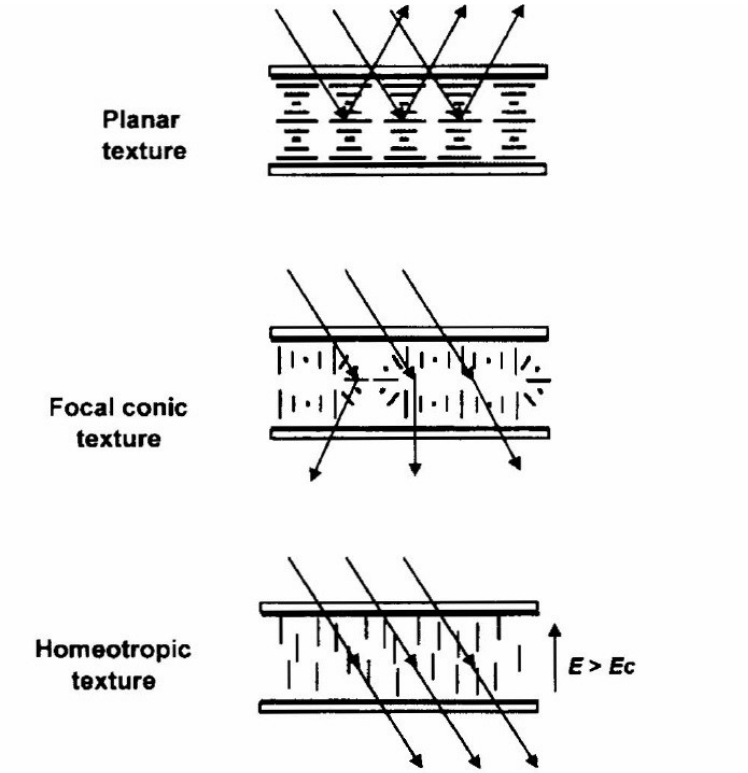

Figure 2.15 The structures of cholesteric textures. (After Ref. [68])

$\lambda_R = n_{av} * P$, where n_{av} is the average refractive index of a CLC. In the planar texture there are usually disclinations called oily streaks, which we observe in the article presented in chapter 5. The CLC can transform to the focal conic texture (Figure 2.15(b)), when an electric field is applied across the planar aligned cell. In the focal conic texture the helical axis of the CLC is more or less parallel to the cell substrates. It is a multiple domain structure, so the material scatters light. When the applied field becomes larger than a critical field E_c, the helical structure is unwound, and focal conic – homeotropic transition occurs. In the homeotropic texture the LC director is perpendicular to the cell substrates (Figure 2.15(c)) like in case of the nematic LCs.

2.6 Light scattering in liquid crystals

The scattering of light is of a great importance in our lives. It is present in many domains of physics, chemistry, and biology. The scattering of light can be much complex in details, and even simple problems of scattering can be hard to solve. While the details can get complex, there are three important things that affect how efficiently a particle scatters light: 1) the size of the particle relative to the light wavelength 2) particle's refractive index relative to the index of surrounding medium 3) particle's shape. The absolute size and the refractive index of particle don't matter [69].

In past century, Rayleigh was investigated a monochromatic plane wave scattering by a small particles [70]. For particles with radii (r) less than about 10% of the wavelength of light (λ), all the portions of the particle experience the incident light as having the same phase and intensity. So they will emit scattered light more or less in phase. The scattered light intensity will be proportional to the $(r/\lambda)^4$, a relation known as Rayleigh's inverse fourth-power law. Thus short wavelengths are scattered more than long wavelengths. The small particles scatter light approximately equally in all directions. The amount of the light scattered in a particular direction can be presented:

$$S \propto \frac{V^2}{\lambda^4}\left(\frac{m^2-1}{m^2+2}\right)^2 (1+cos^2\theta)\,, \qquad (2.10)$$

where m is the ratio of the refractive index of the particle and that of the medium, V is the volume of particle, and θ is the angle relative to the forward direction.

As the characteristic size of scattering particles increases, the scattering behavior becomes more complicated. For the particles in range of radii more than 1/10 the wavelength of the incident light and less than 100 times the wavelength the scattering is difficult to determine, because the different parts of the particle experiences different phases of incident light, and because the incident light is altered by its trip through the particle. The scattering in this range becomes more sensitive to particle dispersion, shape and less sensitive to the light wavelength. In 1908 Mie designed his theory of scattering of light by spherical particles of any size. The tendency of scattered light dependence from particle size is presented in the

Figure 2.16. As we can see from the Figure 2.16, the ratio of forward scattering compared with a back scattering increases with increase of the particle size.

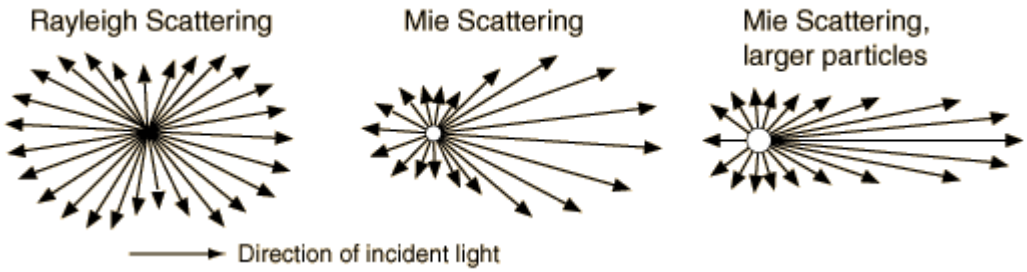

Figure 2.16 Scattering of light depending on particle size: from smaller to larger particles

In pure liquid crystals the scattering of light is generally due to director axis fluctuations of the molecules. The amount of the scattering depends on a several factors, that include cell thickness, boundary conditions, geometry of the cell, external field and optical wavelength. The ability to scatter light easily is an advantage of liquid crystals for various electro-optical applications. The scattering in LC crystals can be significantly improved by using LC / polymer composites. In this case scattering will be defined not only by LC local director axis fluctuations, but also by a local anisotropy of a LC / polymer system. The majority of existing approaches are focused on bulk LC / polymer composites such as PDLC and PSLC. In these systems the light scattering can be dynamically controlled very effectively by applying an electric field that reorients the LC molecules and thus modifies its uniformity of the refractive index, which is responsible for light scattering. The example of using electrically controlled LC light scattering in privacy window application is shown in Figure 2.17. In this work we have used a different approach by using a polymer network "attached" to the surface of the substrate (spin coated onto an anchoring film such as polyimide) instead of being dispersed in the cell volume. The detailed description of this method and obtained results for the cases of nematic liquid crystals and chiral liquid crystals are presented, respectively, in Chapter 4 and Chapter 5 of present thesis.

Figure 2.17 LC Privacy Glass from Innovative Glass Corporation. (From http://www.innovativeglasscorp.com/lc-privacy)

Chapter 3

Thin Orienting Surface Layers with Azobenzen Dyes

The alignment control of liquid crystal molecules by surfaces has a great importance in the applications of the liquid crystal based electro-optical devices. This control requires the ‘‘programming’’ of surface interactions between the liquid crystals and the substrate. The most widely used rubbing method has some limitations as we mentioned already. Some of the important drawbacks are: 1) it is impossible to produce a multi-domain alignment with this method, and 2) pretilt control is very limited [6]. So there is a great interest in developing other alignment modes, which give more control possibilities. Among all the existing alignment modes, the photoalignment is probably the most promising method. The method of photoalignment that we were interested in, in the scope of the present thesis is based on use of the photoreorientation of azobenzene dye.

The interest for azobenzens dyes as photoaligning materials was supported at a remarkably high level in the last three decades. The most interesting applications of azobenzene are based on easy and reversible photoisomerization about the nitrogen-nitrogen double bond, converting between thermally stable *trans* and metastable *cis* isomers. The schematic representation of *trans* form of the mesogenic azobenzen dye used in our study is presented in Figure 3.1. Upon absorption of a photon with the wavelength in the absorption band of the *trans* isomer, azobenzene will convert into the *cis* isomer. A second light wavelength (in absorption band of *cis* isomer) will cause inverse conversion (Figure 3.2). Even without illumination the *cis* isomer will thermally reconvert to the more stable *trans* state, with a time scale ranging from milliseconds to hours, depending on the azobenzen type [71].

The first publication on LC photoalignement [72] showed the possibility of using of reversible cis-trans isomerization of azobenzen monolayer to switch the adjacent LC alignment from homeotropic to planar state. That solid surface attached azobenzen

monolayer is called 'command surface'. Here optical control of LC alignment was produced by changing the wavelength of the non-polarized light illumination.

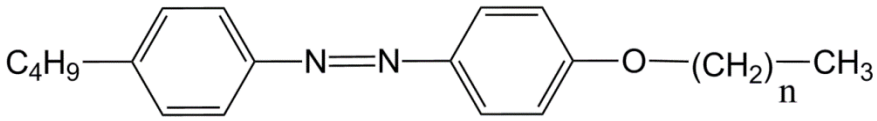

n = 1, 4, 6 and 9

Figure 3.1 Schematic representation of the mesogenic azobenzene dye (Beam 5721) molecular structure used in our study. It is a mixture of 4 components: 4-n-butyl-4'-ethoxyazobezene, 4-n-butyl-4'-pentyloxyazobezene 4-n-butyl-4'-heptyloxyazobezene and 4-n-butyl-4'-decyloxyazobezene.

Later it was shown the alignment of LC could be controlled by irradiating an azobenzen dye doped polymer layer with a polarized laser beam [73]. It is related to the reorientation of the azobenzen molecule under the action of polarized light (Figure 3.3). The azobenzens preferentially absorb the light polarized parallel to their long axes. The molecules aligned along the polarization direction of the incident light will be isomerized *cis* form, and then reconvert to the *trans* form with a new random orientation. The molecules aligned perpendicular to the light polarization will no longer absorb light and will remain fixed (Figure 3.3). Thus, a distribution of azobenzen molecules which is initially isotropic will gradually align with the polarized light.

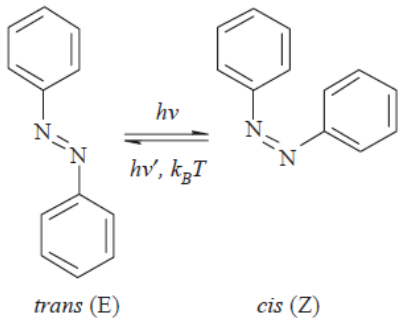

Figure 3.2 Azobenzene molecule can convert betwwen *trans* and *cis* isomers upon absorption of light. (After Ref. [71])

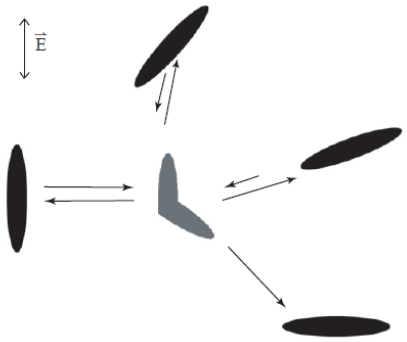

Figure 3.3 Statistical photo-orientation of azo molecules. The molecules aligned along the polarization direction of the incident light absorb, isomerize, and re-orient. The final state of molecules is perpendicular to the light polarization. Those molecules cannot absorb and remain fixed. (After Ref. [71])

The present chapter is based on article that discusses the photo isomerisation and photo induced anisotropy in mesogenic azobenzen dye doped matrices. The aim of this work is to prepare an azobenzenes doped reactive mesogens layer, which can be oriented locally due to reorientation of azobenzen molecules by illuminating with polorized light, and then use the UV photo polymerization of the reactive mesogenic host to fix that reorientation. Then the alignment and electro-optical behavior of the LC cell fabricated with these substrates can be controlled upon application of an electric field.

Resumé de l’article inseré

Étude de la photo isomérisation et anisotropie photo induite d'un mélange de colorant d’azobenzen mésogènique dans diverses matrices solides et liquides

Nous rapportons les analyses de l'anisotropie photo induite générée par un colorant d’azobenzène mésogènique qui est introduit dans des matrices isotropes et anisotropes. En utilisant la spectroscopie polarisée résolue dans le temps et des études de dichroïsme photo induite, nous montrons que ce colorant spécifique subit un processus de photo isomérisation, mais qu’il possède une mobilité angulaire très limitée dans toutes les matrices testées.

Proc. SPIE 9288, Photonics North 2014, 92880N

Study of photo isomerization and photo induced anisotropy of a mesogenic azobenzen dye mixture in various solid and liquid matrices

A. Minasyan, A. Tork and T. Galstian*

Center for Optics, Photonics and Laser,

Department of Physics, Engineering Physics and Optics, Laval University,

Pav. d'Optique-Photonique, 2375 Rue de la Terrasse, Québec, Canada G1V 0A6

* Corresponding author : galstian@phy.ulaval.ca

ABSTRACT

We report the analyses of the photo induced anisotropy generated by a mesogenic azobenzene dye complex that is doped in isotropic and anisotropic matrices. By using time resolved polarized spectroscopy and photo induced dichroism studies, we show that this specific dye composition undergoes photo isomerization process, but has very limited angular mobility in all tested matrices.

Keywords: Photo isomerization, photo induced anisotropy, guest-host, molecular reorientation, spectroscopy, polarization

3.1 Introduction

Azobenzen dyes have attracted attention for very broad range of potential applications, from industrial paint to liquid crystal (LC) displays [74], reversible storage [75] [76] [77],

mechanical ‘‘muscle’’ [78] and nonlinear optics [79] [80] [81]. The mechanisms of photo isomerization (in-plane or out of plane rotation of one of the phenol groups with respect to the second group) of such molecules were widely discussed in the scientific literature [82]. It was shown that the resulting photo induced rotation of the long molecular axis of molecules happens almost in all cases, even when the dye is covalently attached to a polymer matrix [83] [84] [85] or when the molecular packaging is extremely tight to prohibit the photo isomerization reaction (for example, in some Langmuir Blodgett films) [86].

Particularly interesting aspect of studies of azobenzen dyes was their use for LC photo alignment [7]. Indeed, the interest in photo alignment techniques for LC displays [87] propelled the development of various azobenzene molecules (including liquid crystalline or, so called, mesogenic) [88]. The most frequently used mechanism of such alignment was the photo induced reorientation of azobenzen molecules. In the past, we have successfully used azobenzene dye doped systems (in the bulk [63] [64]) or in the surface layer [65] [66] of the nematic LC (NLC)) to induce reorientation of the host matrix by means of the resonant photo excitation of the dye. In addition, surface thin films of reactive mesogen (RM) where doped by an azobenzen dye, exposed by a reorienting laser beam and polymerized by UV exposition to obtain ‘‘photo-programmed’’ alignment of NLC [89]. Encouraged by those results, we have attempted to use a mesogenic azo dye (MAD) (doped into the RM matrix) to increase the efficiency of such rotation thanks to the stronger coupling of the dye dipole moment with the *director* (average orientation of long molecular axis) [1] of the RM host in its liquid crystalline phase. The main idea here was to use the photo induced reorientation (of the dye and then of the director of the host) and UV photo polymerization of the reactive mesogenic (nematic) host that would fix (at least partially) the alignment of its director. However, one of the commercially available MADs appeared to be very specific since, as we have discovered (see hereafter), it readily undergoes photo isomerization reaction, but the photo induced rotation of its long axis is very limited. We have started its study in a thin LC alignment layer, but then explored the photo excitation processes in various bulk matrices, including anisotropy (e.g., an NLC) or isotropy (polymer) media. Spectroscopic, polarizational and dynamic characteristics of the photo isomerization process of that dye are described and discussed in the present work.

3.2 Material systems and samples

We have purchased the MAD (LC 5721, from BeamCo) and doped it in three hosts: two of them where mesogenic (liquid crystalline) in their NLC phase; the first one was a thin RM film and the second one was a bulk NLC. The last host explored was a solid poly(methyl methacrylate)(PMMA) isotropy matrix.

In the case of the RM matrix, we have used the photo-curable composition RMS03-001C (purchased from Merck) without any modification. It was received in the form of a solution, where the MR was diluted to 30 wt.% in a solvent. We have added the MAD (in the NLC phase) to the original solution of RM at the concentration of 1wt.% (before spin coating). The obtained solution was then mixed during 20 minutes in an ultrasonic bath at the temperature of 40°C. Then, we have used a glass substrate that was already covered by a transparent conductive indium tin oxide (ITO) coating to support two additional layers, coated on the ITO surface. First, a thin (≈ 50 nm thick) layer of polyimide (PI-150, from Nissan) was spin-coated on the ITO (following the instructions from Nissan; 3000 rpm for 30 sec), heated (at 280^{o}C) and rubbed to obtain a planar alignment layer for the next layer to be coated. The MAD doped RM solution was afterward spin-coated (10 seconds at 500 rpm followed by 40 seconds at 4000 rpm) onto the rubbed PI-150 layer to obtain a ≈ 600 nm thick aligned (along the rubbing direction of the PI-150) film of uncured RM. The obtained MAD-doped RM layer was then heated for 1 minute at 90°C on a hot-stage to evaporate the original solvent taking care to avoid its polymerization at that stage (see later).

In the case of the bulk NLC matrix, we have used 0.7 wt. % of MAD and 99.3 wt. % of the NLC TL216 (from Merck). To fabricate the "sandwich-like" cell (filled with the mixture of MAD and TL216), we have used two ITO and PI coated substrates (as described above, the PI surfaces still being rubbed, but without the RM layers). Those two substrates were placed parallel to each other and joined together by a UV curable adhesive (dispensed on the periphery of one of substrates) that was containing spherical spacers (of 50 μm

diameter) to provide the desired cell thickness. The NLC-MAD mixture was then injected into the cell by capillary action at room temperature (20°C).

Finally, we have separately prepared chloroform solutions of the MAD and PMMA (from Aldrich) and mixed them to obtain a uniform mixture of concentration 1wt. % of MAD in the PMMA. Then a drop of that solution was dispensed on a horizontally leveled glass substrate (without any coatings) and left to dry in the dark for 24h (to build a film by using the so called "gravity deposition" method). The obtained films had typical thicknesses of 100 μm and surfaces of up to 10 cm^2.

3.3 Photo sensitivity study in two anisotropy matrices

We have started our studies by exploring the photo alignment processes in the thin layer of RM doped by MAD. The MAD/RM layer was exposed by an LED, operating at 375 nm. The LED beam was linearly polarized by a UV polarizer and was focused by a lens to obtain an exposition intensity of ≈ 2.6 mW/cm^2. In all cases of anisotropy matrices (thin RM layer and bulk NLC) the polarization of the LED beam was set parallel to the rubbing direction of the substrate, thus being parallel to the ground state *director*.

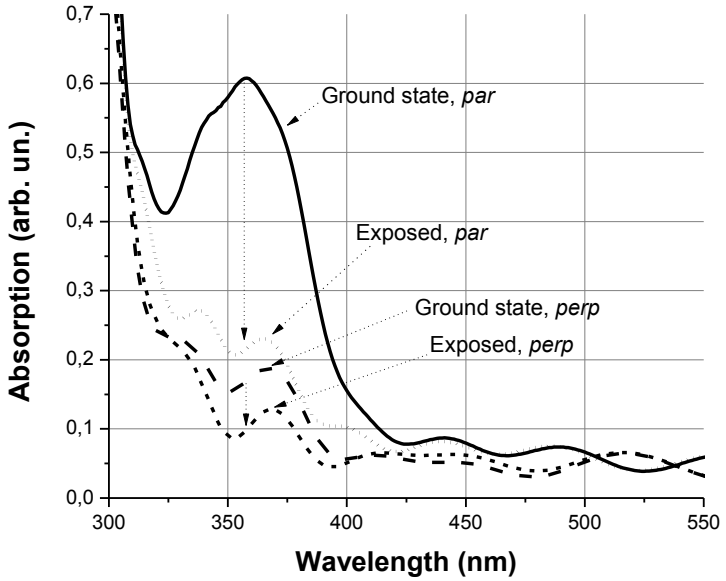

Figure 3.4 Polarization selective absorption spectra of the thin layer of RM doped by MAD. "par" and "perp" are cases when the polarization of the probe beam was, respectively, parallel and perpendicular to the director of the RM. The excitation of the material was done by an LED operating at 375 nm and polarized along the direction of the RM's director.

As one can see, from the Figure 3.4, the ground state transmission spectra are clearly polarization dependent. The parallel (to the director) polarization of the probe beam (solid line) is significantly more absorbed than the perpendicular component (dashed lines with large spacings). This confirms the good alignement of the MAD within the RM matrix (given the positive dichroism of the dye). The transmission of the sample is additionally modulated by the Fabry-Perot effect (more visible for wavelengths >400 nm) due to the thin layer of RM used (without index matching with the air and the substrate). In spite of that, we can clearly observe (solid line) a strong absorption band around ≈ 360 nm (actually a combination of resonances), which, we think, is associated to the *trans* form of the dye. After the LED exposition, this band decreases significantly (from 0.62 down to 0.22). Thus, the photo excitation of the dye induces *trans* to *cis* isomerization. The corresponding increase of the absorption band (that is associated to the cis form) is however not visible clearly. We think that this is because the main spectral changes here happen in the shorter

wavelength range (not accessible with our spectrometer Varian (Cary 500)) and also, in much less extend, in the visible range, but they are compromised by the Fabry-Perot effect.

Most importantly, we do not observe opposed changes of absorption for probe polarizations that are parallel and perpendicular to the LED's polarization. Indeed, the absorption of the trans molecules is reduced in both cases. This was not what we were expecting. As we shall show hereafter, the MAD is not degraded (the study in the NLC matrix shows its reversibility after the LED is switched off). We thus think that this could be related to the mesogenic character of both the guest (MAD) and the host (RM) molecules. This indeed could impose very strong anisotropic interaction of both molecular systems and the anisotropic potential of the host RM would then prohibit the rotation of MAD molecules alone. In the same time, the collective reorientation (both dye and RM) also must be very difficult here since the RM layer is very thin (≈ 0.6 μm) and has very strong boundary conditions (the PI and the air, the last one being able to provide alignment boundary conditions even stronger than the PI).

We have thus decided to exclude this strong boundary condition by doping the same MAD molecules into a bulk NLC of ≈ 50 μm thickness (almost 100 times thicker layer with two PI surfaces). However, even in such a thick layer of NLC, we were not able to observe the characteristic signature of light induced rotation of dye molecules, while the reversible photo induced isomerization was still clearly observed. Indeed, ground state absorptions of probe beams, which are polarized parallel and perpendicular to the NLC's director, are shown in the Figure 3.5. Here also, the observed strong anisotropy of absorption spectra confirms the good ground state orientation of the MAD by the NLC matrix. Here also, the exposition of the material by the same LED generates a strong decrease (depending upon the intensity of exposition) of the trans absorption band (around 355 nm) along with a weak increase of absorption around 442 nm, which, we think is responsible for the cis molecular absorption [90] [91].

It is worth to notice that the photo induced isomerization process here is characterized by a rather localized isobestic point despite the fact that the MAD is a mixture of various azobenzene molecules [92]. Furthermore, we clearly see a spectral shift of the isobestic point when rotating the polarizations of the input probe beam (402 nm for the ordinary

polarized probe and 436nm for the extra ordinary polarized probe). If all trans molecules are aligned along the director (which is the general supposition here) then this shift could be explained, for example, by the spectral transformation of the dye's absorption band due to the strong anisotropy of the host matrix. Indeed, it was already shown [93] [94] [95] that even an isotropic dye would show an effective dichroic absorption when doped into a strongly anisotropy matrix.

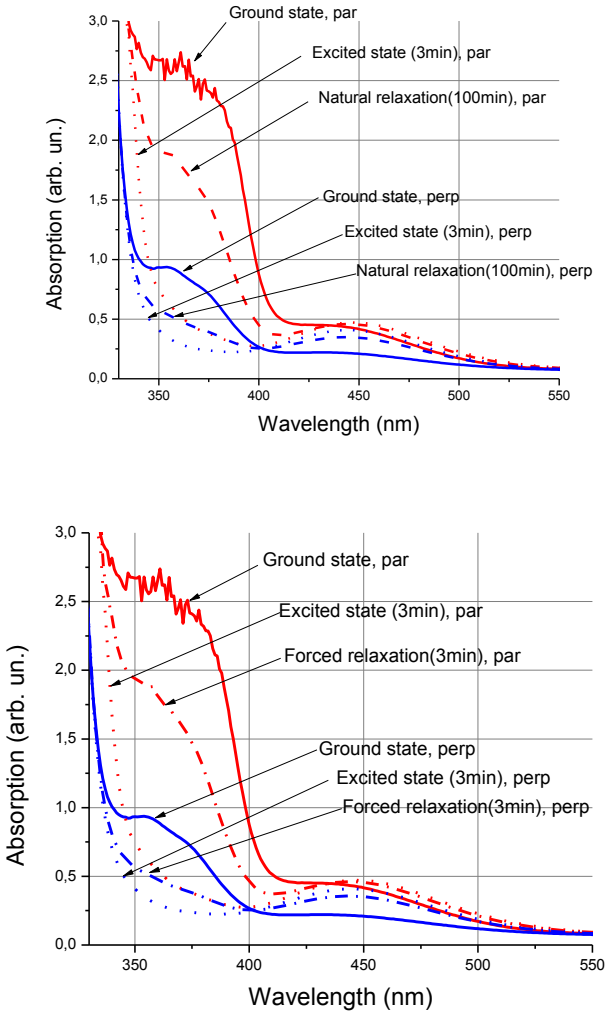

Figure 3.5 Absorption spectra of the MAD doped bulk NLC for probe polarizations, parallel (« par ») and perpendicular (« perp ») to the director. Ground state, excited state by LED, natural (a) relaxation (excitation by Argon ion laser) and forced (b) relaxation cases are presented for both polarizations. Intensity of LED excitation was 2,6mW/cm^2. Power of the argon ion laser was 60 µW (I=0,71mW/cm^2).

Another interesting observation is the stronger photo induced increase of the *cis* absorption for the perpendicularly polarized probe beam. This however could not be considered as a molecular rotation since, very likely, it is related to the fact that the dipole moment of the *cis* molecule may be perpendicular to the long molecular axis of the dye and hence to the director [96]. Thus the increase of the number of *cis* molecules increases the absorption around 445 nm for the probe polarization that is perpendicular to the pump's polarization.

As another important observation; here also, both parallel and perpendicular (with respect to the director) polarization components of the probe show decreasing *trans* absorption under the LED exposition. Thus, the molecular rotation seems to be absent in this bulk NLC matrix too.

It is worth mentioning that, the natural *cis* to *trans* back isomerization was extremely long (days) in the explored two material systems. Because the *trans* molecular reorientation is usually (not always) the result of multiple cycles of *trans* to *cis* and *cis* to *trans* transitions, this long relaxation times could be at the origin of the absence of molecular rotation. To eliminate this possibility, we have used a CW Argon ion laser (operating at 488nm, with a diameter of = 0.29 cm) to excite the *cis* molecules and to accelerate the back transition to the *trans* molecular form. The hope here was to help to perform multiple cycles of excitation and relaxation. Note that such a double exposition process was already used for holographic recording processes in azo dye doped polymers [97] [91]. The polarization of the argon ion laser was set parallel to the director.

The Figure 3.5 demonstrates the obtained results. So the forced relaxation accelerates the back transition almost by a factor of $100/3 \approx 33$, but the overall dependence of spectra from polarization is the same (Figure 3.6: forced relaxation) . Thus, there is no rotation of dye molecules. As we can see, from the Figure 3.6 (derived from Figure 3.5 and dynamic data), we succeeded to change drastically the kinetics of that transition by the exposition of the argon ion laser. For the corresponding demonstration, we have monitored the absorption changes at $\lambda = 450\ nm$ for the case when the LED was simply removed ("natural

relaxation") or when an argon ion laser beam of *713,4 μW/cm²* was added after the removal of the LED ("forced relaxation").

For the wavelengths corresponding to *cis* the changes are more important for perpendicular component. It is the opposite for the wavelengths corresponding to *trans* (for these wavelengths the changes are more important for parallel component). Despite the strong acceleration obtained we did not detect rotational processes for *trans* molecules.

To detect the possible rotation of MAD we have been using pure ''e'' or ''o'' probe beams. One possible mechanism of excitation might be the photo-induced large scale reorientation of the coupled MAD-NLC system. In this case the probe beam migth be ''polarization-guided'' (in the so called Moguin regime, [1]). To exclude this possibility, we have finally decided to study the photo isomerization process of this dye in an isotropy matrix, such as the PMMA.

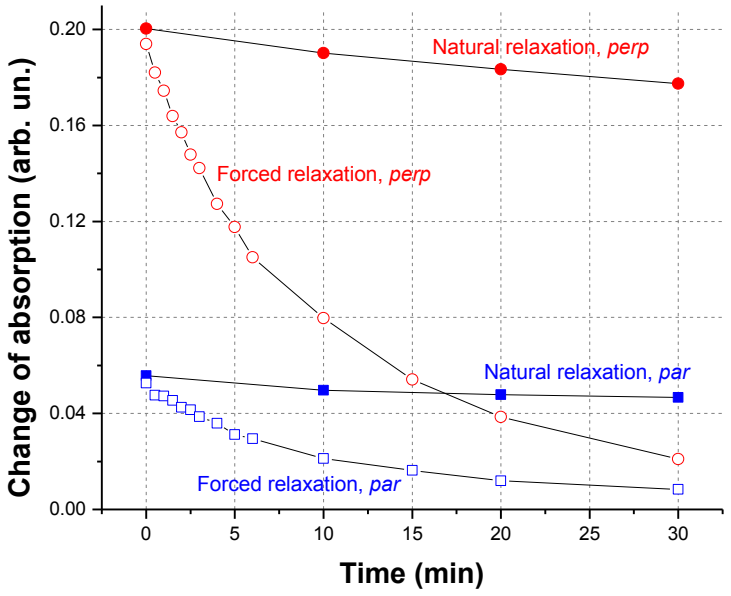

Figure 3.6 The natural and forced relaxation of MAD doped NLC absorption observed at 450 nm (mainly cis absorption) without and with an argon ion laser of 0,71 mW/cm² power.

3.4 Photo sensitivity study in a polymer matrix

The photo excitation of the material was done by means of the same, linearly polarized LED during 3 minutes with the same excitation intensity of 2.6 mW/cm². The corresponding spectra of the dye in its ground state as well as in the established excited states are presented in the Figure 3.7. We see clearly that the original absorption of the material is isotropic and the LED exposition induces spectral changes (absorption reduction for $\lambda < 415$ nm and increase for larger wavelengths; the 415 nm being the unique isobestic point here) corresponding to the *trans* to *cis* isomerization. Here also the relaxation of the dye was very slow (days) and the material system remained always isotropy. While the isotropy of absorption at ground state is quite natural, the isotropy of absorption in the excited state (by a plane polarized LED) is rather unexpected since azobenzen dye doped polymers have readily shown photo induced birefringence (PIB) and photo induced dichroism (PID) at such excitation intensities [98] [99] [28]. Thus, despite the clear presence of photo isomerization we don't observe any anisotropy of absorption even due to the angular hole burning.

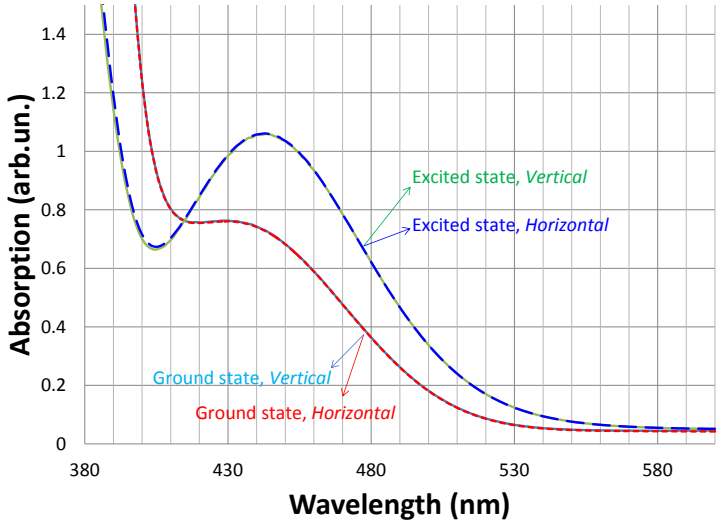

Figure 3.7 Ground state and excited, by a linearly polarized (vertical) UV LED of 2.6 mW/cm2 power (operating at 375 nm) absorption spectra observed with a probe beam polarized parallel and perpendicular to the polarization of the LED.

Finally, we have decided to increase drastically the excitation intensity to further study the behavior of this azobenzen compound. The same MAD doped PMMA sample was positioned between crossed polarizer and analyzer and the film was exposed by the same CW Argon ion laser (since it could provide significantly higher powers) that was polarized at 45° with respect to the polarizer's axis. This choice (imposed by the limited power of the LED) has the consequence of potentially involving (in the excitation) refractive index changes, which are generated by various molecular species (both *cis* and *trans*). A CW He-Ne laser (operating at 632 nm) was used as a probe.

The PIB was indeed observed when the excitation power was rather high (above 10 mW). The Figure 3.8 shows the rise, stabilization and the relaxation of the transmitted (through the analyzer) probe beam that confirms the PIB.

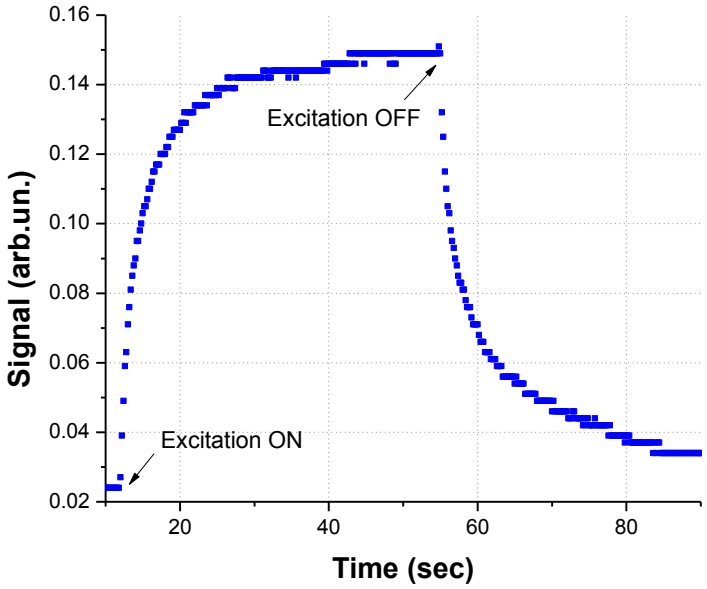

Figure 3.8 Dynamics of the photo induced birefringence of the MAD doped PMMA film induced by using an excitation at λ=488nm and detected at λ=632 nm. The excitation beam is switched on at t ≈ 5 sec and switched off at t ≈ 55 sec.

The analyses of the growth and relaxation of the PIB (by using a double exponential model) shows that there are two characteristic times of excitation. During the excitation (for the excitation intensity of 151,4mW/cm^2) one of them is $\tau_{ex.1} \approx 1.56$ sec and second one is

$\tau_{ex.2}\approx 9.05$ sec. The relative contribution of those "fast" and "slow" excitation modes in the PIB is $A_1/A_2\approx 0.66$. Those contributions are also visible during the relaxation process (when the Argon ion laser is switched off). Thus, here also we observe two typical times; $\tau_{rel.1}\approx 1.38$ sec and $\tau_{rel.2}\approx 13.85$ sec. The relative contribution of those "fast" and "slow" excitation modes in the PIB is $A_1/A_2\approx 1.34$, which shows that the slower mechanism did not relax completely. We believe that the fast mechanism of excitation could be related to the *cis* excitation while the slow one to the rotation of its dipole moment.

The way we decided to further study this process was based on the detection of the PID. To perform this last experiment, we have chosen the polarization of the probe beam to have simultaneously two components, one parallel to the excitation beam's polarization and the second one, perpendicular to it. Those two components were separated after the sample by using a Wollaston prism and detected separately (but simultaneously). The dynamic transmission of those two polarization components was monitored when the Argon ion laser was switched on and off. We have observed slight increase of transmission for the parallel component but almost no changes for the perpendicular component. We think that this rather means a cis to trans back photo isomerization. However, some rotation processes were observed only at very high excitation intensities. An example of such a process is described in the Figure 3.9. As we can see, the transmission of the parallel (with the polarization of the excitation beam) polarized probe beam increases while the perpendicular polarized probe's transmission decreases, which is a typical signature of orientational reoriganization of the dye's dipole moment corresponding to the cis state (given the wavelength of 514 nm, used for excitation).

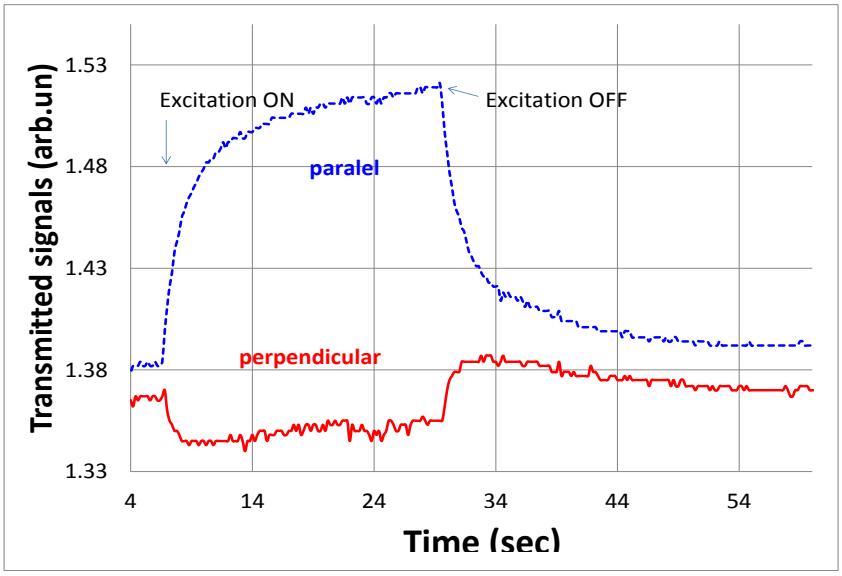

Figure 3.9 Demonstration of the PID in the MAD doped PMMA for excitation intensity of 2,4W/cm^2 at 514 nm.

3.5 Summary and conclusions

To summarize, we have studied the photo isomerization process of the mesogenic azobenzen dye mixture LC 5721 in various matrices, including liquid anisotropy and solid isotropy media. We started our studies in a thin layer of RM doped with MAD, and then explored the photo alignment process in a bulk anisotropy (LC) and isotropy matrices (PMMA). Polarized spectroscopy and photo induced dichroism studies showed that this dye undergoes photo isomerization process, but the rotation of the molecular axis is limited in all these tested matrices. The reason of the limited angular mobility of this dye is not very clear at this stage and additional work is needed to further understand its origins.

A spectral shift of the isobestic point of ≈34nm was observed for the ordinary and extraordinary polarized probe beams when the MAD was doped in the bulk anisotropy matrix. We think that this shift is related to the spectral transformation of the dye's absorption band, which could be caused by the strong anisotropy of the host matrix.

Acknowledgments

We thank Dr. S. Nersisyan for advices. We also acknowledge the financial support of Canadian Institute for Photonic Innovations (CIPI), Fonds Québécois de la Recherche sur la Nature et les Technologies (FQRNT) and Natural Sciences and Engineering Research Council of Canada (NSERC).

Chapter 4

Surface Polymer Stabilized Dual Frequency Nematic Liquid Crystals

The work presented in previous chapter, however, did not confirm the possibility of employment of surface photoalignment approach with mesogenic azobenzen dye. The commercially available mesogenic azobenzene dye that we have used in our research has shown a special behavior, showing very limited photo-induced rotation of its long axis. Another approach of surface alignment by polymer networks and surface control of electro-optical behavior of liquid crystals is explored in present chapter. The approach is based in using a reactive mesogen spin coated at the surface of an anchoring layer. As we have mentioned already the reactive mesogens are liquid crystalline materials which can be polymerized by an UV exposition. The mesogen reactive used for surface alignment have generally two or more polymerizable end groups. In the reactive mesogen there is a photo-initiator of polymerization. Under the action of UV light exposition it will produce radicals that will initiate the polymerization of mesogen. Polymerisation of these materials leads to a densely crosslinked network in which the liquid crystalline order stay fixed [100]. This procedure schematically is presented in Figure 4.1.

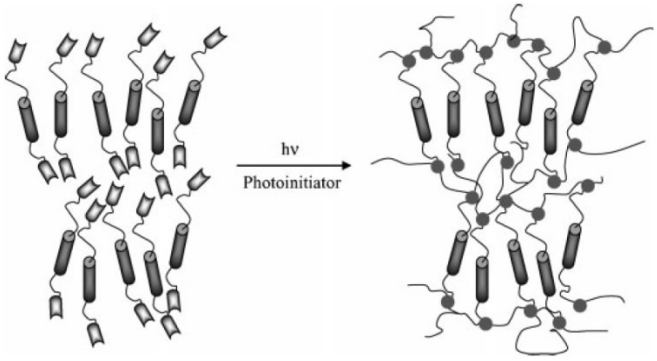

Figure 4.1 Photopolymerization of reactive mesogens: at left we have monomers (free molecules), and at right we have polymer with interconnected monomers. (After Ref. [100])

In our approach we have used the liquid crystalline properties of the reactive mesogen to first align them in their liquid crystalline phase by using electric field, and then fix that alignment by photopolymerisation procedure.

A surface alignment method using reactive mesogens localized in vicinity of the LC layer boundary is shown in ref. [101] (see Figure 4.2). The pretilt angle of the LC crystal cell was controlled by a so called surface localized polymer alignment (SPLA) layer. The LC-RM mixture separation and RM thin layer formation at the interior surface of the LC cell was performed by application of a pre-cure electric field. Then the UV exposition was used to ‘‘freeze’’ that alignment by a polymerization procedure. This procedure is schematically presented in Figure 4.2. However, this method of surface alignment can be problematic as the RM is not ‘‘attached’’ to the surface. The RMs flow in concentration gradients can cause the non-uniformities in alignment by formation of the polymer network in bulk resulting to a light scattering. Therefore the very low concentrations of RMs ($< 1.2\%$) and an accurate polymerisation intensity control is needed for the uniform alignment.

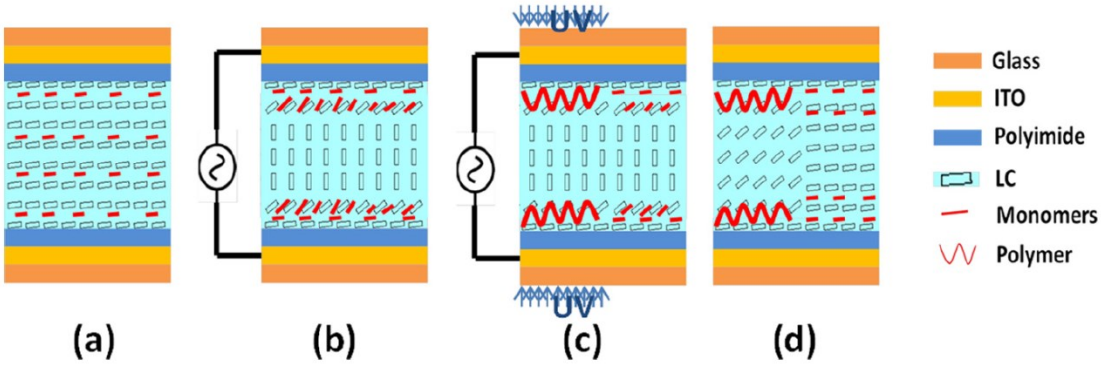

Figure 4.2 Method for the spatial control of the pretilt angle: (a) Planar cell filled with LC-RM mixture; (b) LC-RMs mixture separation in the external electric field (pre-cure voltage); (c) formation of the polymer layer in the vicinity of the LC cell substrates by local UV lightinduced polymerization (UV curing); (d) cell with spatially varied pretilt after curing. (After Ref. [101])

The low concentrations of the reactive monomer (below 5%) dissolved in the bulk LCs is used to fabricate the electrically controllable light scattering devices. In these LC/polymer composites called polymer stabilized liquid crystals (PSLC), a small amount of the monomer and photoinitiator are dissolved in non-reactive LC [102]. The afterward cross-linked polymerization of the monomer (generally mesogenic) results in a polymer network formation in the non-reactive LC (Figure 4.3). This network then stabilizes the liquid crystal alignment and improves the device characteristics (switching speed, lower threshold switching voltage, large viewing angle, haze free performance, etc.). The texture of the LC is not significantly influenced by the network. Application of electric fields then results in light scattering. The light scattering is due to a polymer network which plays the role of the cavities, keeping the LC molecules in vicinity of the polymer walls in their original alignment, while the bulk material reorients under applied field.

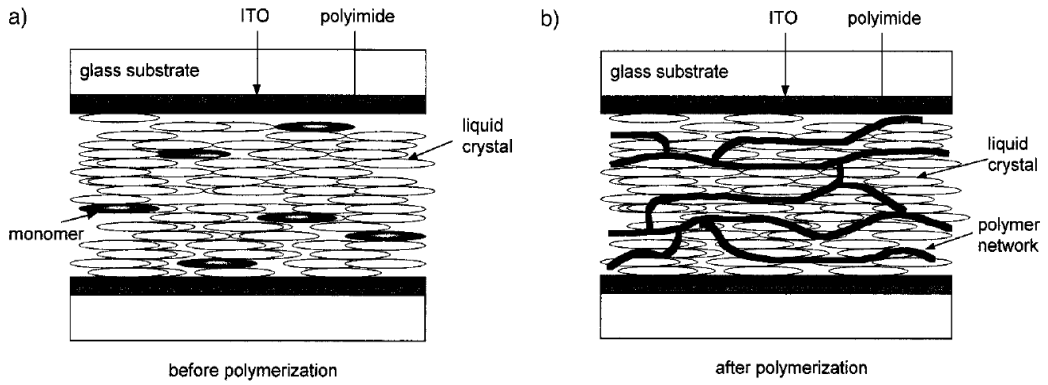

Figure 4.3 Schematic illustration of the fabrication of PSLCs. a) Photoreactive monomers dissolved in a LC before polymerization. b) Polymer network stabilizing the LC orientation after polymerization by UV irradiation (After Ref. [102])

As we have mentioned already in our approach we have used the RM which is not dissolved in bulk LC, but attached to the surface of the cell substrates and only partial interpenetration was allowed between the LC and the polymer network. The use of an interfacial RM layer (spin coated onto an anchoring layer) has shown great potential for the control of the LC alignment, enabling the fabrication of cells with electrically controllable light scattering. We have named the fabrication process of our cells as “programming”, and

taking into account that RM layer is onto the substrate, we call those cells as “surface PSLCs” (S-PSLCs). The programming process of S-PSLCs in details is presented afterward in the article inserted in this chapter.

Several groups have used the dual frequency LCs in order to improve the excitation and relaxation times of PDLC films. Which is typical for PDLC applications, a low frequency signal is used to induce alignment of nematic LC along the field direction and achieve a transparent state. To induce a rapid relaxation response, the low frequency field is removed and a high frequency signal is applied to the film. The negative dielectric anisotropy at high frequencies induces nematic orientation perpendicular to the applied field, which accelerates the relaxation time. 5ms relaxation times were reported with a high frequency signal, compared to 40-50 ms for the same material without applied high frequency [103]. Thus, the combinations of high and low frequency signals can induce a new switching behavior in LC based devices.

The use of dual frequency nematic LCs (DFLCs) provides the choice of programming regimes (at low frequency or at high frequency), and also introduces more possibilities of dynamic control during the post-programming operations of the cell. The noticeably improved contrasts of light scatter modulation and polarization independence by the dual-frequency control are discussed in article inserted in present chapter.

Resumé de l’article inseré

Cristaux liquides stabilisés par un polymère en surfaces avec un contrôle à double-fréquence

Des cristaux liquides (CL) à double-fréquence ainsi que des films minces de mésogènes réactifs (MR), moulé sur les surfaces internes des substrats d’une cellule, sont utilisés pour construire des structures stabilisées par un polymère en surface. Un champ électrique de haute fréquence est utilisé pour orienter les molécules de cristaux liquides à partir du couple diélectrique négatif avant la photopolymérisation des films de MR. Les résultats de la caractérisation électro-optique montrent que les contrastes de modulation de diffusion de la lumière et la dépendance de polarisation sont sensiblement améliorés par le contrôle à double-fréquence. Cependant, il n'y a pas de diminution notable de la durée complète du cycle d'excitation-relaxation-excitation.

Appl. Opt. **52**, E60-E67 (2013)

Surface-polymer stabilized liquid crystals with dual-frequency control

Amalya Minasyan and Tigran Galstian*
Center for Optics, Photonics and Laser, Department of Physics, Engineering Physics and Optics, Laval University, Pav. d'Optique-Photonique, 2375 Rue de la Terrasse, Québec G1V 0A6, Canada
*Corresponding author: galstian@phy.ulaval.ca

Received 2 April 2013; revised 6 May 2013; accepted 6 May 2013;
posted 8 May 2013 (Doc. ID 188156); published 14 June 2013

Abstract

Dual-frequency control liquid crystal (LC) and thin reactive mesogen (RM) films, cast on internal surfaces of cell substrate, are used to build surface polymer stabilized structures. Electric field of high frequency is used to orient the LC molecules by the negative dielectric torque prior to the photopolymerization of RM films. Electro-optic characterization results show that the contrasts of light scatter modulation and polarization dependence are noticeably improved by the dual-frequency control. However, there is no significant shortening in the full cycle duration of excitation–relaxation–excitation.

OCIS codes: (160.1190) Anisotropic optical materials; (160.2100) Electro-optical materials;

(160.3710) Liquid crystals; (160.4670) Optical materials; (160.5470) Polymers.

http://dx.doi.org/10.1364/AO.52.000E60

4.1 Introduction

Liquid crystal (LC) materials [1] [43] have been used in various consumer electronic (LCDs [44] and webcams [46]) and specialized electronic (polarizer [104] and variable optical attenuator, [VOA] [105] [106]) devices. The absence of mechanical movement, low cost, low voltage and power consumption are among the most attractive features of LC-based components. Very often, however, those components are perceived as being slow. In reality, the speed requirements depend upon the type of application, ranging from submilliseconds (shutters), milliseconds (LCDs), tens of milliseconds (network reconfiguration), and up to seconds (privacy windows).

It is well known that the speed of LC-based devices is typically defined by the natural (or free) relaxation time $\tau_{off} \approx \gamma d^2/(K\pi^2)$ of the deformation of their director (average orientation of long molecular axes of the LC [1,2,8], where γ is the rotational viscosity, K is the elastic constant and d is the thickness of the nematic LC (NLC). In the same time, the typical excitation times τ_{on} of those materials are defined as $\tau_{on} = \tau_{off}/((V/V_{th})^2 - 1))$, where V is the excitation voltage and V_{th} is the director's reorientation threshold voltage [43] [107]. Therefore, while the τ_{on} may be controlled by the choice of the voltage V, the τ_{off} is difficult to control dynamically for a given type of NLC material, cell geometry, and operation temperature. Thus, the duration of the full cycle of excitation and relaxation in standard NLCs is mainly defined by the free relaxation time τ_{off} .

To overcome the abovementioned speed limitation, "dual-frequency" NLC (DF-NLC) mixtures were introduced, which have positive dielectric anisotropy $\Delta\varepsilon > 0$ at low frequencies (e.g., at 1 kHz) and negative dielectric anisotropy $\Delta\varepsilon < 0$ at higher frequencies (e.g., for >50 kHz at room temperature). Such mixtures were successfully used, among others, to build fast VOAs [108] and phase modulators [32]. However, usually the uniform NLC cells (both ordinary and DF controlled) require polarizers to obtain intensity modulation. To obtain transmission modulation without polarizers, polymer dispersed LC (PDLC, [16]) and polymer stabilized LC (PSLC) compositions were introduced with ordinary NLCs [109] as well as with DF-NLCs [110]. In those PSLC materials, the

polymer network (bundles, walls, and aggregates) is dispersed in the volume of the NLC. Later, surface polymer stabilized NLCs (S-PSLCs) were introduced [29] [30] [31] with the promise of better control and stability. Those material compositions were using ordinary NLCs. However, in contrast with PSLCs, the polymer matrix here was attached to the surface of the cell substrates and only partial interpenetration was allowed between the NLC and the polymer network. While the obtained response times in all abovementioned cases were noticeably faster (almost by an order of magnitude compared to pure NLCs), the modulation speed and contrast were still rather limited. We were thus interested to see if we could further improve our capacity to configure such components (see hereafter) as well as their performance by using DF-NLCs in the same (S-PSLC) geometry. For the sake of shortness we shall further call them as S-PS-DF-NLC.

Thus, in the present work, we describe the fabrication (photoelectric configuration) and experimental characterization results of S-PS-DF-NLC cells. Given the large variety of possible fabrication processes, we limit this part to one or two examples, while the electro-optic characterization of obtained cells is presented in more detail. The scattering modulation contrast, transition times, and polarization dependences are compared for the cases of excitation followed by natural relaxation as well as for various excitation sequences. As it will be shown hereafter some of the key technical parameters of obtained cells may be in "conflict" and a corresponding choice must be done as trade-off when using DF-NLCs in S-PSLC configuration.

4.2 Materials and Methods

Two commercially available glass substrates (already covered, from one side, by transparent conductive indium tin oxide, ITO, layers) were used to build sandwich-like cells containing our S-PS-DF-NLC. Each substrate was first covered by a layer of ≈50 nm thick polymide (PI-150 from Nissan). Note that we usually apply this polymide to obtain a planar (parallel to the cell substrates) aligning layer through the well-known mechanical rubbing procedure [6]. However, in the present work, we did not rub the PI-150 layers to

eliminate the preferential alignment direction and thus to obtain polarization-independent operation. Note that we had two reasons for the use of PI: to have similar substrate (as those used in previous studies) and to provide good uniformity of the next thin layer. Indeed, a layer (≈600 nm thick) of reactive mesogen (RM) was cast onto each PI layer by spin-coating procedure. Then those RM films were dried and annealed on a hot stage at 60°C for ≈90 s. We have used two such substrates to fabricate the sandwich-like cell by the "drop-fill" technique. This was done without polymerizing the RM layer by UV light (usually it is done right after the deposition of the RM layer). Thus, one of the substrates was positioned horizontally (with the RM layer facing up) and the droplet of the DF-NLC (MLC2048, from Merck) was dispensed onto the surface of the RM layer. The periphery of the substrate was covered by UV curable adhesive walls (AC A1432-Q-S2 from Addisson) containing glass spacers (Ø ≈ 50 μm) to ensure the desired thickness of the cell. Then the second RM-covered substrate was pressed (with the RM layer facing down) on the drop of DF-NLC and the peripheral adhesive was cured (by a UV lamp with spectra between 300 and 450 nm, intensity of ≈10 mW/cm^2, irradiation time ≤10 min) while protecting the central part of the cell (the zone, which was later used for electro-optic tests) by a mask. An electric field (110 V_{RMS}, AC of SIN form at 1 kHz or 70 kHz, see hereafter) was applied to the cell during these 10 min to allow reorientation and partial interpenetration of DF-NLC and RM molecules, prior to the total curing of RM (over the entire surface of the cell) by the same UV lamp during 40 min. After this polymerization step the electric field was switched off (for the sake of shortness, we shall further call the above-described process as cell programming). However, since the polymerization was performed in the nonequilibrium state (field-induced alignment, interdiffusion, and photopolymerization), the cells were subjected to a final voltage pulse (e.g., an AC voltage of U = 110 V and 1 kHz frequency during 1 s) to obtain a stabilized (ground-state) material morphology before their electro-optic study. The five major steps of cell fabrication are summarized in Figure 4.4.

4.3 Experimental Setup and Process

To monitor the programming process, we have used a standard polarimetric setup (Figure 4.5). Namely, the S-PS-DF-NLC cell was placed between crossed polarizer and analyzer (Glan prisms) and the transmission of the probe beam (CW He–Ne laser, operating at 632.8 nm) through the analyzer was monitored dynamically by using a photodetector (the half-wave plate $\lambda/2$ and the diaphragm were added later, for electro-optic scatter measurements only). At the programming stage, the probe beam was at normal incidence on the cell.

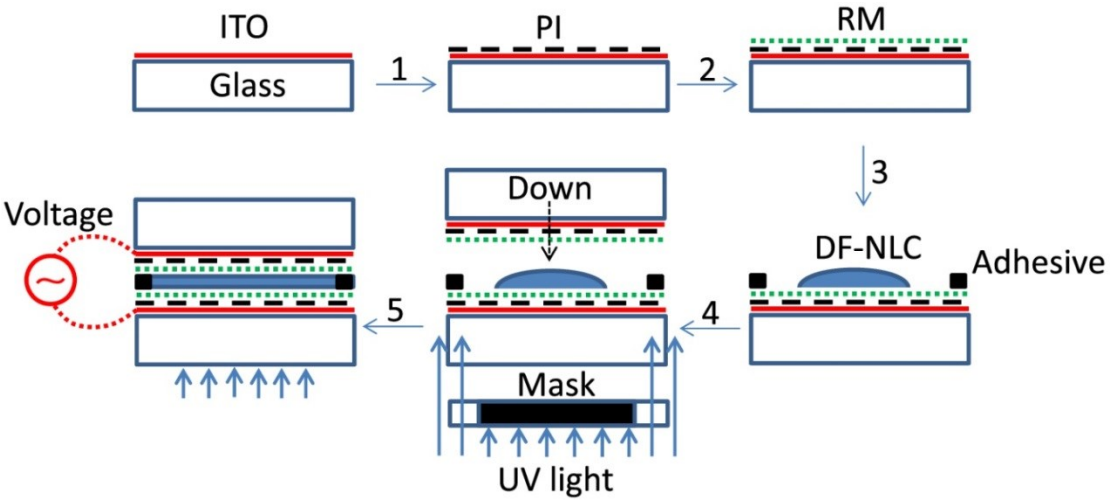

Figure 4.4 Schematic presentation of major steps of the fabrication of S-PS-DF-NLC cell (see text for details).

The original "drop-fill assembled" cells were transparent in their ground state (before the application of the electric field and before the curing of the RM layers), while having a planar-aligned director with large domains delimited by disclination (orientational defect) lines. Thus, the initial transmission of the probe beam was relatively high, which was defined by the local effective birefringence Δn_{eff} and the corresponding phase delay $\Delta\phi = d\Delta n_{eff} 2\pi/\lambda_0$, where λ_0 is the wavelength of light in vacuum and $\Delta n_{eff} \equiv n_e - n_\perp$ is the effective optical birefringence of the NLC. It is well known (see, e.g., [32] and references therein) that the addition of a strong electric field (e.g., U = 110 V; note that all voltages will further be expressed in RMS) reorients the director to become perpendicular to the cell

substrates (often called homeotropic alignment) if the electrical signal has relatively low frequency f (e.g., 1 kHz), at which, the $\Delta\varepsilon(f) > 0$. In contrast, the alignment of the director is "forced" to become planar if the frequency is high (e.g., U = 110 V at 70 kHz), at which the $\Delta\varepsilon(f) < 0$. In the case, if there is no rubbing (preferential direction), this planar alignment is strongly nonuniform. Indeed, in both cases, we observed significant reduction of the transmitted probe signal; in the first case (excited homeotropic state), because of $\Delta n_{eff} = 0$, and in the second case (planar-excited state), because of the strong scattering of light. During the above-mentioned electric-field-induced reorientation, the molecules of MR and DF-NLC underwent mutual interdiffusion [29] [30] [31]. Then, the broadband UV light source was turned on during 40 min to polymerize the RM. Then, the UV light was switched off first and then the electric field was switched off too. The final "remnant" transmission was much lower compared to the initial state.

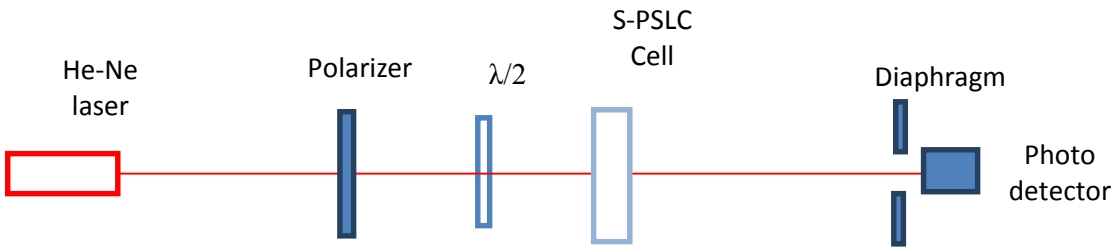

Figure 4.5 Schematics of the general experimental setup used for the "programming" and for the electro-optic study of the haze and angular dependence of light scattering of S-PS-DF-NLC cells. The half-wave plate λ/2 and the diaphragm were used later for electro-optic tests only (see hereafter).

The cells were then subjected to electro-optic measurements (after their electrical "stabilization" or "annealing" by applying U = 110 V at 1 kHz during 1 s). For the following measurements, we have used the same experimental setup that is schematically presented in Figure 4.5. At this stage we have removed the analyzer and added the half-wave plate λ/2 to change the orientation of the linear polarization of the probe beam (vertical or horizontal). The diameter of the diaphragm (also added at this stage), which is positioned just in front of the detector, was $\emptyset \approx 0.5$ mm, and its distance from the cell was

70 cm (providing a total acceptance angle of $\theta \approx 0.04$ rad). We have measured the transmission of the probe beam in different states of the cell. Thus, a low frequency (1 kHz) voltage was applied to the sample to obtain excited homeotropic state. Then the voltage was switched off to observe the natural relaxation of the cell to its ground state. Alternatively, a high frequency voltage (e.g., at 80 kHz) was applied to the cell immediately after the application of the voltage at 1 kHz to obtain planar-excited state instead of natural relaxation. All those measurements were made for two linear polarizations of the probe beam, parallel and perpendicular to the horizontal plane.

4.4 Stationary Mode Characterization

Before describing the detailed results of our electrooptic measurements, we can "visually" appreciate the performance of obtained samples. Figure 4.6 (a) shows the example of a cell, which was programmed with U = 110 V at 1 kHz. As one can see, there are two scattering states (left picture: ground state with U = 0 V, and right picture: excited planar state, with U = 80 V at 80 kHz). The cell is positioned on the top of the bar code pattern and pictures are recorded thanks to the reflected natural light without polarizers. This was made possible since the polarization dependence of our cells was noticeably lower (see hereafter) compared to the case when rubbed PI was used [29]. As we can see [Figure 4.6(a), in the center], the application of the low-frequency control (or excitation) voltage U = 110 V at 1 kHz reduces the light scattering. The analyses of the intensity distribution shows [Figure 4.6(b)] that the modulation depth is noticeably stronger between the excited homeotropic [Figure 4.6(a), center] and excited planar [Figure 4.6(a), right] states.

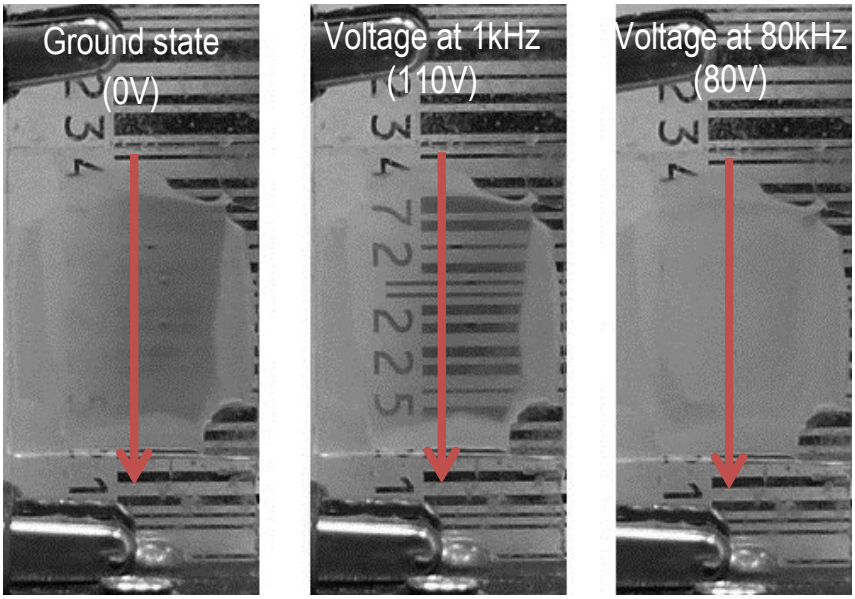

a)

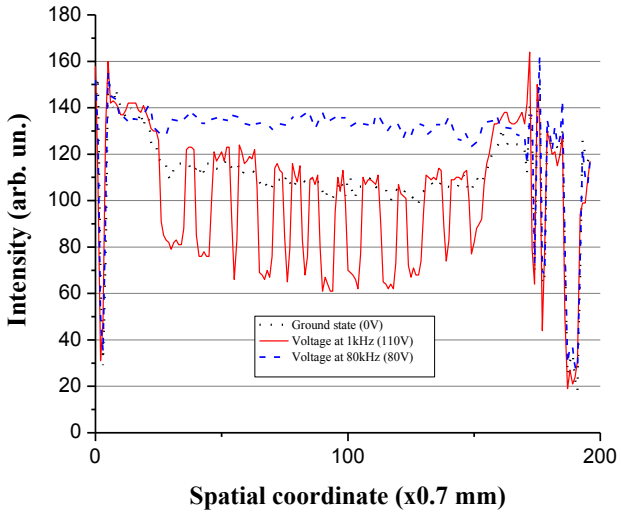

b)

Figure 4.6 Qualitative demonstration of (a) cell's scattering in its ground state (left picture, U _ 0 V), when subjected to U = 110 V at 1 kHz (central picture) and when subjected to U = 80 V at 80 kHz (right picture). (b) The comparative histograms for three key cases (vertical arrows show the scanned zones). The cell was programmed with 110 V at 1 kHz.

Similar cells were used to measure the angular distribution of the scattered light. For this experiment, the setup of Figure 4.5 was used (without the analyzer) with the photodetector and diaphragm turning around the position of the cell (all elements staying in the horizontal plane). As one can see (Figure 4.7), the probe's divergence (originally $\approx 10^{-3}$ rad) is increased by 3 orders of magnitude and it is almost twice larger for the cell that was "programmed" at 1 kHz compared to the cell programmed at 70 kHz.

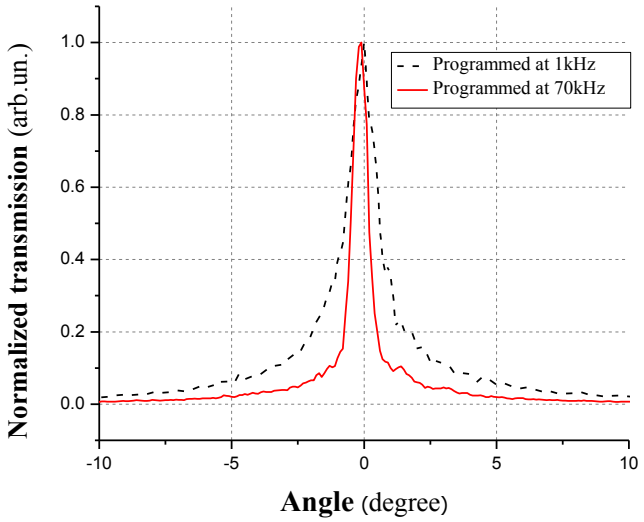

Figure 4.7 Normalized (ground state; U = 0 V) angular distribution of scattered light power for the S-PS-DF-NLC cells programmed in the presence of an electric field of 110 V at 1 kHz (dashed curve) and at 70 kHz (solid curve).

We then performed electro-optic measurements of ballistic transmission of light at normal incidence on the cell (the couple of the diaphragm and photodetector facing the incident probe beam). However, we have already presented the electro-optic characterization results of "simple" S-PSLC cells (using standard NLCs) that were programmed thanks to the positive dielectric torque (with $\Delta\varepsilon > 0$) by using electric voltages at 1 kHz [29] [30] [31]. That is why we shall describe here the behavior of cells programmed thanks to the negative dielectric torque. Thus, Figure 4.8 shows an example of the electro-optic control of light transmission in a cell that was programmed by using an electric voltage U = 110 V at 70 kHz (where $\Delta\varepsilon < 0$).

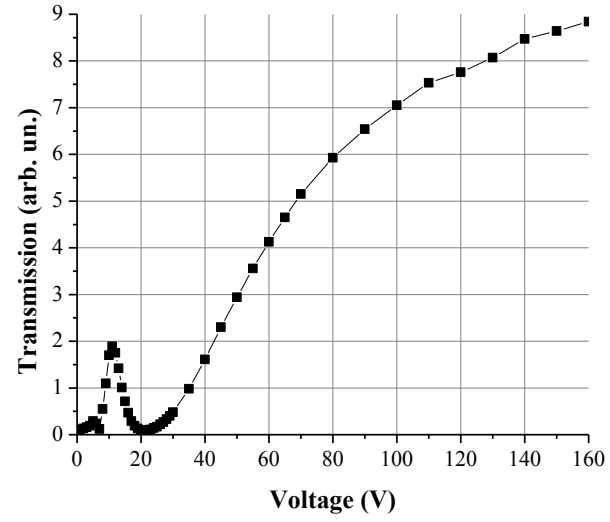

a)

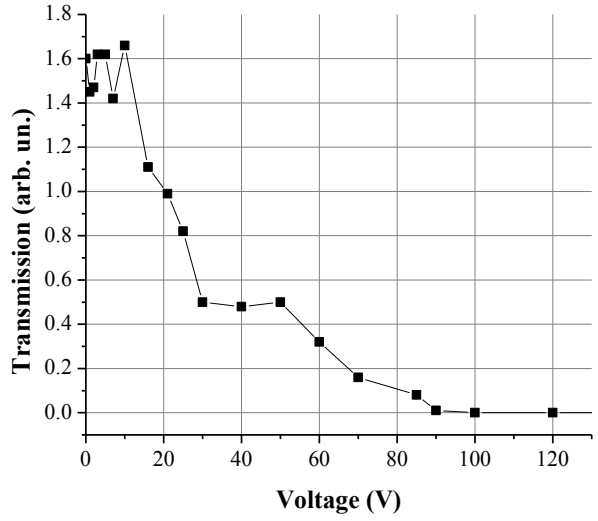

b)

Figure 4.8 Stationary dependence of ballistic light transmission upon the voltage applied to the S-PS-DF-NLC cell with frequency (a) 1 kHz and (b) 70 kHz. The cell was programmed with U = 110 V at 70 kHz.

As one can see [Figure 4.8(a)], light transmission is relatively low at ground state (when U = 0 V) and then increases with the increase of the excitation voltage at 1 kHz. The growth is not monotonic. We observe an initial increase, followed by a decrease and a final

increase of transmission. As we can see also [Figure 4.8(a) and Figure 4.8(b)], there is some weak transmitted signal in the ground state. The application of voltages at 70 kHz reduces the transmitted signal [Figure 4.8(b)] further improving the contrast of scattering modulation. Note that, here also, we see some initial oscillations, which, however, have different character (higher "frequency" and smaller modulation depth).

It is well known that the traditional scattering based devices (such as PDLCs [16]) have significant angular dependence in the transparent state (haze). We have performed haze measurements by using the setup of Figure 4.5. In contrast with previous experiments all elements of the setup were kept immobile while the cell was rotated around its vertical axes for three key states of the cell. We can see (Figure 4.9) that the light transmission drops below 50% of the value of normal incidence at approximately ±30° of probe beam's incidence angle beyond which the Fresnel reflection losses contribute significantly in the further drop of transmission.

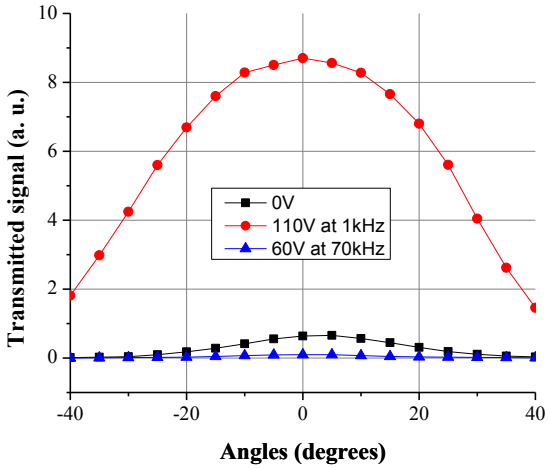

Figure 4.9 Angular dependence of the probe beam's transmission of the S-PS-DF-NLC cell that was programmed with U = 110 V at 70 kHz. Squares, circles, and triangles represent, respectively, ground state (U = 0 V) as well as excited homeotropic (110 V at 1 kHz) and excited planar (60 V at 70 kHz) states.

4.5 Dynamic Characterization

Dynamic electro-optic measurements were then conducted to analyze the transitions between different states of the cell. First, the transmission was measured (Figure 4.10) when a low-frequency excitation (110 V at 1 kHz) was applied to the cell to bring it to the excited homeotropic (transparent) state. Then the transmitted signal was monitored during the natural relaxation of director's orientation, after switching off the excitation voltage (U = 0V at t ≈ 5.6 s). Finally, the same voltage (110 V at 1 kHz) was re-established (at t ≈ 12.4 s) to transfer the cell from the ground state back to the homeotropic excited state. As expected, this last transition is very fast (being "forced"), lasting less than 10 ms.

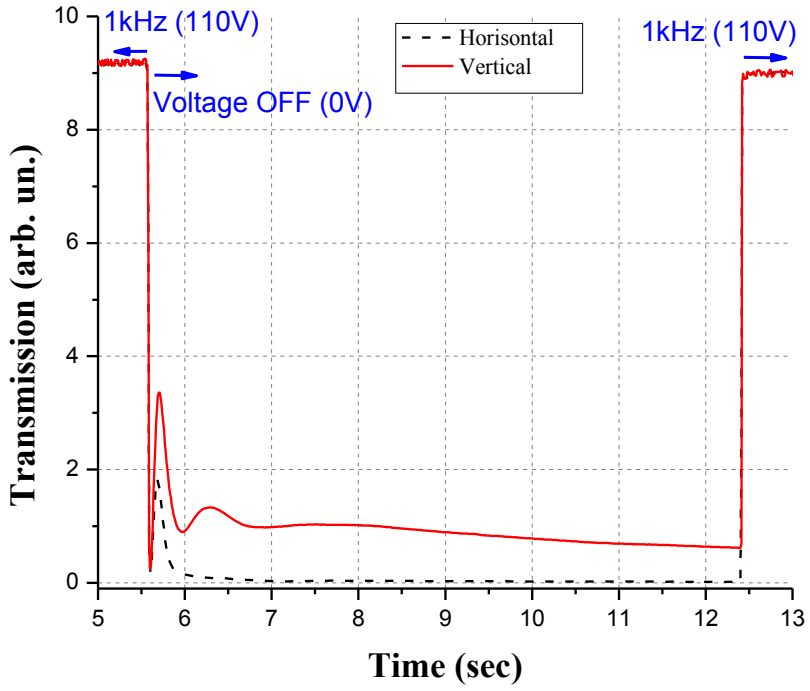

Figure 4.10 Transmission versus time for different transitions for two perpendicular polarizations (solid line, vertical; dashed line, horizontal). Excitation switching is performed (at t ≈ 5.6 s) from 110 V at 1 kHz to 0 Vand then (at t ≈ 12.4 s) from zero to 110 V at 1 kHz. The S-PS-DF-NLC cell was programmed with 110 V at 70 kHz.

The natural relaxation process being particularly interesting, we present (in Figure 4.11) a "zoom" of the initial stages of this process (from Figure 4.10). As we can see, the relaxation process is nonmonotonic and relatively long (≈0.5 s). We can also see (Figure 4.11) that the established (in the ground state) transmission values are still noticeably high while differing for vertical and horizontal polarizations of the incident light. Thus, the contrast of transition (or modulation depth) between the transparent (excited homeotropic) and scattering (ground) states is not very high and, in addition, it is different for two polarizations. An alternative type of dynamic transition was studied (Figure 4.12) by initially applying a low-frequency voltage (110 V at 1 kHz), but the excitation signal was not switched off. Instead, the voltage and frequency of excitation were directly changed to 80 V at 80 kHz (at t ≈ 4.4 s). Thus, the cell was transferred directly from the excited homeotropic state to the excited planar state. Finally, the initial excitation signal (110 V at 1 kHz) was re-established at t ≈ 11.2 s.

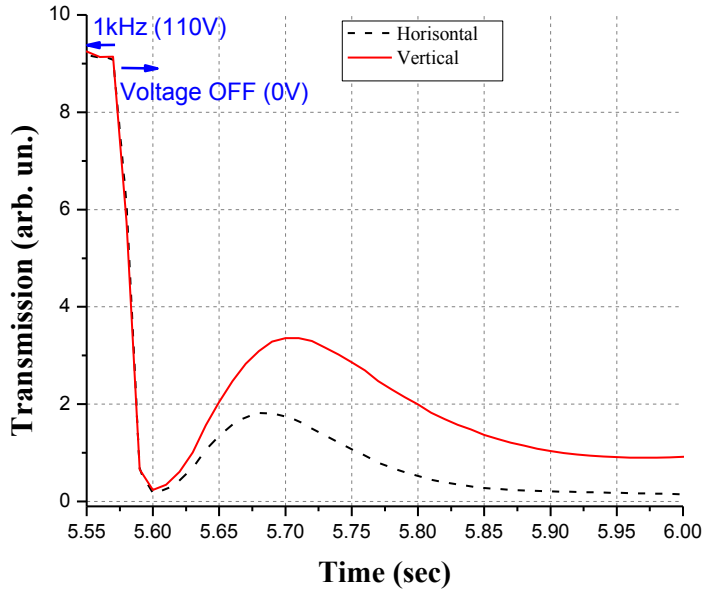

Figure 4.11 Transmission versus time during the natural relaxation process for two perpendicular polarizations (solid line, vertical; dashed line, horizontal). The S-PS-DF-NLC cell was programmed with 110 V at 70 kHz.

We can see (Figure 4.12) the following specificities in the case of switching the control frequency from 1 to 80 kHz: First, the transition from the homeotropic excitation state (110

V at 1 kHz) to the planar excitation state (80 V at 80 kHz) is monotonic and noticeably faster (≤10 ms) compared to the free relaxation (≈0.5 s). Second, the polarization dependence is now practically eliminated. Third, the transmission in the planar-excited state is very low. Thus, the modulation contrast M is significantly higher. However, we can also see (Figure 4.12) that the back transition (from excited planar to excited homeotropic state) is now noticeably slower (≈0.3 s) compared to the transition from the ground state to the excited homeotropic state (≤10 ms, Figure 4.10).

4.6 Discussion

The electro-optic and photopolymerization procedure (programming) used in our work has provided cells with strong light scattering in their ground state (U = 0 V) in contrast to the case of volume (or bulk) dispersed DF-NLC material systems, reported in [110], which were transparent at U = 0 V. Those bulk composites became scattering when high-frequency voltage was applied to the cell. In our case also the cell is scattering when being excited by high frequency electric signal. However, the application of low-frequency electric voltage brings our cell into the transparent state. There are other features in our material system (for example, the nonmonotonic behavior), which require further morphological characterization to better understand their origin. For the moment, we could speculate that the nonmonotonic behavior of transmission [upon voltage, Figure 4.8(a)] could be related to the coherent quenching phenomena since we are using a coherent probe beam and we capture the transmitted signal (through the diaphragm) in a rather small acceptance angle [111] [112]. The different character of nonmonotonic decrease (higher "frequency" and smaller modulation depth) in the case of using negative torque [Figure 4.8(b)] could be related to smaller director clusters and higher granularity (more grains with smaller sizes) of the scattered speckle pattern.

It is interesting to analyze the observed dynamic changes that were introduced by the use of DF-NLC in the surface polymer stabilized cells (instead of simple NLCs [29] [30] [31]). First of all, we were expecting that the use of DF-NLC would allow us to obtain very fast

transitions. Indeed, the transition from excited homeotropic to excited planar states is significantly faster compared to the free relaxation.

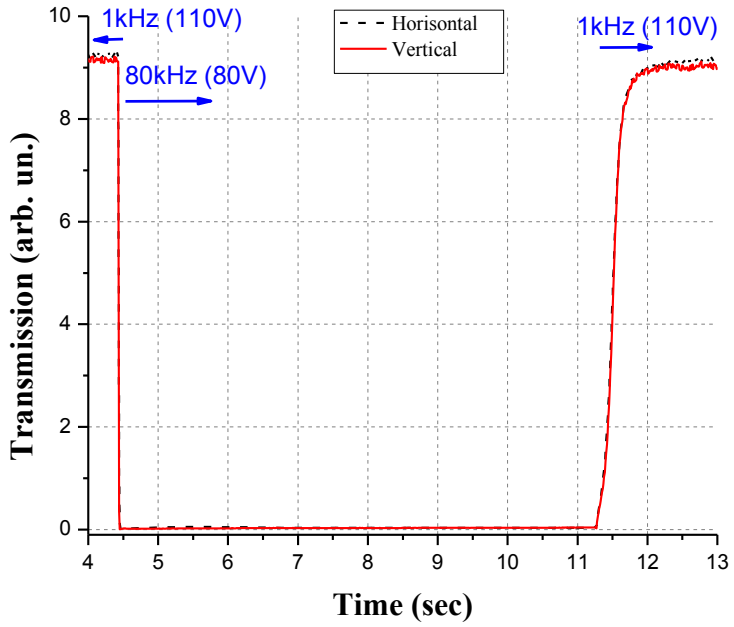

Figure 4.12 Transmission versus time for an S-PS-DF-NLC cell that was programmed at 70 kHz. Switching is performed at t ≈ 4.4 s from 1 kHz (110 V) to 80 kHz (80 V) and back to 1 kHz (110 V) at t ≈ 11.2 s. Curves for two polarizations (solid line, vertical; dashed line, horizontal) are practically coinciding.

For comparison purposes, we can use the typical value of $\gamma \approx 300$ mPas [113] and $K \approx 15.8$ pN [114] of the used DF-NLC mixture to estimate the characteristic free relaxation time $\tau_{off} \approx 4.8$ s of the standard (pure) DF-NLC layer of thickness $d = 50$ μm. As we can see from Figure 4.11, the light transmission is first quickly reduced (within ≤20 ms) followed by a slow stabilization of ≈0.5 s. We believe that the fast transition might be related to the presence of small-scale director orientation defects, predominantly near to the cell surfaces. This is confirmed by our preliminary morphological studies (Figure 4.13). Indeed, we can see that the typical nonuniformities of the director orientation defects range from <5 μm up to 50 μm. Note that the slower relaxation mode (≈0.5 s) is still significantly faster (almost by an order of magnitude) compared with the pure NLC's relaxation (≈4.8 s).

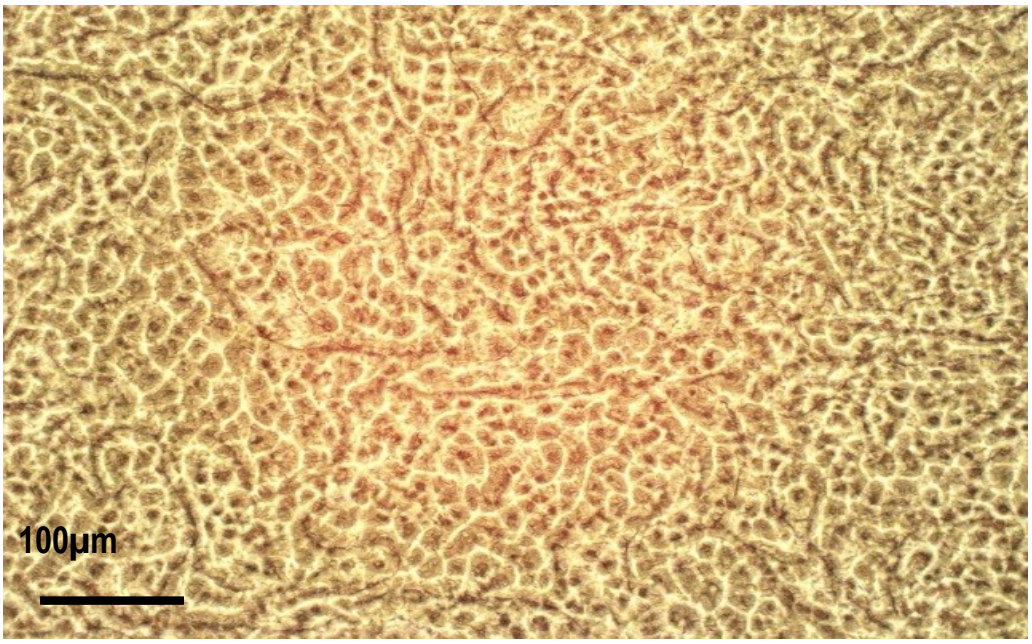

Figure 4.13 Ground-state microphotography (by using Zeiss polarization microscope) of the S-PS-DF-NLC cell that was programmed at 70 kHz.

We can also see (from Figure 4.10 and Figure 4.11) that there is still some polarization dependence (despite the fact that the PI surfaces were not rubbed) and the contrast M of light transmission's modulation between the transparent (excited homeotropic) and ground state (via free relaxation) is not very high, ranging (for two polarizations) from M = 10 to M = 58. We believe that this polarization dependence may be related to the fact that the initial drop of NLC was mechanically dispersed (by us) on the cell surface to cover the entire working zone. We can finally see (from Figure 4.10) that the transition from the ground state to the excited homeotropic state (at approximately t = 12.4 s) is rather fast (≤10 ms), which is not surprising since, as we have already mentioned, the typical excitation of the NLC's forced reorientation may be reduced by applying stronger excitations voltages [43] [107].

Most importantly, we can see from Figure 4.12 that the above-mentioned drawbacks (slow relaxation, polarization dependence, and low contrast) are eliminated if we use "forced relaxation" (see below) thanks to the DF-NLC. Indeed, in this case, the transition time between the transparent (excited homeotropic) and scattering (excited planar) states is

much faster (milliseconds). In addition, the modulation depth is significantly improved (M ≈ 173) and the polarization dependence is eliminated.

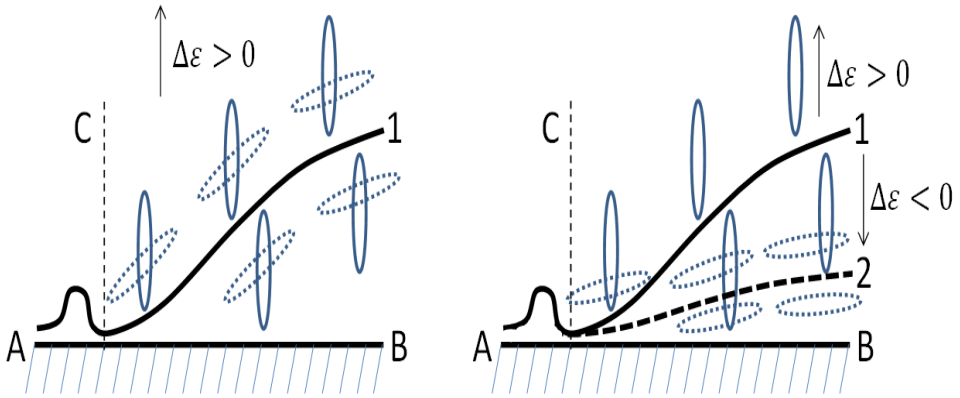

Figure 4.14 Schematic demonstration of the possible mechanism of slowing of the S-PS-DF-NLC's reaction due to the difference between (a) free relaxation and (b) forced back reorientation. The polymer aggregate (solid curve 1) is bent (dashed curve 2) toward the surface AB by the negative torque.

However, we now face another problem, which is the back transition to the transparent (excited homeotropic state). Unfortunately, it appears (Figure 4.12) that this transition now is slowed significantly. We think that this could be related to the strong repulsion of the director during the negative torque (excited planar state), which could eventually force the polymer aggregates of the surface to participate in the reorientation process as it is schematically demonstrated in Figure 4.14. Thus, Figure 4.14(a) shows the freely relaxed NLC molecules (dotted ellipses) in their ground state after being reoriented by an electric field of low frequency (via the positive torque) to be perpendicular (solid ellipses) to the cell substrate's surface AB. The solid bold curve 1 shows an angularly "mobile" part of a polymer aggregate, which is "attached" to the substrate on the left side of the image (the zone that is delimited by the vertical dashed line C). Figure 4.14(b) shows the same case of reoriented molecules (solid ellipses) as well as the case when the NLC molecules are "pushed" away (dotted ellipses) from the electric field with high frequency (via the

negative torque) to be parallel to the surface AB. The bold dashed curve 2 [in Figure 4.14(b)] shows the resulting possible reorientation of the polymer aggregate due to negative torque and the anchoring of NLC molecules to that aggregate.

The reorientation of molecules toward the normal of the surface AB (by the positive torque) may thus be relatively faster, for the case described in Figure 4.14(a), compared to the case of Figure 4.14(b) since, in the second case, the polymer aggregate would also participate by adding an additional "slow step" in the reorientation process.

4.7 Conclusion

In conclusion, we believe that the use of DF-NLC in the S-PSLC geometry may bring noticeable benefits. First of all, it allows various modes of cell programming (negative or positive torques). Second, as we saw in this work, it may greatly improve the contrast and polarization independence of light scattering. In addition, we achieved very short transition times when switching the low-frequency excitation to high frequencies (at the order of 1 ms, in the best case). However, its promise of significantly shortening the cycle of on–off–on transition was not demonstrated, very likely because of the specific surface polymer morphology. At this stage, we do not know yet how to improve the "slowed" transition without changing the surface of the cell and without allowing further interpenetration of the RM and NLC molecules (which would bring the material system closer to the PSLC case, [110]). However, we believe that, if needed, the total on-off-on cycle duration may be further optimized by the appropriate choice of the excitation amplitudes at higher frequencies (via the negative torque). Also, another potential drawback must be taken into account (when considering the use of DF-NLCs) that is the strong temperature dependence of the excitation frequency zones for negative and positive torques [113] [114].

We acknowledge the financial support of the Natural Sciences and Engineering Research Council of Canada (NSERC). We are also grateful to TLCL Optical Research Inc. and LensVector for their material support.

Chapter 5

Surface Polymer Stabilized Dual Frequency Chiral Liquid Crystals

There are a multitude of liquid crystalline textures, most of which are based on chiral systems. The properties and textures of chiral liquid crystals, as we have seen in introduction section, can vary significantly from their non-chiral analogues.

Cholesteric liquid crystals have two sets of properties that do not exist in non-chiral nematics and that can be used to generate electro-optical effects [1]. One of these properties is the selective reflection of light of a particular wavelength or circular polarization. For the light travelling parallel at the helical pitch of a cholesteric material, selective reflection occurs for light of a wavelength of circular polarization and $\lambda_0 = \bar{n} \times p$. Here, λ_0 is the wavelength in air and $\bar{n}$ is the average refractive index. The pitch p is defined as the distance required for the director for the rotation by 2π around the helical axis. The modification of pitch (by changing the temperature or by the application of an external field) can change the wavelength of the selective reflection.

Another useful property for electro-optical effects is the existence of several stable textures for a cholesteric material. These are the planar texture and the focal conic texture and the homeotropic texture, wherein the helix is unwound by external forces. These textures have different polarization and scattering properties and devices can be built to switch between these different textures by applying an electric field. The planar and focal conic textures can each be stable, so that the bistable devices can be constructed.

Here the method we used is based on the use of dual-frequency liquid crystal mixed with chiral dopant in S-PSLC geometry presented in chapter 4. By mixing CL dual frequency with a small amount of chiral molecules we get a chiral LC (CLC), and we assume that it must retain the properties of "dual frequency". So we have a dual frequency CLC (DF-CLC). To destroy the helical structure, we apply an electric field, which corresponds to a

positive dielectric anisotropy of material, and to reform the helical structure, we will apply another field, corresponding to a negative dielectric anisotropy of material. The helical structure (planar state) is equilibrium state for the negative dielectric anisotropy, which is why the field "helps" and speeds up the relaxation process. So the DF-CLC mixture may be used to obtain a controllable light backscattering (and so controllable energy flow) and different stable textures using the chiral properties of this mixture and simultaneously improve contrast ratios and relaxation times using the "double frequency" properties of this mixture.

This chapter is based on the review article, where we describe the use of *chiral* DFCLs to build surface polymer-stabilized dual frequency cholesteric liquid crystal (S-PS-DF-CLC) cells with our method of surface programming. Given the rich variety of possible programming conditions, in the article we focus our attention on the influence of the prepolymerization duration parameter of the RM and demonstrate that it plays a crucial role in the behavior of the cell. The corresponding spectral and electro-optical characteristics, also the results of dynamic, angular and morphological studies of obtained cells are presented as well.

Resumé de l’article inseré

Cristaux liquides chiraux à double fréquence stabilisé par un polymère en surface

Les matériaux composites polymères-cristal liquide (CL) offrent des moyens rentables pour atteindre des fonctionnalités électro-optiques améliorées. Des morphologies de types volume-dispersé et phases-séparé (de degrés divers) ont été intensivement étudiés dans le passé et sont brièvement décrits dans ce travail. En outre, on considère le cas particulier où les structures CL-polymère sont formées à proximité des substrats de la cellule. Pour ce faire, des revêtements polymères partiellement durcies et orientés sont utilisés comme couches d'alignement pour CL chiral à double fréquence. Le durcissement partiel est destiné à permettre une interpénétration partielle entre les molécules de CL et celle du polymère pour former des réseaux de polymère stabilisées en surface. Après une période d'interpénétration courte (entre les revêtements de polymère et le CL en volume), un couple diélectrique positif est appliqué et l'exposition UV est utilisée pour durcir définitivement le système. Nos études électro-optiques, spectroscopiques et microscopiques montrent que la durée du pré-durcissement joue un rôle crucial dans le comportement de la cellule. Il est montré que l’interdiffusion moléculaire génère des défauts d'alignement des cristaux liquides autour des agrégats de polymère sur les surfaces internes de la cellule. L'alignement hors du plan et les petits agrégats polymères obtenus sont à l'origine de la diffusion contrôlable de la lumière. Entre autres, certains défauts linéaires sont formés par le couple positif, qui sont éliminés quand un couple diélectrique négatif est appliqué.

Liquid Crystals Reviews, 2014
Vol. 2, No. 1, 60–71, http://dx.doi.org/10.1080/21680396.2014.947528

Surface polymer stabilized dual frequency chiral liquid crystals

Amalya Minasyan and Tigran Galstian

Center for Optics, Photonics and Lasers, Department of Physics, Engineering Physics and Optics, Laval University, Pav. d'Optique-Photonique, 2375 Rue de la Terrasse, Québec, Canada G1V 0A6

(Received 8 April 2014; accepted 19 July 2014)

Abstract

Polymer-liquid crystal (LC) composite materials provide cost-effective ways to achieve enhanced electro-optic functionalities. Corresponding bulk-dispersed and phase-separated (of various degrees) morphologies were intensively studied in the past and are shortly described in this work. In addition, we consider the specific case when the polymer-LC structures are formed near to the cell substrates. To achieve this, partially cured and oriented polymer coatings are used as alignment layers for dual frequency chiral LC. The partial curing is intended to allow a partial interpenetration between the LC and the polymer molecules to form surface-stabilized polymer networks. After a short interpenetration period (between the polymer coatings and the bulk LC), a positive dielectric torque is applied and UV exposition is used to definitely cure the material system. Our electro-optical, spectroscopic and microscopic studies show that the pre-curing duration plays a crucial role in the behavior of the cell. It is shown that the molecular interdiffusion generates defects of LC alignment around polymer aggregates on the cell's internal surfaces. The obtained out-of-plane alignment and small polymer aggregates are at the origin of formation of controllable light scattering. Among others, some linear defects

are formed by the positive torque, which are, however, eliminated when a negative dielectric torque is applied.

Keywords: chiral liquid crystals; reactive mesogen; photopolymerization; pretilt; scatter; defects

5.1 Introduction

Liquid crystal (LC) materials have several well-known applications, including displays, [44] image conversion [115] and polarization control [116] as well as focusing and imaging [117]. The ground-state (non-excited) alignment of LC molecules is very important in majority of those applications where it is used as a default state that is retrieved once the excitation is switched off. Various methods, ranging from mechanical rubbing, vacuum deposition and photo alignment, were developed to obtain a predetermined ground-state alignment of the LC [6] [7]. This was mainly obtained via the surface-mediated interactions between the "pure" LC layer (it is a mixture of various LC molecules in most cases) and the solid "discrete" interfaces (typically rubbed polyimide) [6]. Those surfaces were proven to be very efficient (and widely accepted in the industry) for the uniform alignment of LC, but their market acceptance remains rather limited both for in-plane patterning [7] and for out-of-plane pretilt control [8] [9] [118], while, if successfully implemented, they might enable more functionalities and new interesting applications.

To further increase the functionality of LC-based devices, various composite solutions were experimented, including polymer-dispersed LCs (PDLCs) [16] and polymer-stabilized LCs (PSLCs) [109]. Both of those approaches were typically using an initial mixture of LC with a photo-polymerizable monomer composition to build bulk non-uniform polymer-LC dispersions. For example, in the case of the PDLC, the initial monomer content may be very high (at the order of 75 wt%) and it must be chosen to be miscible with the LC, but must repulse the LC molecules from the polymerized areas (obtained by photo or thermal

curing of the monomer or by solvent evaporation), thus forming sub-micrometric phase-separated droplets of LC (Figure 5.1). The operation principle of those films is based on light scattering, which is typically high without electrical voltage applied to the cell (the effective refractive index $n_{LC}(V_0=0)$ of LC droplets being different from the refractive index *nP* of the polymer matrix, $n_{LC}(V_0 = 0) \neq n_P$*)* and which becomes low when the *director* (the local average orientation of long axes of LC molecules) is aligned along the applied electric field, providing thus the "refractive hiding" (or optical matching) condition: $n_{LC}(V_0 \neq 0) \approx n_P$. While such films have already found certain market acceptance (e.g. as privacy windows with relatively short relaxation times τ_{PDLC}*)*, there are still significant challenges remaining, which are of rather fundamental character. One of them is the *haze*: the scattering dependence upon the light incidence angle. Indeed, if the optical matching may be achieved for the normally incident beams (Ray A, Figure 5.1), the rays at tilted incidence (Ray B, Figure 1) may still be scattered (Ray B', Figure 5.1) because of the local anisotropy of the LC.

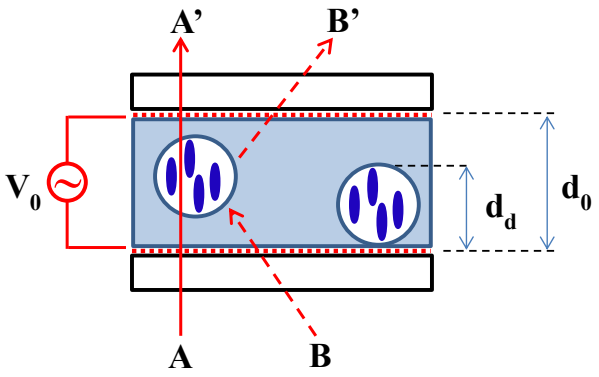

Figure 5.1 Schematic presentation of a PDLC cell and its operation principle. Dotted horizontal lines (at distance d0) show transparent electrodes (e.g., ITO). Two circles (of diameter dd) show the LC droplets (filled vertical ellipses showing the LC molecules; when voltage V0 is applied to the ITOs) dispersed within the polymer matrix. A and B represent incident rays at normal and tilted angles, while A' and B' show the transmitted and scattered rays, respectively.

The second drawback of those material systems is the high driving voltage required. Indeed, the driving voltages in a pure LC cell must be at the order (above) of certain

threshold value V_{th}, defined as $V_{th} = \pi[K(\varepsilon_0|\Delta\varepsilon|)]^{1/2}$, [43] where K is the elastic constant of the LC, ε_0 is the dielectric constant of the vacuum and $\Delta\varepsilon$ is the dielectric anisotropy of the LC. Thus, it is easy to estimate that the typical values of V_{th} are at the order of 1V. Given the geometrical factors of the PDLC layer (Figure 5.1), the applied voltage V_0 will be split into a part (drop of electrical potential) applied on the polymer and another part applied on the LC droplet. For a simple estimation of corresponding required voltages, let us consider the right droplet (Figure 5.1). For the sake of estimation, we shall consider the dielectric constants of the polymer matrix and of the LC droplet as $\varepsilon_P \approx 5$ and $\varepsilon_{LC} \approx 7$, respectively. In this case, the voltage drop on the LC droplet will be expressed as $V_{LC} \approx V_0/[1 + \varepsilon_{LC} (d_0 - d_d)/(\varepsilon_P d_d)]$ [46]. Thus, if we consider $d_0 \approx 10\mu m$ and $d_d \approx 0.1\mu m$, then the values of voltage V_0 (applied to the transparent electrodes of the PDLC film) must be almost two orders of magnitude higher than those applied to pure LC cells. This requires electrical certification before its installation in residential buildings (there are also cost and format issues, which complicate the broad commercialization of this product).

The typical approach for the fabrication of bulk PSLCs is schematically represented in Figure 5.2. The initial material system (Figure 5.2(a)) is a mixture of a monomer (short horizontal lines) and a LC (horizontal filled ellipses), at typical concentrations of ≈3 wt% and ≈96 wt%, respectively (less than 1 wt% being typically used for the polymerization initiation system). After the polymerization of the monomer, polymer chains, walls and aggregates are formed (Figure 5.2(b)). In the example schematically shown here, the material system remains uniform and light at different angles of incidence (rays A and B) is not scattered (A' and B'). The application of the electric field induces reorientation of the director, which is not uniform in space (Figure 5.2(c)) since the polymer network plays the role of distributed "cavities". In this case, light is scattered (A–A' and B–B', Figure 5.2 (c)), the corresponding voltages required being slightly higher than those for pure LC cells of the same thickness d_0, since the effective cavity sizes d_d are smaller here (for similar reasons described earlier). The relaxation times τ_{PSLC} here are shorter than those in pure LC cells (τ_{LC}), which are defined by the rotational viscosity γ and the elastic constant K of the LC, as well as the effective cavity size d_d as $\tau_{LC} \approx \gamma d_d^2/(K\pi^2)$ [119]. It is worth noting that, depending on the way how the PSLC is made, the light scattering may be strongly

polarization dependent and also of inversed mode (scattering without electric voltage and transparent when a strong voltage is applied) [105].

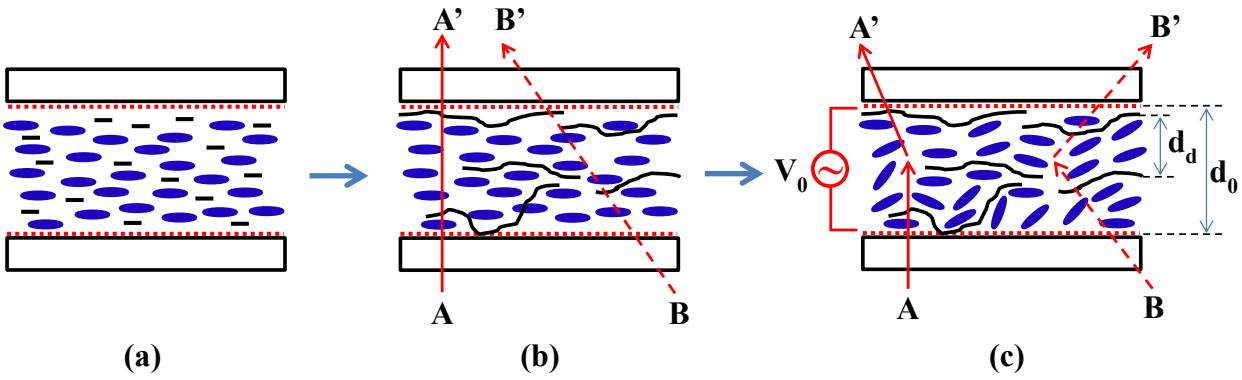

Figure 5.2 Schematic presentation of a PSLC cell and its operation principle. Dotted horizontal lines (at a distance d0) show transparent electrodes. Short horizontal lines (a) show the monomer molecules (not necessarily aligned along the LC molecules, shown by horizontal filled ellipses). Large curved lines (b) show the polymer walls and bundles. The application of voltage V0 initiates nonuniform LC reorientation (c) and corresponding light scatter.

The aforementioned schematic presentation of the PSLC suggests a more or less uniform polymerization process. In some previous efforts, a longitudinal gradient (from the center of the cell to the interface between the LC and the cell substrate) was demonstrated (Figure 5.3) by using the photopolymerization that was initiated from one of the external sides of the cell (Side B, Figure 5.3(a)). Indeed, in this case the UV light (for example, used to build the PSLC cell) is strongly absorbed at interfacial slices of that mixture. Thus, the polymerization process is initiated in those areas [101] and the diffusion of monomers (from the center to interface B of the LC layer) may create higher density of the obtained polymer network near substrate B of the cell. Thus, a gradient of polymer network is obtained, which may be configured (either in the longitudinal [101] or in the lateral directions [120]) to enable additional useful functionalities.

In parallel, authors of ref. [22] have shown that very limited degree of interpenetration (between the LC molecules and the polyimide alignment layer) may be obtained with an appropriate thermal treatment of LC cells in the presence of external fields (here, magnetic). This brought the attention of several research groups (including our) to the possibility of having "soft" polymer interfaces

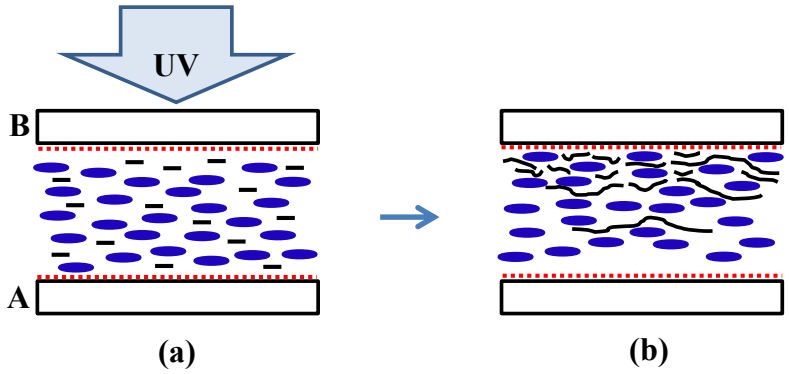

Figure 5.3 Schematic presentation of fabrication of a nonuniform PSLC cell. The original mixture is exposed from one side of the cell (a) and the diffusion of monomers creates higher polymer network density from that side of the cell (b).

where this interpenetration might be more efficient and provide more flexibility for the configuration of the ground-state LC alignment, which, consequently, may affect the performance of the LC cell in the excited state. An attractive avenue, in this direction, was the use of reactive mesogen (RM) molecules in a mixture with LCs [101]. Alternatively, the RM layers were also cast on the internal surfaces of cell substrates (as partially cured distinct layers, Figure 5.4) and used to fabricate LC cells, enabling several interesting properties [29] [30] [31] [121] [89] (see also, for example, refs. [122] [123] [124] [125]).

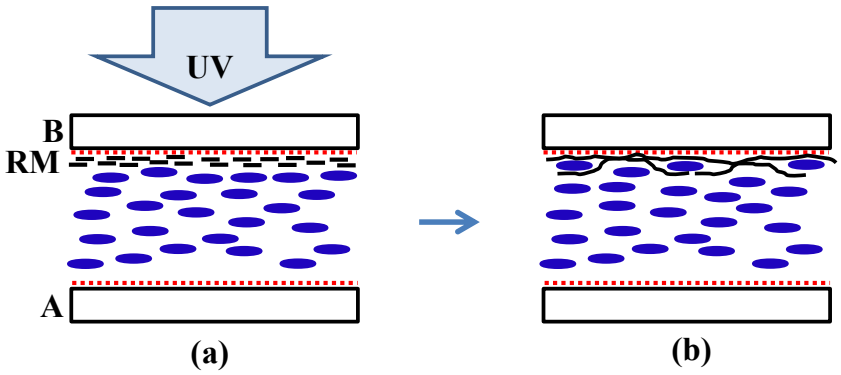

Figure 5.4 Schematic presentation of the fabrication of a S-PSLC. The partially cured RM layer is cast and aligned on the internal surface of the cell (a). Partial interpenetration between the RM and LC molecules is allowed before the photo polymerization of the RM (b).

Our group was exploring this avenue in the hope to control both the in-plane organization of LC molecules (photopolymerization via an amplitude mask) and their out-of-plane pretilt (photopolymerization in the presence of external fields) [29] [30] [31] [121] [89]. We have observed some fascinating phenomena, including 2D molecular self-organization [29] and photo-controlled wetting and capillarity [89] in the interface between the LC and the RM. However, the precise control of the pretilt angle appeared to be a rather difficult task for us. Despite this, the use of a separate interfacial RM layer has shown great potential for the control of the ground-state LC alignment, enabling the fabrication of cells with electrically controllable light scattering (for such applications as privacy windows, smart lighting, etc.). Among the important advantages of such systems (e.g. versus the PDLCs) is the fact that the alignment defects here are formed mainly at the LC interface and the haze is significantly reduced in the on-state (when the LC adopts homeotropic alignment, see later in the article).

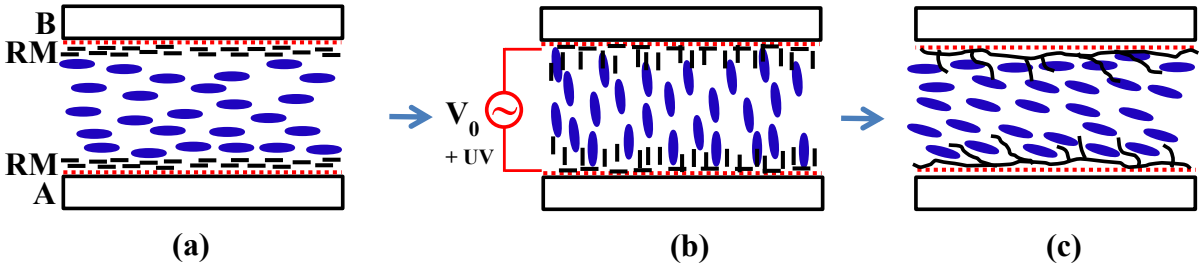

Figure 5.5 Schematic presentation of the fabrication of an oriented (programmed) S-PSLC cell. The partially cured RM layers are cast and aligned on the internal surface of the cell (a). Partial interpenetration between the RM and LC molecules is allowed under an applied electric field (b) before the photo polymerization of RM layers (c).

The typical approach here (Figure 5.5) consists in starting the cell fabrication by spin coating a thin (typically few 100 nm) layer of RM on a substrate having already transparent electrodes (indium tin oxide, ITO) and unidirectionally rubbed polyimide layers (see later for details). The critical step in cell fabrication is the period between the moments when the LC is drop-filled into the sandwich (composed of two earlier mentioned RM-coated substrates, with RM layers facing each other inside the cell) and when the RM layer is photopolymerized. Molecular interdiffusion is allowed between two liquids (LC and RM) during this delay (before the RM is photopolymerized). A limited degree of partial polymerization or pre-polymerization (or pre-cure) can be used to control this process. In addition, the application of external fields may affect significantly this interdiffusion. For example, such fields may align the composite material system during the final photopolymerization, enabling thus specific out-of-plane orientational states. We have named this process as "programming" of the transitional material zone (between the "hard" polyimide interface and the bulk LC), and given the proximity of the RM layer to the substrate, we call those systems as "surface PSLCs" (S-PSLCs) [29] [30] [31] [121]. In fact, there are many parameters that can be used to control the programming process: the choice of LC and RM molecules, the LC–RM contact time (before RM's polymerization), the degree of pre-polymerization of RM (defined by the duration of pre-polymerization Δt_{pp} for a given curing intensity and temperature) and the electric (or magnetic) field induced reorientation of molecules. In addition, given that the molecular diffusion here is strongly anisotropic, one can expect significant differences if the LC and RM molecules are parallel

to the surface (e.g. without an electric field or with a field generating a negative dielectric torque; when the LC's dielectric anisotropy is $\Delta\varepsilon < 0$) or perpendicular to it (in the presence of an electric field with a frequency corresponding to the positive dielectric anisotropy $\Delta\varepsilon > 0$ of the LC). The use of dual frequency nematic LCs (DFLCs) may enable not only obtaining both the aforementioned programming regimes [121], but also introducing more possibilities of dynamic control during the post-programming operations of the cell.

In the present work, we describe the use of *chiral* DFCLs to build surface polymer-stabilized dual frequency cholesteric liquid crystal (S-PS-DF-CLC) cells, which, in addition to the controllable light scattering, exhibit also resonant reflection phenomenon. This may be used for color control and light reflection (thus potentially extending the use of our films in the so-called smart window applications). Given the rich variety of possible programming conditions, in the present work we shall focus our attention only on the influence of one parameter: the prepolymerization duration Δt_{pp}. Thus, various durations of Δt_{pp} will be considered to demonstrate its role. The corresponding (for each Δt_{pp}) spectral and electro-optical characteristics (at different control conditions) of obtained cells will be presented. The results of dynamic, angular and morphological studies also will be provided.

5.2 Materials and methods

We have used commercial microscope slides (Fisher Scientific) as glass substrates (of 1mm thickness) which were covered (in-house) by uniform ITO coatings to build our S-PS-DF-CLC sandwich-like cells. As briefly mentioned earlier, two additional layers were coated on the ITO surfaces prior to the LC cell construction. The first one was a standard layer of ≈50-nm-thick polyimide (PI-150 from Nissan). The PI-150 was spin-coated on the ITO glass substrate (3000 rpm for 30 sec), cured (at 280◦C) and then rubbed to obtain planar alignment layer. The second one was a layer of RM (RMS03-001C, delivered from Merck as a 30% (w/w) solution in propylene glycol monomethyl ether acetate solvent) of positive

anisotropy (n_{oRM}=1.525, Δn_{RM}=0.155) that was spincoated (3000 rpm for 30 sec) onto the rubbed PI-150 layer to obtain ≈ 600-nm-thick RM film. The thicknesses of the thin films were measured sequentially by using the profilometer DekTak (the height difference was measured by using the profilometer between an untouched film section and a section where the film has been removed). The obtained substrate was then dried and annealed (by heating for ≈ 90 sec at 60◦C on a temperature-controlled hot stage). Then the RM layer was pre-polymerized at different degrees (see later) by exposing it to UV light for different durations (Δt_{pp} ranging from 0 to 30 min for different cases). Two such substrates were used to build (within few minutes after the pre-cure) the sandwich-like cell of the S-PS-DF-CLC by using the so-called drop-fill method. The first substrate was placed horizontally with the RM layer facing up and a droplet of the mixture (9.72% by weight) of a chiral dopant: (R,R) 1-phenyl-1,2-bis[4-(trans-4- pentylcyclohexylbenzenecarbonyl)]ethane (purchased from AWAT Comp.) with the DFLC: MLC2048 (90.28% by weight) was placed onto the surface of the RM layer (the MLC2048 is a well-known LC mixture with clearing point =106°C, n_{oLC}=1.4978, optical anisotropy Δn_{LC}=0.2214 and dielectric anisotropy $\Delta\varepsilon_{LC}$=3.22 at 1kHz and $\Delta\varepsilon_{LC}$=-3.40 at 100kHz at 20°C). The periphery of the substrate was covered by using UV curable adhesive walls (AC A1432-Q-S2 from Addisson) containing glass spacers (diameter ∅ ≈ 5μm) to provide the desired thickness of the cell. Then the second (identical) substrate was quickly pressed (with the RM layer facing down) on the drop of the LC mixture and the peripheral adhesive was cured by a UV lamp (with spectra between 300 and 450 nm, intensity of ≈ 10mW/cm^2, irradiation time ≤ 10 min, exposition at room temperature T = 22◦C, with particular attention to avoid heating) while protecting the central part of the cell (that is, the two RM layers) by a mask.

The obtained cell was then stored in the dark, but subjected to a programming electric field (root mean square (RMS) voltage U = 40VRMS, alternative current (AC) of sinusoidal (SIN) form at 1 kHz) during Δt_d = 10 minutes to allow some molecular reorientation (supposing homeotropic state of alignment) and partial interpenetration of LC and uncured RM molecules, prior to total curing of RM by using the same UV lamp for 40 min. Since the polymerization was performed in the nonequilibrium state, the obtained cells were subjected to a critical voltage pulse (e.g. an AC voltage of $U = 110V_{RMS}$ and 1 kHz

frequency for 1 sec) to obtain a stabilized (ground-state) material morphology prior to its characterization (we shall further omit the index RMS for convenience of writing).

5.3 Experimental setup and process

The typical characterization of obtained cells was done by measuring the transmission spectra for different states of the cell. These spectra were measured by using Sciencetech spectrometer (the monochromator was placed at 3 cm from the cell; the opening of the monochromator was 0.5 mm). First, the transmission spectrum of the sample was measured at the "ground state" (no voltage applied). Then, we measured transmission spectrum of the cell by applying a low frequency (1 kHz) voltage to obtain excited homeotropic state (thanks to $\Delta\varepsilon_{LC} > 0$). Then, the electrical excitation was switched to a high frequency voltage (e.g. at 90 kHz) to "force" the LC into "helicoidal" excited state (since $\Delta\varepsilon_{LC} < 0$). The natural relaxation was observed by simply switching off the applied voltage.

As a reference (for qualitative comparison only of possible orientational states), we have also built similar cells by using a "single frequency" cholesteric LC with $\Delta\varepsilon_{LC} > 0$ (MDA-02-3211, from Merck). The PI-150 was not rubbed here. The cell's thickness was ≈ 8μm. The cell was subjected to an electric field $U = 60$V (AC of SIN form at 1 kHz) during the programming. The RM layer was not pre-cured ($\Delta t_{pp} = 0$ min). We measured the transmission spectra of this cell before programing (just after the assembly of the cell, see Curve 1 in Figure 5.6), also for the programmed cell at the ground state ($U = 0$V, Curve 2 in Figure 5.6) and when a low frequency voltage was applied to the cell ($U = 75$V at 1 kHz, Curve 3 in Figure 5.6). As can be seen, we obtained (as expected) a resonant character of transmission (Curve 1 in Figure 5.6, $U = 0$ V, before programming) when we recorded the spectrum before applying the electric field. This resonant character disappeared once the programming was done (application of an electric field and then photopolymerization); we observed low transmission for the cell at its ground state (Curve 2 in Figure 5.6, $U = 0$ V, after programming) and a relatively high transparency (Curve 3 in Figure 5.6, $U = 75$V at 1 kHz, after programming) corresponding to the homeotropic state of the cell. As the RM

was not procured here, it could diffuse into the bulk of the LC and the focal conic polymer-stabilized texture could be formed in the low light transmission state [126]. While the spectral characteristics of this cell are very interesting in general, the transitions between the transparent (homeotropic) and scattering states are relatively slow and the resonant character of reflection is lost after the programming (impossible to recover by the field).

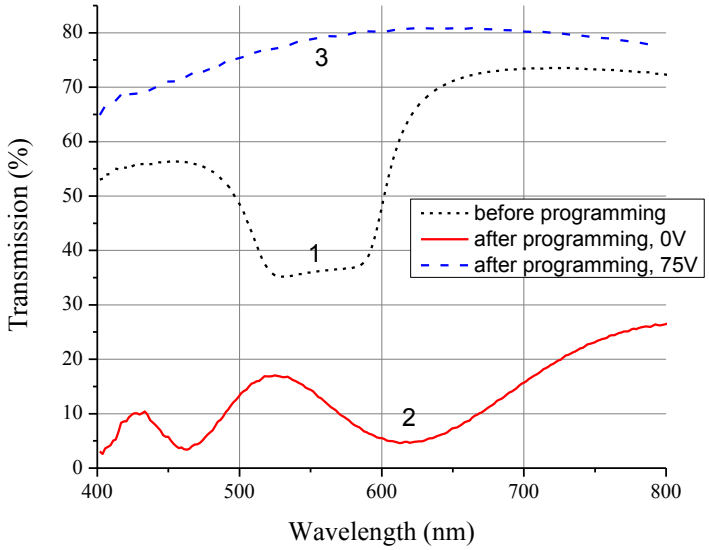

Figure 5.6 Transmission spectra of the S-PS-CLC cell that was programmed with U=60V voltage at 1kHz. A single frequency CLC was used as LC. The RM wasn't cured before applying the programming voltage (Δtpp = 0 min.). Curves 1 – before programming and 2 – after programming (in ground state, U=0V); 3 – after programming (excited by U=75V at 1kHz).

This is the reason why the use of dual frequency chiral LC becomes very attractive (all the following cells of S-PS-DF-CLCs will be based on such LCs). Those cells were characterized for different pre-polymerization durations Δt_{pp}. To compare with the previous case, we start with the case of $\Delta t_{pp} = 0$ min. The transmission spectra of this S-PS-DF-CLC cell were measured for three key states: ground state (no voltage applied, $U = 0$ V), homeotropic state (an excitation voltage is applied at low frequencies, $U = 120$V at 1 kHz) and planar state (the same excitation voltage is applied, but at high frequencies, $U =$

120V at 90 kHz). We can see from Figure 5.7 that in all cases, the obtained curves are more or less similar. Thus, not only did we not observe a resonant character (in the visible spectra), but our capacity to change the transmission regime (from transparent to scattering and vice versa) was also completely lost because of the too strong interpenetration of LC and RM molecules. Indeed, this is very likely a complete dilution and, given the thickness of each RM layer (≈ 0.6μm) and of the LC cell (≈ 5μm), this mixture would correspond to an almost 24% of RM mixture with the LC matrix.

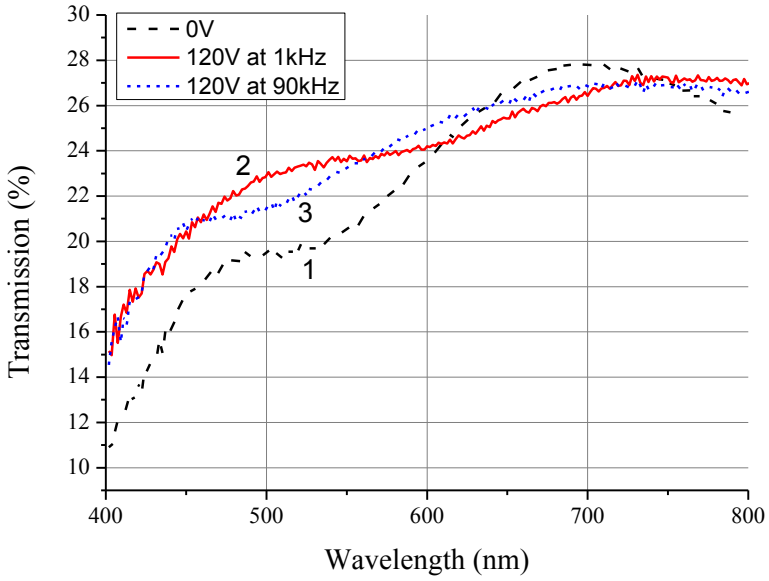

Figure 5.7 Transmission spectra of the S-PS-DF-CLC cell programmed with U=40V at 1kHz. The RM was not cured before applying the programming voltage (Δtpp = 0 min). Curves 1 - 0V; 2 – 120V at 1kHz; 3 – 120V at 90kHz.

The extreme opposite case of cell programming would be the complete curing of RM layers. We can see, from Figure 5.8, that in the case of almost complete curing of RM (Δt_{pp} ≈ 30 min), as expected, we obtained again the typical resonant character (Curve 1) for the "ground state" (U = 0 V). The transmission drop corresponds to the resonant wavelength of $\lambda_R \approx 630$ nm. The same type of behavior (Curve 3, Figure 5.8) with slightly reduced resonant wavelength (at $\lambda_R \approx 620$ nm) is obtained for the forced "helicoidal" excited state (with U = 90V applied at 90 kHz). Finally, the resonance disappears (Curve 2, Figure 5.8) when a low frequency excitation voltage (U = 90V at 1 kHz) is applied to the cell.

Unfortunately, two of three "most interesting" states (with high and low transmission, as shown by Curves 3 and 2 of Figure 5.6) are not achieved with this cell. However, in contrast to the reference case, at least all the three key states can be recovered by changing the frequency of excitation. Also, the relaxation process here can be significantly accelerated.

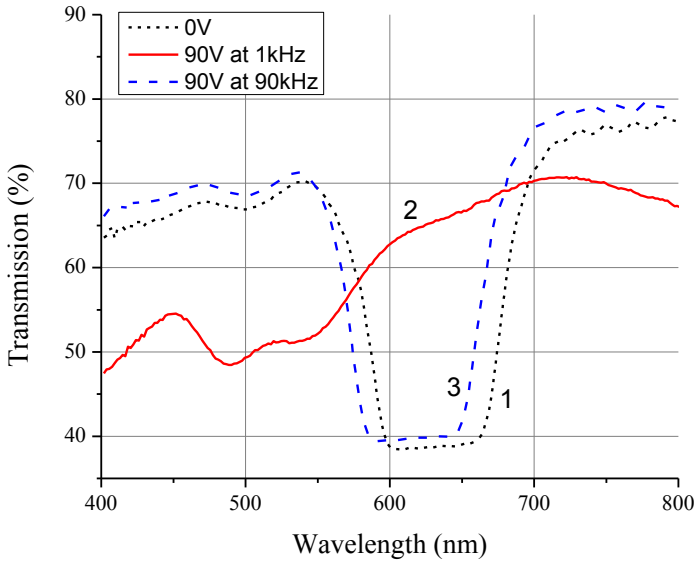

Figure 5.8 Transmission spectra of the S-PS-DF-CLC cell (programmed with U=40V voltage at 1kHz with the RM cured for Δtpp = 30 minutes). Curves 1 - 0V; 2 – 90V at 1kHz; 3 – 90V at 90kHz.

Indeed, we have done several dynamic studies with this cell (see later in the article). This was done by using an integration sphere in a reflection geometry, allowing us at the same time to clarify the nature of the resonant drop of transmission. The corresponding spectral reflectivity measurement setup is presented in Figure 5.9. The beam of a white light source WLS (SuperK COMPACT – Supercontinuum White Light Laser, from NKT Photonics) was split by the beam splitter (BS). The reflected beam (from the BS) was directed on the S-PS-DF-CLC sample (S) at normal incidence. The reflected light (from the sample) was then detected by the integrating sphere (IS), positioned at the opposite side of the BS. The

sample was placed at a distance of 15mm from the IS, the opening diameter of which was 9.5 mm.

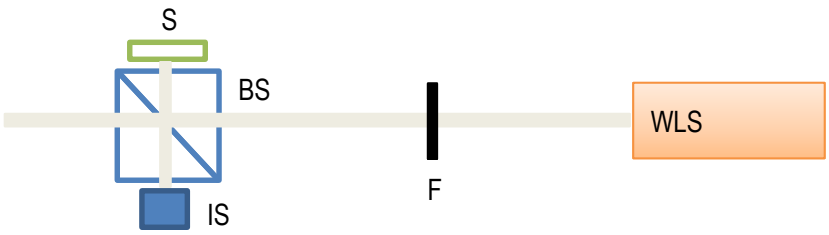

Figure 5.9 Schematic representation of the experimental setup used for the measurement of the reflection spectra. WLS - Supercontinuum White Light Laser, S-sample, F - neutral density filter, BS – beam splitter cube, IS - integrating sphere.

The transition dynamics of this cell (RM cured for Δt_{pp} = 30 min) was measured during the natural (or free) and forced relaxations. In the case of the natural relaxation, the previously applied excitation voltage was simply switched off. In the case of forced relaxation, the initial excitation voltage and frequency were directly changed to 80V at 80 kHz.

In Figure 5.10 and Figure 5.11, Curve 1 (0 sec) corresponds to the "low-reflecting" state of the excitation when a low frequency voltage (U = 80V at 1 kHz) is applied to the cell. In that state, the LC molecules are aligned homeotropically and thus the cell is more transparent (less reflective). During the relaxation process, the helicoidal molecular alignment is restored and we see the resonance curves appearing gradually (Curves 2–4). In the case of natural relaxation (Figure 5.10), this transition takes about 21 min, while in the case of forced relaxation (Figure 5.11), the process is faster by a factor of 63 (it takes about 20 sec). Thus, the use of the S-PS-DF-CLC cells enables us to switch between the homeotropic and the planar twisted states back and forth. In addition, we can do this quickly. However, the privacy window application requires also the presence of the broadband scattering state, which is not observed here. We have thus explored other pre-polymerization durations to achieve such a state (see later in the article).

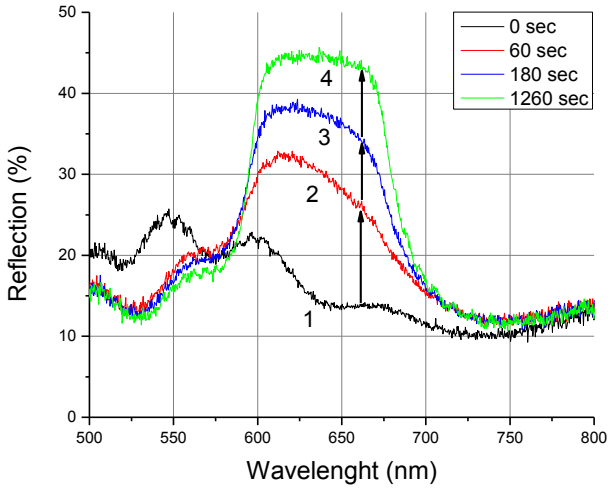

Figure 5.10 Reflection spectra of the S-PS-DF-CLC cell (programmed at U=40V at 1kHz with RM cured for Δtpp = 30 minutes) during the natural relaxation from homeotropic (U=80V at 1kHz) to ground state (U=0V). Curves 1 – 0 sec; 2 –60 sec; 3 – 180 sec; 4 – 1260 sec.

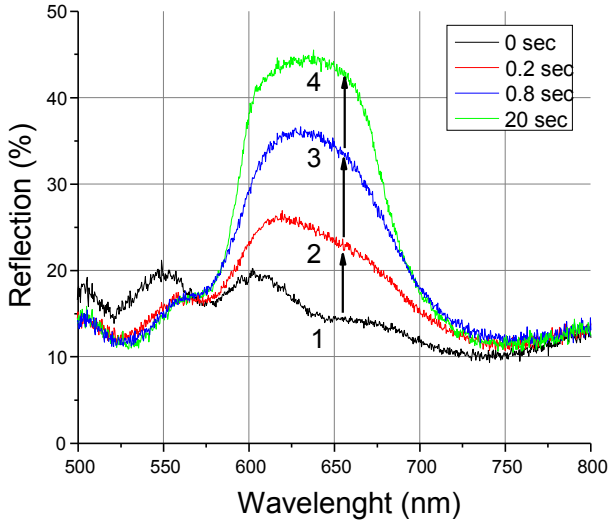

Figure 5.11 Reflection spectra of the S-PS-DF-CLC cell (programmed at U=40V at 1kHz with RM cured for Δtpp = 30 minutes) during forced relaxation (from 80V at 1kHz to 80V at 80kHz). Curves 1 – 0 sec; 2 –0.2 sec; 3 – 0.8 sec; 4 – 20 sec.

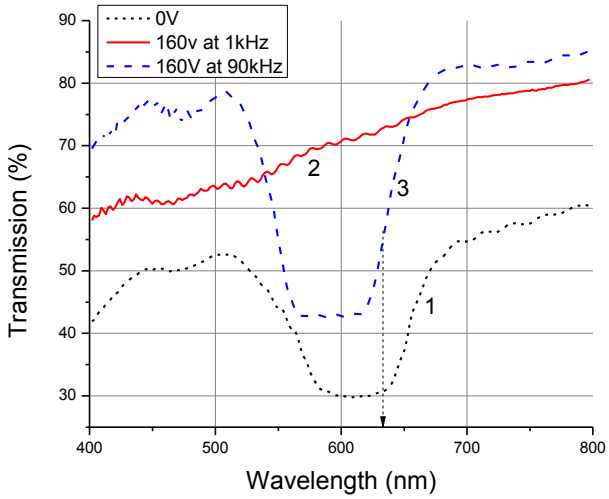

Figure 5.12 Transmission spectra of the S-PS-DF-CLC cell (programmed at U=40V at 1 kHz, with the RM precured for Δtpp = 1.5 minutes) in stationary states. 1 - 0V; 2 – 160V at 1kHz; 3 – 160V at 90kHz. The vertical dashed arrow shows the wavelength (632.8nm) used for haze measurements.

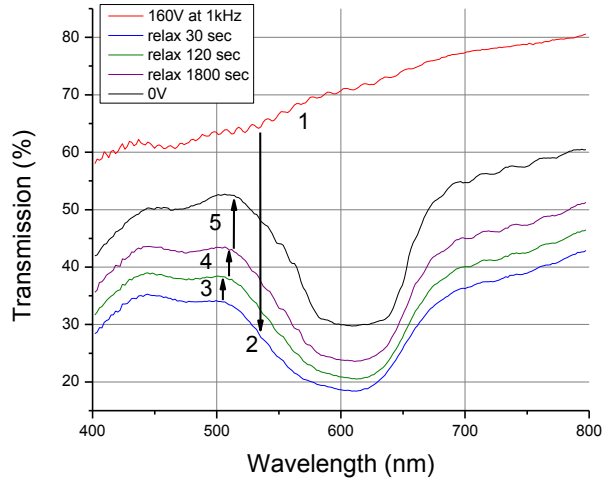

Figure 5.13 Transmission spectra of the S-PS-DF-CLC cell (programmed at U=40V at 1kHz, with the RM pre-cured for Δt_{pp} = 1.5 minutes) during the natural relaxation after the switch off of the voltage from the state with 160V at 1kHz. Curves 1 – 160V at 1kHz; 2 –relax 30 sec; 3 – relax 120 sec; 4 – relax 1800 sec; 5 – 0V.

The relaxation dynamics (Figure 5.13 and Figure 5.14) of the S-PS- DF-CLC cell with RM pre-cured for Δt_{pp} = 1.5 min was measured during the natural and forced relaxations, when the "initial" excitation voltage (1 kHz) to obtain a homeotropic alignment (Curve 1, Figure 5.14). Then the voltage and frequency of excitation were quickly changed to 160V at 90 kHz. The first spectrum was recorded 500 msec after the switching (Curve 2, relax 0.5 sec, Figure 5.14). Then the spectra were recorded periodically during the relaxation process. The final curve (Curve 5: 160V at 90 kHz, Figure 5.14) was recorded ≈ 5 sec after the switching. It corresponds to the field-stabilized "helicoidal" (or planar) excited state (U = 160V at 90 kHz). As one can see, in addition to the strong acceleration of the transition (by a factor of ≈ 720), we can regenerate and even increase the depth of the resonance, thanks to the suppression of defects via the negative dielectric torque (see later).

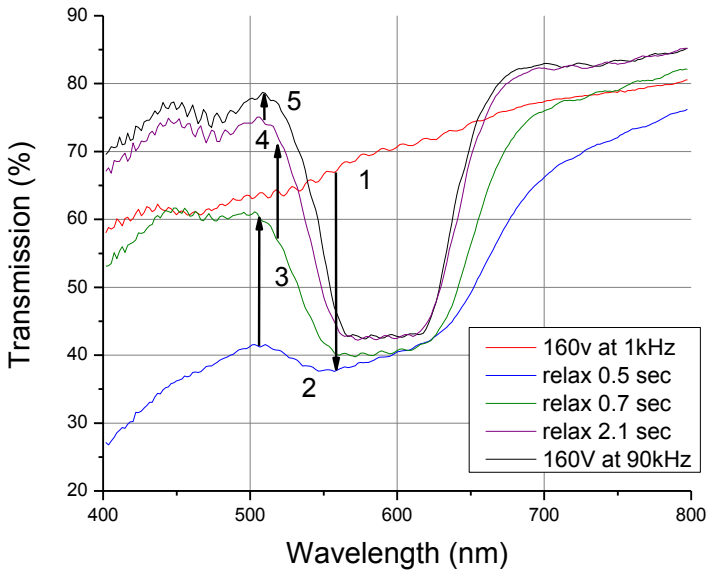

Figure 5.14 Transmission spectra of the S-PS-DF-CLC cell (programmed at U=40V at 1 kHz, with the RM pre-cured for Δtpp = 1.5 minutes) during the forced relaxation after the switching the voltage from the state 160V at 1kHz to 160V at 90kHz. 1 – 160V at 1kHz; 2 – relax 0.5 sec; 3 – relax 0.7 sec; 4 – relax 2.1 sec; 5 – 160V at 90kHz.

5.4 Haze measurements

We have performed haze measurements for the sample with RM pre-cured for 1.5 min. The corresponding experimental setup is described in Figure 5.15. During the measurements, all elements of the setup were kept immobile while the cell was rotated around its vertical axes for the three key states of the cell (ground state, and low and high frequency voltages applied). The photo-detector (Det110 from Thorlabs) was placed at a distance of 19 cm from the sample (noted as S-PSLC). The aperture of the photo-detector was ≈ 0.7 cm. The transmission through a standard uniform glass window (without antireflection coatings) was used as a reference. A plane polarized (in vertical direction) beam, obtained from a CW He-Ne laser (operating at 632.8 nm), was used as probe.

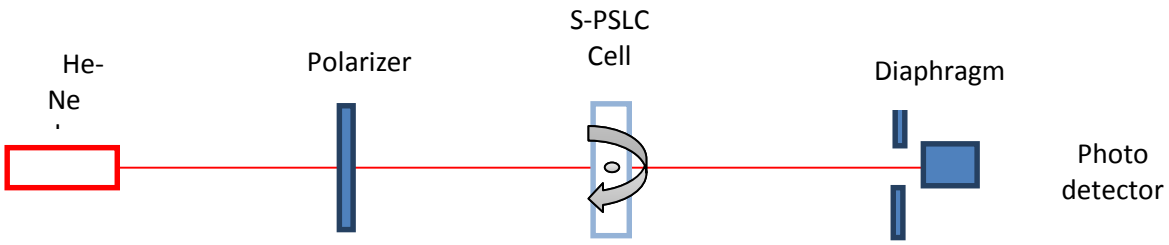

Figure 5.15 Schematics of the experimental setup used for the electro-optical haze measurements of S-PS-DF-CLC cells.

As one can see (Figure 5.16), the angular dependence of transmission (the haze) for our cell is rather similar to the glass reference (defined by Fresnel reflections only) in the case of the homeotropic state (U = 160V at 1 kHz). However, the overall transmission is lower by a factor of ≈ 1.4. We observe a drastic drop in transmission for incidence angles above ±20◦ in the forced helical state (U = 160V at 90 kHz). This might appear rather surprizing since the resonant diffraction of periodic structures is blue shifted for tilted incidence angles and our probe wavelength is positioned at the long wavelength side of the resonance. However, it appears that, for the used LC and RM materials, their average refractive indexes (calculated as $n_{av} = [n_e + 2n_o]/3$) are almost the same for normal incidence (n_{avLC} = 1.5716 and n_{avRM} = 1.5766). Thus, the polymer aggregates must be "hidden" (or index matched) in

the LC matrix for the normal incidence of the probe, while they are "revealed" (or index mismatched) at tilted light incidence since then the n_{avLC} tends toward the n_o, which is lower than the n_{avRM}. This would increase the light scattering at higher incidence angles. In contrast, the index mismatch of polymer defects (and thus the scattering) is higher for the normal incidence in the homeotropic state of the cell (U = 160V at 1 kHz) and the polymer defects become "less visible" (and thus less scattering) with the increase in incidence angle (for comparison, see the index matching role in PSLCs, e.g. in ref. [127]).

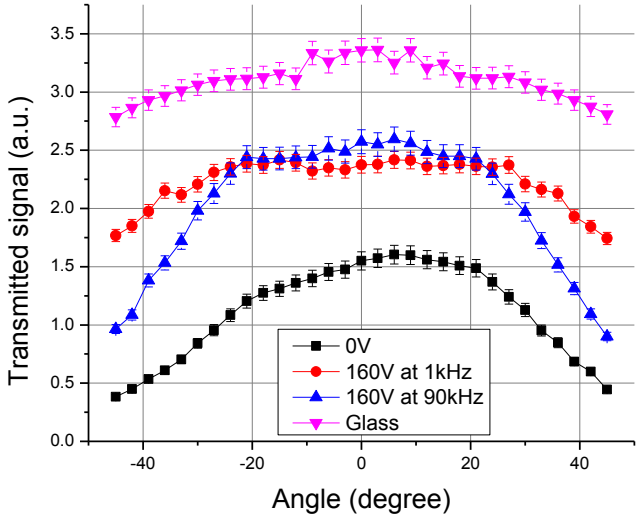

Figure 5.16 The angular dependence of the probe beam's transmission (haze) of the S-PS-DF-CLC cell (programmed with U=40V at 1kHz with RM procured for Δtpp = 1.5 minutes). Squares, circles and triangles represent respectively ground state (U=0V), excited homeotropic (160V at 1kHz) and excited "helicoidal" (160V at 90kHz) states. Inverted triangles (top curve) correspond to the reference glass plate.

5.5 Discussion

The results obtained by using the three typical pre-curing conditions (Δt_{pp} = 0, 1.5 and 30 min) demonstrate the trade-offs we are facing when building our cells. The complete curing of RM layers (Δt_{pp} = 30 min) is not really interesting since it would reproduce the same alignment conditions as the typical polyimides (Figure 5.8). The uncured RM (Δt_{pp} = 0

min) is strongly dissolved in the bulk of the LC material, eliminating almost completely the dynamic control possibilities (Figure 5.8). The idea of programming was to use two aligned liquid layers (RM and LC molecules, Figure 5.5(a)), which are reoriented by an electrical field (Figure 5.5(b)) and interdiffused before being "frozen" by the photopolymerization of the RM (Figure 5.5(c)). The goal of the programming step consisted in creating alignment defects in the ground state (to scatter light), the energy of which, however, would be low enough enabling the electrical switching of the material system to two other key states with high transparency (homeotropic alignment) and resonant reflection (planar alignment). Thus, in an ideal scenario, we should obtain all three key states when using reasonable values of driving voltages (≈ 100 V). However, as we can see from Figure 5.12, the programming conditions must still be improved since, even in our optimized (preliminary) samples, we are far from our goal. Indeed, in the ground state (Curve 1, Figure 5.12), the spectrally averaged (in the visible spectral region, between 400 and 700 nm) transmission is not low enough (approximately 40% versus the desired 10%) to be used for privacy windows. Thus, the light scattering (as broadband as possible) must be further increased in the ground state. In contrast, we observed a clear resonant character of light reflection (with $\lambda_R \approx 610$ nm, Curve1, Figure 5.12), which should be related to the relatively important presence of helicoidal domains (see later). The application of a repulsing torque (U = 160V at 90 kHz, Curve 3, Figure 5.12) reconstructs a very good resonance (with $\lambda_R \approx 593$ nm and almost 50% resonant reflection for unpolarized probe beam). The "blue-shift" of the resonance is related to the small reduction of the cholesteric pitch [128]. We can also see (Curve 2, Figure 5.12) that the application of a positive torque (U = 160V at 1 kHz) is not able to bring the system to the uniform homeotropic alignment; we are not able to achieve high enough spectrally averaged transmission (approximately 70% versus the desired 80%). Apparently, there are still defects, which scatter light (stronger in the short wavelength region). Very likely those defects are defined by the polar "out-of-plane" anchoring conditions (since the programming of the cell was performed by using an electrical voltage at 1 kHz) and "stabilized" by some 3D polymer aggregations.

To confirm these hypotheses, we have proceeded to some additional microscopic analyses of our samples. We have started with optical polarizing microscopy studies (the cell was placed between crossed polarizers). The micro-photography of the S-PS-DF-CLC cell was

made (in transmission) for the three key states. First, the low frequency excitation voltage (U = 160V at 1 kHz) was applied to the cell to obtain homeotropic alignment (Figure 5.17(a)). Then the voltage was directly switched to U = 160V at 90 kHz, providing excited planar (twisted) state (Figure 5.17(b)). Finally, the excitation voltage (160V at 1 kHz) was switched off (U = 0 V), and the photos were recorded during the natural relaxation process. Some examples of such natural relaxation may be seen in Figure 5.17(c) (10 sec after switching off) and Figure 5.17 (d) (20 min after switching off). We can see (Figure 5.17 (a)) that the overall color of the image is reddish (in transmission) for the excitation conditions U = 160V at 1 kHz. Along with the corresponding data, obtained in Figure 5.12(Curve 2; without resonant reflection), we can conclude that this color is defined by the dispersion of white light probe's polarization rotation, thanks to the presence of chiral molecules in the cell, which can generate light polarization rotation event for a homeotropic alignment of LC molecules. By using a digital zoom on obtained (in Figure 5.17) images, we can notice also the presence of closed-loop linear nonuniformities of circular (e.g. Zone 1, Figure 5.18 (a)) or more extended linear forms (zone 2, Figure 5.18(a)). The application of the repulsing torque (U = 160V at 90 kHz, Figure 5.18(b)) brings the system to the planar twisted state. We see that the linear (circular or elliptic) nonuniformities disappear confirming their orientation character (defects). These are the so-called pi-wall defects, which are present during the focal conic-to-homeotropic transition, and can even persist when the applied field is higher than the focal conic-to-homeotropic transition's threshold Ec. We calculated this threshold field for our material, by using the formula $E_c = (\pi^2/P)(K_{22}/\varepsilon_0 \Delta\varepsilon)^{1/2}$ [68] (see also [129]), where P is the pitch of the helix, K_{22} is the twist elastic constant and the $\Delta\varepsilon$ is the local dielectric anisotropy of the LC. The pitch was calculated from the well-known formula for the resonance wavelength $\lambda_R = n_{av} * P$, where $n_{av} = \frac{2*n_\perp + n_\parallel}{3}$ is the average refractive index of the LC, $n_\perp$ and $n_\parallel$ being the local ordinary and extraordinary refractive indexes of the LC, respectively. The value of λ_R was taken from Curve 1 of Figure 5.12, corresponding to the state when no voltage is applied to the cell. While Curve 3 of Figure 5.12 also shows the resonant character, the pitch of the helix could

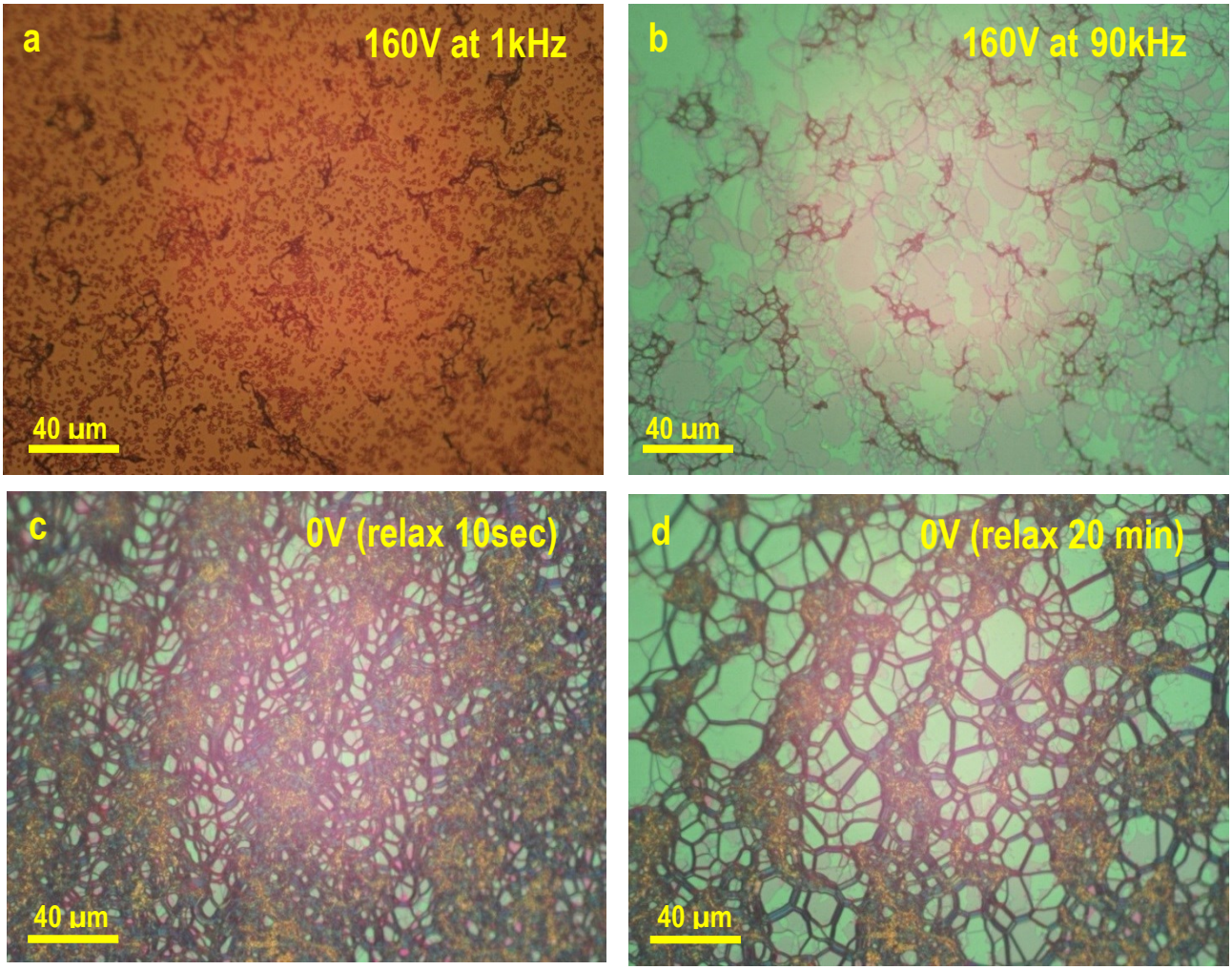

Figure 5.17 Micro photography of the S-PS-DF-CLC cell (in transmission) with RM cured for Δtpp = 1.5 minutes, recorded by using polarizing microscope (crossed polarizers). The corresponding driving conditions are shown on the right top corners of images.

be modulated (reduced) as a result of the application of the "stabilizing" voltage at 90 kHz [128]. In a rough approximation, we can use the values of the parameters ($n_{\perp}$ = 1.4978, $n_{\parallel}$ = 1.7192, $K22$ = 19pN and $\Delta\varepsilon$ = 3.22 at 1 kHz) of the dual frequency NLC (MLC-2048) used in our mixture. The estimated threshold field is E_c = 20.797∗ (V/μm), and the corresponding threshold voltage for our cell of d = 5μm

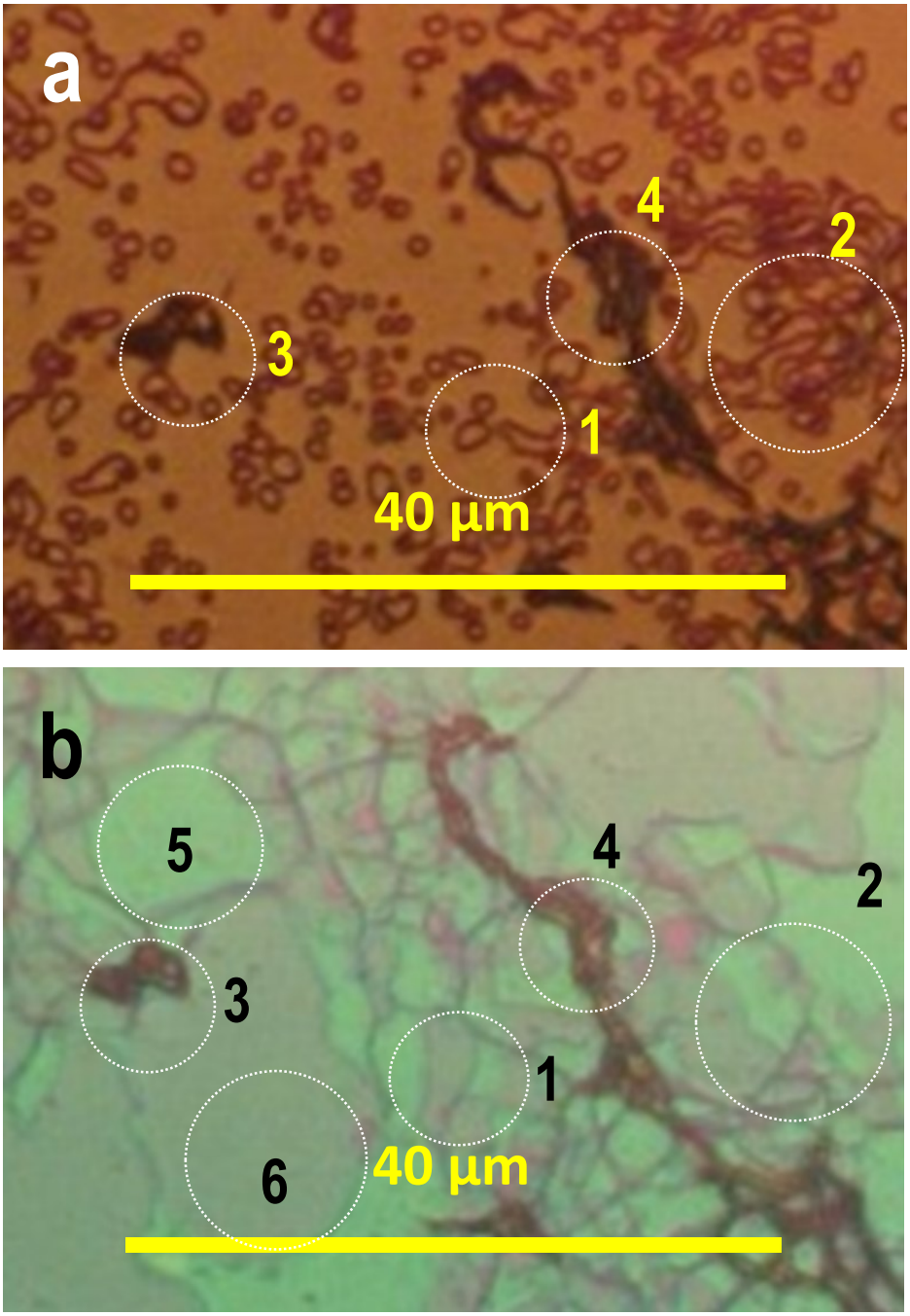

Figure 5.18 Digital zoom on the Figure 5.17 images (recorded in transmission by the polarizing microscope) to demonstrate the defect structures a-in the homeotropic and b-in the planar excited states. The outlined zones are linear defects (1 and 2), polymer rich region (3 and 4) and planar cholesteric structures with different numbers of half periods (5 and 6).

thickness is $U_c = E_c * d$ = 103.985 V. We can see from Figure 5.19 that initially the transmission drops when the applied voltage is increased. In this stage, we have a transition from planar to focal conic texture. With further increase in the voltage, we see that the transmission begins to rise above U = 100 V, and so the helical structure begins to unwind, and focal conic-to-homeotropic transition takes place. So we presume there is a good agreement with the aforementioned theoretical estimations.

We can see also that so-called oily streaks (other type of orientational defects) are present in the planar state (presented in Figure 5.17(c) and Figure 5.17(d)). The theoretical analyses of the electrical field induced similar linear defects may be found in ref. [33]. Another distinctive type of nonuniformity is shown by Zones 3 and 4 (Figure 5.18(a)). These zones remain almost unchanged suggesting that those are zones rich of polymer aggregates, which limit the orientational mobility of the LC. In contrast, the areas with linear defects are transformed into large uniform areas (Zones 5 and 6, Figure 5.18(b)) with slightly different colors. These should be planar helicoidal areas with slightly different rotative power of the cell (in those areas), which might be related to the local differences in concentrations of chiral molecules and respectively to the number of half periods of the molecular helix.

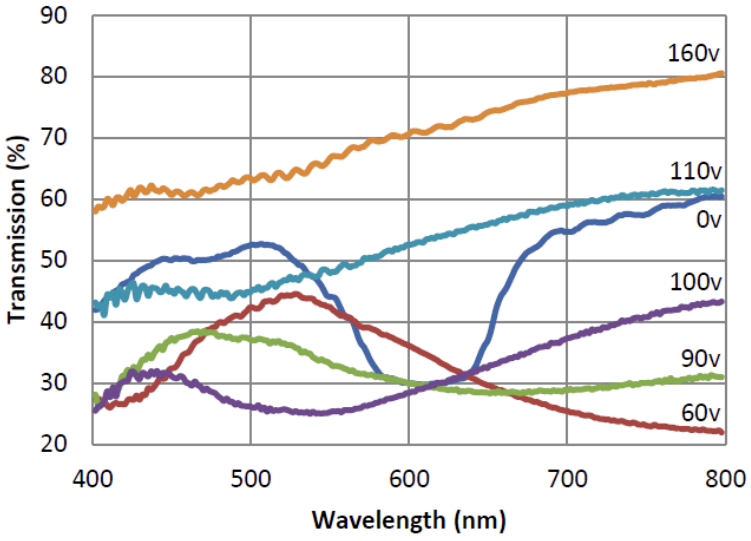

Figure 5.19 Transmission spectra of the S-PS-DF-CLC cell (programmed at U=40V at 1 kHz, with the RM precured for Δt_{pp} = 1.5 minutes) for various stationary voltages applied at 1kHz.

We think that the observed (by the optical microscope) defects should be intimately related to the "programmed" surface anchoring conditions and to the morphology of the polymer on the surface of the substrate. NanoScope VVeeco atomic force microscope (AFM) was used to study this morphology. First, two substrates of the cell were separated by a knife. The LC was then removed from the substrates by leaving those substrates in isopropanol for 2 h. A vacuum pump was then used for few hours to expel the rest of the residue from the substrates. After these cleaning processes were completed, a scan of the surface was made using the AFM. The results of those scans are presented in Figure 5.20. The surface morphology in 3D is presented in Figure 5.20(a). As we can see, there are aggregations of polymer and thus the obtained molecular interdiffusion was not uniform. There are many aggregates of small size (≈ 1.5μm lateral and tens of nanometers of height) as well as of larger size (≈ 10μm lateral and hundreds of nanometers of height) polymer aggregates. Thus, the original RM monomer layer (≈ 600 nm) is dramatically modified. The larger defects should be in the origin of defects observed in Zones 3 and 4 (Figure 5.18), while the smaller defects might be in the origin of linear (circular) defects, described by Zones 1 and 2 (Figure 5.18).

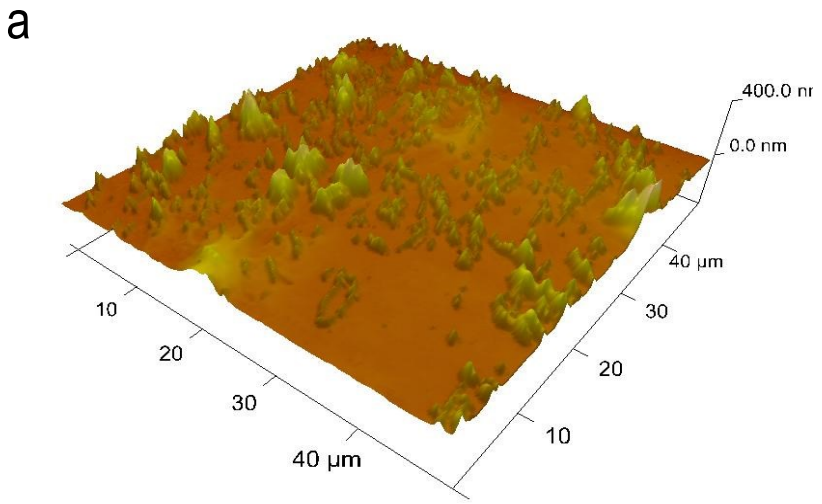

b

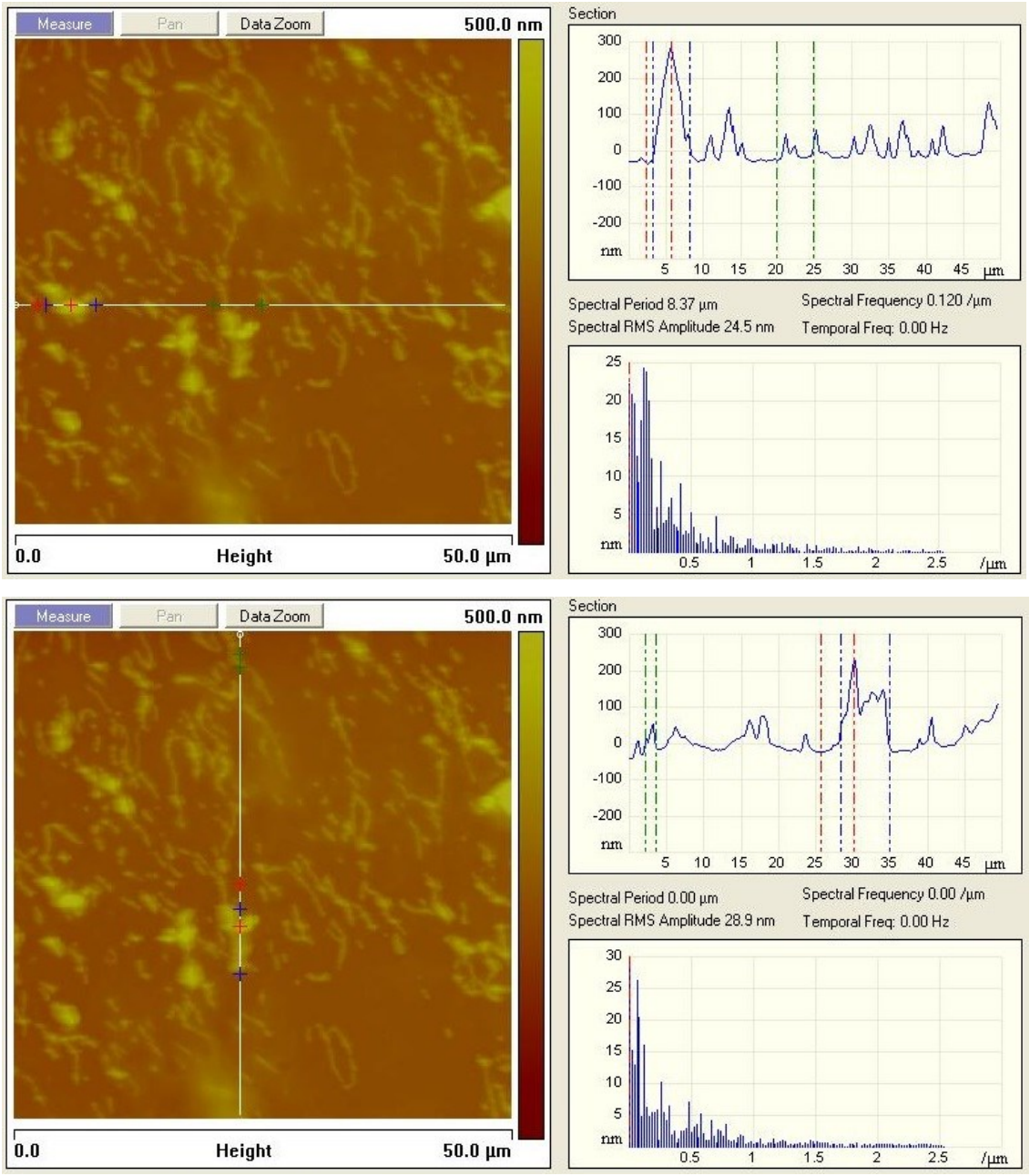

Figure 5.20 AFM scan of the substrate with RM pre-cured for Δtpp = 1.5 minutes. (a) – Surface morphology in 3D and (b) – surface presented in 2D (left) and amplitude profiles (right) in two perpendicular directions (top and bottom).

We present also (Figure 5.20 (b)) the basic surface analyses (amplitude profiles along two perpendicular lines), which might be used to build a theoretical model of defect formation as well as for light scattering. However, this is out of the scope of the present work.

5.6 Conclusions

We have studied the influence of pre-polymerization degree on the formation of various LC alignment states in the specific case of a dual frequency chiral LC. Positive dielectric torque was used during the cell programming (interpenetration and curing under torque). Based on the obtained results, we think that (a) – the programming of the cell favors the out-of-plane anchoring conditions, which are influencing (along with small polymer aggregates) linear circular defects that are present in the excited homeotropic state of the cell and (b) – the obtained interdiffusion (between the LC and the RM molecules) is not uniform. Very likely, it is initiated by large-scale fluctuations [29], which, in addition, are further increased by the photopolymerization process. The RM monomers being attracted by the RM-rich areas (where the photopolymerization started earlier) might result in more attraction of RM molecules, resulting in local phase separation on the surface of the cell. Such polymer aggregation generates defects, including LC alignment defects (in the ground state of the cell) that are difficult to completely eliminate by the application of a positive dielectric torque. It is possible that the programming technique itself prohibits the high transparency due to the formation of linear circular defects (under the positive torque). Note, however, that these defects are eliminated by a negative torque, as described in ref. [130]. Further studies and optimization of programming conditions are required to better understand the physics behind this programming process.

Acknowledgements

We would like to acknowledge the financial support of NSERC-Canada.

Chapter 6

Conclusion

The alignment control of liquid crystals is of great interest both from scientific and practical points of view. With aim of producing a new surface alignment method for liquid crystals, we have used the polymer networks near the surfaces to align the liquid crystals of a non-mechanical way and then control their electro-optical behavior by that surface polymer network. We have started our study, by exploring the possibility of photoalignment of a mesogenic azobenzen dye doped in mesogen reactive host matrix, with aim to use the photo induced reorientation of the dye to reorient the host and then fix that alignment by an UV photo polymerization process. However, this mesogenic azobenzene dye showed specific behavior, as it undergoed photo isomerization reaction, but the photo induced rotation of its long axis was very limited [131].

In the second approach we developed the surface alignment method by using a layer of a reactive mesogen cast onto the surface of an anchoring layer (the polyimide). The contact of the non precured RM with LC molecules allowed a partial interdiffusion procces. Such anisotropic molecular diffusion processes, which take place in the presence of aligning fields are very interesting and were observed also in azo dye/host LC [132] and self-organizing systems [63] . Application of an electric field during the programming process (interdiffusion and UV curing) influenced the morphology and electro-optical behavior of obtained S-PSLC cells. The similar effect of influence of the alignment fields (electric or magnetic) during UV curing was also observed in bulk PDLC [133] and PSLC systems [134].

We saw in Chapter 4 that using of DFNLCs make the S-PSLC systems more interesting and promising. The use of DFNLC allows not only the various modes of cell programming, but also improves the contrast and polarization independence of light scattering. We obtained a short transition times at the order of 1 ms, when switching the low-frequency voltage to high frequencies. However, significantly shortening of the on–off–on transition

cycle was not demonstrated. This was very likely because of the strong interaction between surface polymer network and the LC under the negative torque, preventing a fast transition when switching from high frequency to low frequency voltage. Future consideration of the total on-off-on cycle duration shortening may be the application of the lower amplitude voltages at higher frequencies.

There are many parameters that can be used to control the programming process of S-PSLC cells: the choice of LC and RM molecules, the LC–RM contact time before RM's final polymerization, the duration of the pre-polymerization of RM and the electric field induced reorientation of molecules. For example, the different degrees of pre-polymerization of RM layers showed a completely different electro-optical behavior of the nematic LC cells ([135]). The cells fabricated with RM films pre-cured for more than 2 minutes were shown a uniform alignment [29], and cells with RM film with not pre-cured before their contact with the LC were showed a strong light scattering behavior after programming process. It was shown in Chapter 5, that pre-polymerization degree plays a crucial role on an electro-optical behavior when DF-CLC mixture was used in the S-PSLC geometry [136]. Three key states were obtained with the partially pre-polymerized thin RM layers. We obtained light scattering ground state (one of the key states) by creating out-of-plane alignment defects (polymer aggregates) during the programming process. Application of an electric field at low and high frequencies then allowed electrical switching of the material system between other two key states with high transparency (homeotropic alignment) and resonant reflection (planar alignment). The programming conditions must still be improved since, light transmission in scattering ground state was not low enough and the light transmission in homeotropic alignment was not high enough for permitting to use these systems in device applications. In a future the utilisation of a DF-CLC with a higher dielectric anisotropy than that we used in our research will allow to achieve a higher transparency homeotropic state with lower values of driving voltages. In addition, the application of the higher voltages during the programming step will allow more efficient interdiffusion between the MR and LC, and reaching of a low transparency ground state (scattering state).

The experimental nature of our research and existence of many experimental parameters complicates the understanding the physics behind the programming process and

comparison of obtained systems with already existing ones. Study of role of experimental parameters, such thickness of RM layer and LC cell, polymerisation degree of pre-polymerized RM layer, electric field effect on mutual orientation and interpenetration of the molecules, photo-polymerization conditions, will be done for the better comprehension of the programming process. For example, the photo-polymerization kinetics can affect the polymer aggregate size on the surface, thus altering the electro-optical behavior (for ex. off-on response time) of the cell.

Further systematic morphological studies of surfaces (by AFM, SEM) with the different programming parameters can give insight into the formation process of polymer aggregates and their behavior upon application of the electric field. Afterward, the control of the polymer aggregates' sizes and their distribution during programming process will allow better performance of the S-PSLC cells. After the optimization of programming conditions, one can consider these systems promising for practical applications, including polarization independent displays, privacy/smart windows and variable light illumination systems.

Bibliography

[1] P. G. Gennes and J. Prost, *The Physics of Liquid Crystals*, 2nd ed.: Oxford University, 1995.

[2] D. Demus, J. W. Goodby, G. W. Gray, H.-W. Spiess, and V. Vill, *Handbook of liquid crystals*. New York: Wiley, 1988, vol. 1.

[3] G. W. Gray, *Molecular Structure and the Properties of Liquid Crystals*. London: Academic Press, 1962.

[4] G. W. Gray, *Advances in Liquid Crystals*.: Academic Press, 1976.

[5] D. Demus, J. W. Goodby, G. W. Gray, H.-W. Spiess, and V. Vill, *Physical Properties of Liquid Crystals*. New York: Wiley, 1999.

[6] K. Takatoh et al., *Alignment Technologies and Applications of Liquid Crystal Devices*.: Taylor & Francis, 2005.

[7] V. G. Chigrinov, V. M. Kozenkov, and H. S. Kwok, *Photoalignment of Liquid Crystalline Materials: Physics and Applications*. New York: Wiley, 2008.

[8] J. Y. Ho, V. Chigrinov, and H. S. Kwok, "Variable liquid crystal pretilt angles generated by photoalignment of a mixed polyimide alignment layer," *Appl Phys Lett.*, vol. 90, p. 234506, 2007.

[9] D. Ahn, Y-C. Jeong, and S. J. Lee, "Control of liquid crystal pretilt angles by using

organic/inorganic hybrid interpenetrating networks," *Opt Express.* , vol. 17, no. 19, pp. 16603–16612, 2009.

[10] G. P. Crawford and S. Zumer, *Liquid Crystals in Complex Geometries: Formed by Polymer and Porous Networks*. London: Taylor & Francis, 1996.

[11] P. S. Drzaic, "Polymer dispersed nematic liquid crystals for large area displays and light valves," *J. Appl. Phys*, vol. 60, pp. 2142–2148, 1986.

[12] J. W. Doane, N. A. Vaz, B.-G. Wu, and S. Zumer, "Field controlled light scattering from nematic microdroplets," *Appl. Phys. Lett*, vol. 48, pp. 269–271, 1986.

[13] T. Kajiyama, A. Miyamoto, H. Kikuchi, and Y. Morimura, "Aggregation states and electro-optical properties based on light scattering of polymer/(liquid crystal) composite films," *Chem. Lett*, vol. 18, no. 5, pp. 813–816, 1989.

[14] U. Maschke, X. Coqueret, and M. Benmouna, "Electro-optical properties of polymer-dispersed liquid crystals," *Macromol. Rapid Commun.*, vol. 23, no. 3, pp. 159–170, 2002.

[15] R. A. M. Hikmet, "Anisotropic gels in liquid crystal devices," *Adv. Mater.*, vol. 4, no. 10, pp. 679–683, 1992.

[16] J. W. Doane, A. Golemme, J. L. West, J. B. Whitehead Jr, and B.- G Wu, "Polymer Dispersed Liquid Crystals for Display Application," *Molecular Crystals and Liquid Crystals Incorporating Nonlinear Optics*, vol. 165, no. 1, pp. 511-532, 1988.

[17] A. J. Lovinger, K. R. Amundson, and D. D. Davis, "Morphological Investigation of UV-Curable Polymer-Dispersed Liquid-Crystal (PDLC) Materials," *Chem. Mater*, vol. 6, pp. 1726-1736, 1994.

[18] L. Bouteiller and P.Le Barny, "Polymer-dispersed liquid crystals: Preparation, operation and application," *Liquid Crystals*, vol. 21, no. 2, pp. 157-174, 1996.

[19] G.P. Crawford and S. Zumer, *Liquid Crystals in Complex Geometries*. London: Taylor & Francis, 1996.

[20] R.A. Hikmet, "Electrically induced light scattering from anisotropic gels," *Journal of Appl. Phys*, vol. 68, no. 9, pp. 4406-4412, 1990.

[21] G. P. Crawford, A. Scharkowski, Y. K. Fung, and J. W. Doane, "Internal surface, orientational order, and distribution of a polymer network in a liquid crystal matrix," *Phys. Rev. E*, vol. 52, p. 1273, 1995.

[22] M. I. Boamfa, S. V. Lazarenko, E. C. M. Vermolen, A. Kirilyuk, and Th. Rasing, "Magnetic field alignment of liquid crystals for fast display applications," *Adv Mater.*, vol. 17, no. 5, 2005.

[23] F. S. Y. Yeung, Y. W. Li, and H. S. Kwok, "Fast response No-Bias-Bend LCD," *IDW'05*, p. 41, 2005.

[24] L. Goodman, "Topography of Obliquely Evaporated Silicon Oxide Films and its Effect on Liquid Crystal Orientation," *IEEE*, vol. 24, no. 7, pp. 795-804, 1977.

[25] H. J. Ahn et al., "Liquid crystal pretilt angle control using adjustable wetting properties of alignment layers," *Appl. Phys. Lett.*, vol. 90, no. 25, p. 253505, 2007.

[26] Kim D-H et al., "Controllable Pretilt Angles for Liquid Crystal Molecules using a Rubbing Treated Mixture Layer ," *Transactions on Electrical and Electronic Materials*, vol. 10, no. 4, pp. 140-142, 2009.

[27] Y.-J. Lee et al., "Control of liquid crystal pretilt angle by anchoring competition of the stacked alignment layers," *Appl. Phys. Lett.* , vol. 94, p. 041113 , 2009.

[28] P.-A. Blanche, Ph. C. Lemaire, M. Dumont, and M. Fischer, "Photoinduced orientation of azo dye in various polymer matrices," *Optics Letters*, vol. 24, no. 19, pp. 1349-1351, 1999.

[29] J.-P. Bédard-Arcand and and T. Galstian, "Self-organization of liquid-crystal and reactive-mesogen into 2D surface-stabilized structures," *Macromolecules* , vol. 44, pp. 344–348, 2011.

[30] J.-P. Bédard-Arcand and T. Galstian, "Surface-polymer stabilized liquid crystals," *Mol. Cryst. Liq. Cryst.*, vol. 560, pp. 170–182, 2012.

[31] J.-P. Bédard-Arcand and T. Galstian, "Programmable and electrically controllable light scattering from surface-polymer stabilized liquid crystals," *J. Opt. Soc. Am. A*, vol. 29, pp. 1675–1679, 2012.

[32] A. B. Golovin, S. V. Shiyanovskii, and O. D. Lavrentovich, "Fast switching dual-frequency liquid crystal optical retarder, driven by an amplitude and frequency

modulated voltage," *SID Digest*, vol. 34, pp. 1472–1475, 2003.

[33] F. Reintzer, *Monatsh. Chem.*, vol. 9, no. 1, p. 421, 1988.

[34] O. Lehmann, *Z. Phys. Chem.*, vol. 4, 1889.

[35] P.J. Collings, *Liquid crystals: Nature's delicate phase of matter*, 2nd ed.: Princeton University Press, 2002.

[36] I. C. Khoo, *Liquid Crystals*, 2nd ed.: Wiley, 2007.

[37] Richard A Pethrick, *Polymer Structure Characterization: From Nano To Macro Organization*, 1st ed.: Royal Society of Chemistry, 2007.

[38] W. Maier and A. Saupe, *Z. Naturforsch. A*, vol. 13, p. 564, 1958.

[39] J. N. Israelachvili, *Intermolecular and Surface Forces*, 3rd ed.: Academic Press, 2011.

[40] A. J. Stone, "Intermolecular forces," in *The Molecular Physics of Liquid Crystals*. London: Academic, 1979, ch. 2, pp. 31–50.

[41] J. G. Gay and B. J. Berne, "Modification of the overlap potential to mimic a linear site-site potential," *J. Chem. Phys.*, vol. 74, pp. 3316–3319, 1981.

[42] L. M. Blinov, *Structure and Properties of Liquid Crystals*.: Springer, 2011.

[43] L.M. Blinov and V.G. Chigrinov, *Electrooptic Effects in Liquid Crystal Materials*.:

Springer, 1994.

[44] P. Yeh and C. Gu, *Optics of liquid crystal displays*, 2nd ed. New York: Wiley, 2010.

[45] N. Konforti, S.-T. Wu, and E. Marom, "Phase-only modulation with twisted nematic liquid-crystal spatial light modulators," *Opt. Lett.*, vol. 13, pp. 251-253, 1988.

[46] K. Asatryan et al., "Optical lens with electrically variable focus using an optically hidden dielectric structure," *Opt. Express*, vol. 18, pp. 13981-13992, 2010.

[47] G. Nahum, "Imaging spectroscopy using tunable filters: a review," *Proc. SPIE 4056, Wavelet Applications VII*, pp. 50-64, 2000.

[48] J. P. Riehl, *Mirror-image asymmetry: an introduction to the origin and consequences of chirality*.: Wiley, 2010.

[49] M. Mitov and N. Dessaud, "Going beyond the reflectance limit of cholesteric liquid crystals," *Nature Materials*, vol. 5, 2006.

[50] M. E. McConney et al., "Thermally Induced, Multicolored Hyper-Reflective Cholesteric Liquid Crystals," *Advanced materials*, vol. 23, no. 12, pp. 1453-1457, 2011.

[51] M. Schadt, "Liquid crystal materials and liquid crystal displays," *Annu. Rev. Mater. Sci.*, vol. 27, pp. 305–379, 1997.

[52] H. Xianyu, S-T Wu, and C-L Lin, "Dual frequency liquid crystals: a review," *Liquid*

Crystals, vol. 36, no. 6-7, pp. 717–726, 2009.

[53] Y. Yin, S. V. Shiyanovskii, A. B. Golovin, and O. D. Lavrentovich., "Dielectric Torque and Orientation Dynamics of Liquid Crystals with Dielectric Dispersion," *Phys. Rev. Lett.*, vol. 95, p. 087801, 2005.

[54] G. Heppke, J. Kayed, and U. Muumlller, "Influence of Molecular Structure on the Low Frequency Dielectric Relaxation ofp-Cyano-substituted Liquid Crystals in Nematic Solution," *Mol. Cryst. Liq. Cryst.*, vol. 98, pp. 309–319, 1983.

[55] E.I. Rjumtsev, A.P. Kovshik, B.S. Saburov, and R.M. Umursokov, "Dielectric relaxation in mixtures of liquid crystals of different molecular length," *Mol. Cryst. Liq. Cryst.*, vol. 303, pp. 331–339, 1997.

[56] H. Sato, A. Sawada, A. Manabe, and S. Naemura, "Dielectric relaxation of nematic liquid crystals with different molecular shapes," *Mol. Cryst. Liq. Cryst.*, vol. 366, pp. 2165-2172, 2001.

[57] J. Cognard, "Alignment of nematic liquid crystals and their mixtures," *Mol. Cryst. Liq. Cryst.*, vol. Supp. 1, pp. 1-77, 1982.

[58] W. Chen, M. B. Feller, and Y. R. Shen, "Investigation of anisotropic molecular orientational distributions of liquid-crystal monolayers by optical second-harmonic generation," *Phys. Rev. Lett.*, vol. 63, p. 2665, 1989.

[59] Tiezheng Qian, Xiaowei Zhuang, and Y. R. Shen, "Surface-monolayer-induced bulk alignment of liquid crystals: From nematic to smectic-A phase," *Phys. Rev. E*, vol.

59, no. 2, 1999.

[60] C. Mauguin, "Sur les cristaux liquides de Lehman," *Bull. Soc. Fr. Miner.*, vol. 34, pp. 71–117, 1911.

[61] B. Broughton, *Handbook of Liquid Crystals: 8 Volume Set*, 2nd ed., J. W. Goodby et al., Eds.: Wiley, 2014.

[62] R. Shen, "Surface properties probed by second-harmonic and sum-frequency generation," *Nature (London)*, vol. 337, pp. 519–525, 1989.

[63] B. Saad, M. M. Denariez-Roberge, and T. V. Galstyan, "Diffusion of photoexcited azo dye in a liquid-crystal host," *Optics Letters*, vol. 23, no. 9, pp. 727-729, 1988.

[64] T. V. Galstyan, B. Saad, and M. M. Denariez-Roberge, "Excitation transfer from azo dye to nematic host during photoisomerization," *J. Chem. Phys.*, vol. 107, pp. 9319-9325, 1997.

[65] O. Thibault-Maheu, T. Galstian, A. Bessette, and Y. Zhao, "Light-configured mesogenic azopolymer stabilized liquid crystals," *Appl. Phys. Lett.*, vol. 97, p. 153301, 2010.

[66] V. Presnyakov, K. Asatryan, T. Galstian, and V. Chigrinov, "Optical polarization grating induced liquid crystal micro-structure using azo-dye command layer," *Optics Express*, vol. 14, no. 22, pp. 10558-10564, 2006.

[67] Tigran Galstian, Introduction à la photonique, 2012, Université Laval. Base de la

photonique GPH 3100.

[68] S-T. Wu and D-K. Yang, *Reflective liquid crystal displays*.: Wiley, 2001.

[69] S. Johnsen, *The Optics of Life: A Biologist's Guide to Light in Nature*.: Princeton University Press, 2012.

[70] H. Ch. Hulst, *Light Scattering by Small Particles*.: Science , 1977.

[71] K. G. Yager and Ch. J. Barrett, "Light-Induced Nanostructure Formation using Azobenzene Polymers," in *Polymeric Nanostructures and Their Applications*, H. S. Nalwa, Ed., pp. 1-38.

[72] K. Ichimura and Y. Suzuki, "Reversible change in alignment mode of nematic liquid crystals regulated photochemically by ‘command surfaces’ modified with an azobenzen monolayer," *Langmuir*, vol. 4, p. 1214, 1988.

[73] W. M. Gibbons, P. J. Shannon, Sh.T. Sun, and B. J. Swetlin, "Surface-mediated alignment of nematic liquid crystals with polarized laser light," *Nature*, vol. 351, pp. 49–50, 1991.

[74] V. Chigrinov, "Liquid crystal devices based on photoalignment and photopatterning materials," *Proc. SPIE 9004, Emerging Liquid Crystal Technologies IX, 90040A*, 2014.

[75] A. Natansohn, P. Rochon, J. Gosselin, and S. Xiel, "Azo Polymers for Reversible Optical Storage. 1. Poly[4'- [[2- (acr yloyloxy)ethyll ethylaminol-4-ni troazo

benzene]," *Macromolecules*, vol. 25, no. 8, pp. 2268–2273, 1992.

[76] A. Natansohn and P. Rochon, "Photoinduced Motions in Azo-Containing Polymers," *Chem. Rev.*, vol. 102, pp. 4139-4175, 2002.

[77] D. Y. Kim et al., "Polarized Laser Induced Holographic Surface Relief Gratings on Polymer Films," *Macromolecules*, vol. 28, pp. 8835-8839, 1995.

[78] C. J. Barrett, J.-I. Mamiya, K. G. Yager, and T. Ikeda, "Photo-mechanical effects in azobenzene-containing soft materials," *Soft Matter*, vol. 3, pp. 1249-1261, 2007.

[79] I. Janossy, A. D. Lloyd, and B. S. Wherrett, "Anomalous optical Freedericksz transition in an absorbing liquid crystal," *Mol. Cryst. Liq. Cryst.*, vol. 179, pp. 1-12, 1990.

[80] L. Marucci and D. Paparo, "Photoinduced molecular reorientation of absorbing liquid crystals," *Phys Rev. E.*, vol. 56, pp. 1765-1772, 1997.

[81] N. Tabiryan, U. Hrozhyk, and S. Serak, "Nonlinear refraction in photoinduced isotropic state of liquid crystalline azobenzenes," *Phys. Rev. Lett.*, vol. 93, no. 11, p. 113901, 2004.

[82] H. J. Rau, "Further evidence for rotation in the π,π* and inversion in the n,π* photoisomerization of azobenzenes," *Photochem.*, vol. 26, p. 221, 1984.

[83] C. Fiorini et al., "All-optical manipulation of azo-dye molecules," *Macromolecular Symposia*, vol. 137, no. 1, pp. 105-113, 1999.

[84] P. Rochon and E. Batalla, "Optically induced surface gratings on azoaromatic polymer films," *Appl. Phys. Lett.*, vol. 66, p. 136, 1995.

[85] D. Y. Kim, S. K. Tripathy, L. Li, and J. Kumar, "Laser induced holographic surface relief gratings on nonlinear optical polymer films," *Appl. Phys. Lett.*, vol. 66, p. 1166, 1995.

[86] M. Schonhoff, M. Mertesdorf, and M. Losche, "Mechanism of photoreorientation of azobenzene dyes in molecular films," *J. Phys. Chem.*, vol. 100, pp. 7558-7565, 1996.

[87] D.-K. Yang and S.-T. Wu, *Fundamentals of Liquid Crystal Devices*. New York: Wiley, 2006.

[88] U. Hrozhyk et al., *Proc. SPIE 7050, Liquid Crystals XII*, p. 705007, 2008.

[89] G. Goubert and T. Galstian, "Observation of a photo wetting effect on anisotropic liquid-solid interfaces," *Optics Express*, vol. 17, no. 12, p. 9637, 2009.

[90] A. Yavrian, T. G. Galstian, and M. Piche, "Circularly polarized light-induced rearrangement of optical axis in photoanisotropic recording media," *Opt. Eng.*, vol. 41, no. 4, pp. 852-855, 2002.

[91] V. P. Pham, T. Galstyan, A. Granger, and R. Lessard, "Novel Azo Dye-Doped Poly(Methyl Methacrylate) Films as Optical Data Storage Media," *Jpn. J. Appl. Phys.*, vol. 36, p. 429, 1997.

[92] U. Hrozhyk, S. Serak, N. Tabiryan, and al., "High optical nonlinearity of azobenzene

liquid crystals for short laser pulses," *Proc. SPIE 7050, Liquid Crystals XII*, p. 705007, 2008.

[93] T. Galstyan and K. E. Asatryan, "New intrinsic optical bistability in nematics," *Zh. Technic. Fiz Letters*, vol. 7, no. 11, p. 85, 1991.

[94] K. E. Asatryan, T. Galstyan, and L. Petrosyan, "Optical Freedericksz transition's hysteresis induction by means of light wave attenuation," *Opt. and Spectrosc. (USSR)*, vol. 71, no. 3, p. 471, 1991.

[95] L. Blinov, *Electro-optical and Magneto-optical Properties of Liquid Crystals*.: John Wiley & Sons Ltd, 1983.

[96] A. Yavrian, T. V Galstian, and M Piche, "Photoinduced absorption and refraction in azo dye doped PMMA films: the aging effect," *Optical Materials*, vol. 26, no. 3, pp. 261-265, 2004.

[97] A. Yavrian, K. Asatryan, T. Galstian, and M. Piche, "Real-time holographic image restoration in azo dye doped polymer films," *Optics Communications*, vol. 251, no. 4-6, pp. 286-291, 2005.

[98] P. S. Ramanujam et al., "Erasable holographic storage in azobenzene polyesters and peptides," *Proc. SPIE 3011*, p. 319, 1997.

[99] M. L. Dumont and Z. Sekkat, "Dynamical study of photoinduced anisotropy and orientational relaxation of azo dyes in polymeric films: poling at room temperature,"

Proc. SPIE 1774, Nonconducting Photopolymers and Applications, p. 188, 1993.

[100] H. Thiem, P. Strohriegl, M. Shkunov, and I. McCulloch, "Photopolymerization of Reactive Mesogens," *Macromolecular Chemistry and Physics*, vol. 206, no. 21, 2005.

[101] L. Lu, T. Sergan, V. Sergan, and P. J. Bos, "Spatial and orientational control of liquid crystal alignment using a surface localized polymer layer," *Appl Phys Lett.*, vol. 101, p. 251912, 2012.

[102] I. Dierking, "Polymer Network-Stabilized Liquid Crystals," *Adv. Mater.*, vol. 12, no. 3, 2000.

[103] T. Gotoh, H. Murai, and G. Saitoh, "Response time improvement for liquid crystal/polymer composite films using dual frequency addressable liquid cryctals," *Chem. Lett.*, pp. 901-904, 1991.

[104] H. Ren and S.-T. Wu, "Anisotropic liquid crystal gels for switchable polarizers and displays," *Appl. Phys. Lett.*, vol. 81, pp. 1432–1434, 2002.

[105] V. V. Presnyakov and T. V. Galstian, "Light polarizer based on anisotropic nematic gel with electrically controlled anisotropy of scattering," *Mol. Cryst. Liq. Cryst.*, vol. 413, pp. 545–551, 2004.

[106] T. Galstian, A. Zohrabyan, A. Tork, D. Dumont, and R. Birabassov, "In-guide control of optical propagation," U. S. patent 6,859,567, February 22, 2005.

[107] C. Khoo and S. T. Wu, *Optics and Nonlinear Optics of Liquid Crystals*.: World

Scientific, 1993.

[108] X. Liang et al., "Dual-frequency addressed variable optical attenuator with submillisecond response time," *Jpn. J. Appl. Phys.*, vol. 44, pp. 1292–1295, 2005.

[109] R. A. M. Hikmet and H. M. J. Boots, "Domain structure and switching behavior of anisotropic gels," *Phys. Rev. E*, vol. 51, pp. 5824–5831, 1995.

[110] Y.-H. Fan, H. Ren, X. Liang, Y.-H. Lin, and S.-T. Wu, "Dual-frequency liquid crystal gels with submillisecond response time," *Appl. Phys. Lett.*, vol. 85, pp. 2451–2453, 2004.

[111] S. Bassene and T. Galstian, "Coherent recovery of the degree of polarization of light propagating in random anisotropy media," *Opt. Lett.*, vol. 35, pp. 3294–3296, 2010.

[112] S. Bassene and T. Galstian, "Interferential quenching of light transmission in microsphere dispersions of liquid-crystal clusters," *Opt. Lett.* , vol. 34, pp. 1663–1665, 2009.

[113] Y. Yin, M. Gu, A. B. Golovin, S. V. Shiyanovskii, and O. D. Lavrentovich, "Fast switching optical modulator based on dual frequency nematic cell," *Mol. Cryst. Liq. Cryst.*, vol. 421, pp. 133–144, 2004.

[114] N. J. Mottram and C. V. Brown, "Pulsed addressing of a dualfrequency nematic liquid crystal," *Phys. Rev. E*, vol. 74, p. 031703, 2006.

[115] V. A. Berenberg and A. P. Onokhov, "Optically addressable liquid crystal spatial

light modulators for recording hologram correctors in observational optical systems," *J Opt Technol.*, vol. 68, no. 9, pp. 672–676, 2001.

[116] Z. Zhuang, S-W. Suh, and J. S. Patel, "Polarization controller using nematic liquid crystals," *Opt Lett.*, vol. 24, no. 10, pp. 694–696, 1999.

[117] T. Galstian, *Smart mini-cameras*.: Boca Raton: CRC Press, Taylor & Francis group, 2013.

[118] Y-J. Lee, J. S. Gwag, Y-K. Kim, and J-H. Kim, "Continuous pretilt angle control of LC alignment," *SID, P-12, IDRC 08*, pp. 173–176, Available from: http://ddlab.hanyang.ac.kr/inner_ image/publication/proceeding/151.pdf.

[119] X. Nie, R. Lu, H. Xianyu, T. X. Wu, and S-T. Wu, "Anchoring energy and cell gap effects on liquid crystal response time," *J Appl Phys.*, vol. 101, p. 103110, 2007.

[120] V. V. Presnyakov and T. V. Galstian, "Variable focal length lens based on polymer-stabilized nematic liquid crystals," *Mol Cryst Liq Cryst.*, vol. 413, no. 1, pp. 435–441, 2004.

[121] A. Minasyan and T. Galstian, "Surface-polymer stabilized liquid crystals with dual-frequency control," *Appl Opt.* , vol. 52, no. 22, pp. E60–E67, 2013.

[122] Y-J. Lee et al., "Surface-controlled patterned vertical alignment mode with reactive mesogen," *Opt Express.*, vol. 17, no. 12, pp. 10298–10303, 2009.

[123] Y-K. Moon et al., "Control of liquid crystal pre-tilt angle using reactive mesogen,"

SID Symp. Dig. Tech. Pap., vol. 42, no. 1, pp. 1630–1632, 2011.

[124] Y-J. Lee et al., "Liquid crystal alignment control using reactive mesogen mixed with alignment layers," *FMC5 – 1. IDW '09*, pp. 747–750, Available from: http://ddlab.hanyang.ac.kr/inner_image/ publication/proceeding/175.pdf.

[125] O. Yaroshchuk et al., "Stabilization of liquid crystal photoaligning layers by reactive mesogens," *Appl Phys Lett.*, vol. 95, p. 021902, 2009.

[126] D. K. Yang, L. C. Chien, and J. W. Doane, "Cholesteric liquid crystal/ polymer gel dispersion for haze-free light shutter," *Appl Phys Lett.*, vol. 60, p. 3102, 1992.

[127] J-H. Lee et al., "Enhanced contrast ratio and viewing angle of polymerstabilized liquid crystal via refractive index matching between liquid crystal and polymer network," *Opt Express*, vol. 21, no. 22, pp. 26914–26920, 2013.

[128] K. Allahverdyan and T. Galstian, "Electrooptic jumps in natural helicoidal photonic bandgap structures," *Opt Express*, vol. 19, no. 5, pp. 4611–4617, 2011.

[129] V. A. Belyakov, "Untwisting of the helical structure in a plane layer of chiral liquid crystal," *JETP Lett.*, vol. 76, no. 2, pp. 88–92, 2002.

[130] O. D. Lavrentovich and D-K. Yang, "Cholesteric cellular patterns with electric-field-controlled line tension," *Phys Rev E.*, vol. 57, no. 6, pp. R6269–R6272, 1988.

[131] A. Minasyan, A. Tork, and T. Galstian, "Study of photo isomerization and photoinduced anisotropy of a mesogenic azobenzen dye mixture in various solid and

liquid matrices," *Proc. SPIE 9288, Photonics North 2014, 92880N*, 2014.

[132] L.-C. Chien, N. Boyden, J. Walz, G. Shenouda, and M. Citano, "Photopolymerization in Self-organizing Systems," *Molecular Crystals and Liquid Crystals Science and Technology. Section A. Molecular Crystals and Liquid Crystals*, vol. 31, 1988.

[133] J. D. Margerum, A. M. Lackner, E. Ramos, K. C. Lim, and W. H. Smith, "Effects of off-state alignment in polymer dispersed liquid crystals," *Liq. Cryst.*, vol. 5, pp. 1477-1487, 1989.

[134] E. Shimada and T. Uchida, "Control of polymer orientation in polymer dispersed liquid crystal (PDLC)," *Jpn. J. Appl. Phys, Part 2*, vol. 31, pp. L352-L354, 1992.

[135] Bédard-Arcand Jean-Philippe, Contrôle électrique et magnétique de surfaces mésogènes pour cellules électro-optiques, 2013, Mémoire de maîtrise, Québec, Université Laval.

[136] A. Minasyan and T. Galstian, "Surface polymer-stabilized dual frequency chiral liquid crystals," *Liquid Crystals Reviews*, vol. 2, no. 1, pp. 60-71, 2014.

[137] M. Xu, F.D. Xu, and D.-K. Yang, "Effects of Cell Structure on the Reflection of Cholesteric Liquid Crystal Display," *J. Appl. Phys*, vol. 83, pp. 1938-1955, 1988.

[138] J-H. Lee et al., "Enhanced contrast ratio and viewing angle of polymerstabilized liquid crystal via refractive index matching between liquid crystal and polymer network," *Opt Express*, vol. 21, no. 22, pp. 26914–26920, 2013.

[139] G. W. Gray, *Molecular Structure and the Properties of Liquid Crystals*. London: Academic Press, 1962.

[140] Xiao LIANG, Yan-Qing LU, Yung-Hsun WU, Fang DU, Hai-Ying WANG and Shin-Tson WU, "Dual-Frequency Addressed Variable Optical Attenuator with Submillisecond Response Time," *Japanese Journal of Applied Physics*, vol. 44, no. 3, pp. 1292–1295, 2005.

[141] Andrii B. Golovin, Sergij V. Shiyanovskii, Oleg D. Lavrentovich, "Fast Switching Dual-Frequency Liquid Crystal Optical Retarder, Driven by an Amplitude and Frequency Modulated Voltage," *SID*, pp. 1472 -1475, 2003 DIGEST